Menoufia University

Faculty of Engineering

Electrical Engineering Department

A Proposed Non-isolated High Gain DC-DC Converter for PV Application

The thesis submitted by:

Eng. Eman Mohammed Abd El-ghany Mohammed Sarhan

B.Sc. 2014, Alazhar University

In Partial Fulfillment of the Degree of M.Sc.

In

Electrical Engineering

Supervised by

Prof. Dr. Awad E. Elsabbe

Professor of Power Electronics

Electrical Engineering Department

Faculty of Engineering

Menoufia University

( )

Dr. Arafa S. Mansour

Associate Professor

Electrical Engineering Department

Faculty of Engineering

Menoufia University

( )

Dr. Dina S. Osheba

Associate Professor

Electrical Engineering Department

Faculty of Engineering

Menoufia University

( )

2022

Menoufia University

Faculty of Engineering

Electrical Engineering Department

A Proposed Non-isolated High Gain DC-DC Converter for PV Application

The thesis submitted by:

Eng. Eman Mohammed Abd El-ghany Mohammed Sarhan

B.Sc. 2014, Alazhar University

In Partial Fulfillment of the Degree of M.Sc.

In

Electrical Engineering

Approved by

Prof. Dr. Azza M. E. Lashin

Professor of Power Electronics

Electrical Engineering Department

Faculty of Engineering

Menoufia University

( )

Prof. Dr. Awad E. Elsabbe

Professor of Power Electronics

Electrical Engineering Department

Faculty of Engineering

Menoufia University

( )

Prof. Dr. Mahmoud Mohammed Salem

Professor of Power Electronics

Dean of the College of Industry and Energy Technology

Delta Technological University in Quesna

( )

2022

ACKNOWLEDGEMENTS

First, I would like to express my deepest gratitude and thanks to **ALLAH**, the creator of all, for enormous and continuous help that is the magnificent factor in achieving and making this work a reality.

I would like to express my deep and sincere gratitude to my supervisors, **Prof. Dr. Awad Elsabbe**, **Assoc. Prof. Dr. Arafa S. Mansour and Assoc. Prof. Dr. Dina S. Osheba** for their wide knowledge and their logical way of thinking which have been of great value for me. Their understanding, encouraging and personal guidance have provided a good basis for the present thesis.

Special and deep thanks to my husband, my father-in-law, and my mother-in-law for their moral support and motivation. Without their encouragement, it would have been impossible for me to finish my work.

All my thanks, appreciation, love and respect to my parents, my brothers and my sister for their real love. I will never forget how they supported and encouraged me in all forms.

Lastly, I offer my regards and blessings to all of those who supported me during the completion of my thesis.

Eng. Eman M. Sarhan

ABSTRACT

The increase demand of electrical energy due to the industrial development and world population has made the traditional energy resources entered the age of insufficiency. Recently, an increase attention has been given to the renewable energy sources, especially photovoltaic (PV) energy systems as an alternative energy resource available everywhere in Egypt. And offer substantial advantages over conventional power resources such as reliability, low maintenance cost, no fuel cost, reduced sound pollution, safety and high performance.

DC-DC boost converter is inserted between the source and the load as power conditioning unit to regulate and boost up photovoltaic voltage to desired output voltage**.** But the conventional boost converter give output voltage not exceeds about twice of the input for stable operation, this not sufficient for distribution level voltage. So, high gain DC/DC converter is ideal solution to achieve high voltage level at the output with high efficiency to convert the electrical power to useable form.

There are a lot of topologies of high gain DC/DC converter that used with PV. In this thesis introduces a proposed non isolated high gain DC/DC converter used to convert low voltage solar PV panels to distribution level voltage. To do this, a converter used a single switch with switched inductor technique that is able to produce high gain power transmission and continuous input current.

This thesis the steady state analysis and operation modes of the proposed converter are explained in detail for continuous conduction mode (CCM) and discontinuous conduction mode (DCM) operation. Also, the mathematical analysis implementation and voltage gain derivation is carried out for the proposed converter.

Computer simulations are carried out for the proposed topology by Matlab/Simulink software. The prototypes of the proposed converter for CCM and DCM cases were built and tested in the laboratory. A DSP 1104 platform was used for evaluation board closed loop performance and open loop performance in order to verify the theoretical analysis. The experimental setup and hardware implementation are described. Several of experimental results for the proposed topology are included and discussed. The simulation and experimental results of the proposed converter are studied for closed loop case with static load by using resistive load and dynamic load by using separately excited DC motor.

The proposed converter is compared with other recent converters and it is cleared from this comparison the advantages of the proposed with respect to others that shows the proposed converter has lower compensative components (capacitors and inductors), lower voltage stress

for semi-conductor device (switch and diodes) and higher efficiency. The simulation and experimental results are proved these advantages for the proposed converter and in good agreement.

CONTENTS

ABSTRACT……i

CONTENTS……iii

LIST OF FIGURES……v

LIST OF TABLES……viii

LIST OF ABBREVIATIONS AND SYMBOLS ……ix

CHAPTER (1) 1

INTRODUCTION 1

1.1 General Power Electronic DC-DC Converter 1

1.2 Thesis Objectives 6

1.3 Thesis Outlines 7

CHAPTER (2) 8

DESCRIPTION AND ANALYSIS OF THE PROPOSED HIGH GAIN DC/DC CONVERTER 8

2.1 Summary 8

2.2 Circuit Description 8

2.3 Operation Modes 8

2.3.1 Continuous current operation modes (CCM) 8

2.3.2 Discontinuous conduction mode operation (DCM) 11

2.4 Parameter Design 13

2.4.1 Inductor design 13

2.4.2 Capacitor design 13

CHAPTER (3) 15

PERFORMANCE EVALUATION OF HIGH GAIN DC/DC CONVERTER 15

3.1 Summary 15

3.2 Simulation Results in CCM 15

3.2.1 Steady state results at different duty ratios 16

3.3 Simulation Results in DCM 23

3.3.1 Simulation results at different duty ratios D=0.3, D=0.5 and D=0.6 23

3.4 Simulation Results of Closed Loop Control at Static Load Performance ... 29
3.4.1 Input voltage change ... 30
3.4.2 Load change ... 31
3.4.3 Reference voltage change ... 32

CHAPTER (4) ... 33

EXPERIMENTAL SETUP OF HIGH GAIN DC/DC CONVERTER ... 33

4.1 Summary ... 33

4.2 Experimental Setup Description for Open Loop Control System ... 33
4.2.1 Main power circuit ... 35
4.2.2 Isolating and base driving circuit ... 35
4.2.3 Voltage and current transducers ... 35
4.2.4 DSP1104 controller board ... 37

4.3 Experimental Results for CCM ... 38

4.4 Voltage Gain with Duty Ratio in CCM ... 45

4.5 Experimental Results at DCM Performance ... 45
4.5.1: Experimental results at different duty ratios ... 45

4.6 Voltage Gain with Duty Ratio in DCM ... 52

4.7 Experimental Results of Closed Loop Control at Static Load ... 53
4.7.1 Input voltage change ... 53
4.7.2 Load change ... 55
4.7.3 Reference voltage change ... 56

4.8 Experimental Results of Closed Loop at Dynamic Load Performance ... 57
4.8.1 Voltage control ... 57
4.8.2 Speed control ... 59

4.9 Comparisons of The Proposed Converter with Previous Work ... 61

4.10 Converter Efficiency ... 64

CHAPTER (5) ... 65

CONCLUSIONS AND FUTURE WORK ... 65

5.1 Conclusions ... 65

5.2 Future Work ... 66

LIST OF PUBLICATIONS ... 67

REFERENCES ... 66

APPENDICES ... 70

LIST OF FIGURES

Fig. (1.1) Coupled inductor with intermediate energy storage capacitor converter 2

Fig. (1.2) Coupled inductor with voltage multiplier converter 3

Fig. (1.3) Coupled inductor with diode capacitor converter. 3

Fig. (1.4) Single-ended primary inductance converter (SEPIC). 4

Fig (2.1) The proposed converter 8

Fig. (2.2) Operating mode (1) 9

Fig. (2.3) Operating mode (2) 10

Fig. (2.4) Operating mode (3) 11

Fig. (2.5) The typical key waveforms of the proposed converter in CCM 12

Fig. (2.6) The typical key waveforms of the proposed converter in DCM 13

Fig. (3.1) Performance of output voltage and input voltage at different duty ratios (a) D = 0.3, (b) D = 0.6 and (c) D = 0.8 respectively 17

Fig.(3.2) Performance of output current at different duty ratios (a) D = 0.3, (b) D = 0.6 and (c) D = 0.8 respectively 18

Fig. (3.3) Performance of the input current at different duty ratios (a) D = 0.3, (b) D = 0.6 and (c) D = 0.8 19

Fig. (3.4) Performance of inductor voltage and current at different duty ratios (a) D=0.3, (b) D=0.6 and (c) D=0.8 21

Fig. (3.5) Performance of switch voltage and current at different duty ratios (a) D = 0.3, (b) D = 0.6 and (c) D = 0.8 22

Fig. (3.6) Performance of output voltage and current at different duty ratios (a) D = 0.3, (b) D = 0.5 and (c) D = 0.6 24

Fig. (3.7) Performance of output voltage and current at different duty ratios (a) D = 0.3, (b) D = 0.5 and (c) D = 0.6 25

Fig. (3.8) Performance of input current at different duty ratios (a) D = 0.3, (b) D = 0.5 and (c) D = 0.6 26

Fig. (3.10) Performance switch voltage and current at different duty ratios (a) D = 0.3, (b) D = 0.5 and (c) D = 0.6. 29

Fig. (3.11) Input voltage at input change 30

Fig. (3.12) Reference and output voltage under input change 30

Fig. (3.13) Output current under input change 31

Fig. (3.14) Reference and output voltage under load change 31

Fig. (3.15) Load current change 32

Fig. (3.16) Reference and output voltage under reference change 32

Fig. (4.1) Experimental setup for the proposed converter 34

Fig (4.2) The real view of driving circuit 35

Fig. (4.3) a- The voltage transducer, b- Current transducer and c- Real view of current and voltage transducer 36

Fig. (4.4) DSP port connection 38

Fig. (4.5) Performance waveforms of output and input voltage at different duty ratios (a) D = 0.3, (b) D = 0.6 and (c) D = 0.8 40

Fig. (4.6) Performance waveforms of input current at different duty ratios (a) D = 0.3, (b) D = 0.6 and (c)D = 0.8 41

Fig. (4.7) Performance waveforms of gate signal, switch voltage at different duty ratios (a) D = 0.3, (b)D = 0.6 and (c) D = 0.8 43

Fig. (4.8) Performance waveforms of inductor voltage and current at different duty ratios (a)D = 0.3, (b) D = 0.6 and (c) D = 0.8 44

Fig. (4.9) Voltage gain versus duty ratio 45

Fig. (4.10) Performance waveforms of output and input voltage at various duty ratios (a) D = 0.3, (b) D = 0.5 and (c) D = 0.6 47

Fig. (4.11) Performance waveforms of input current at various duty ratios (a) D = 0.3, (b) D = 0.5 and (c) D = 0.6 49

Fig. (4.12) Performance waveforms of inductor voltage and it's at various duty ratios (a) D = 0.3, (b) D = 0.5 and (c) D = 0.6 50

Fig. (4.13) Performance waveforms of gate signal pulse and switch voltage at various duty ratios (a) D = 0.3, (b) D = 0.5 and (c) D = 0.6 52

Fig. (4.14) Voltage gain versus duty ratio at experimental and mathematical results 52

Fig. (4.15) Input voltage change 54

Fig. (4.16) Reference and output voltage under input change 54

Fig. (4.17) Output current under input change 55

Fig. (4.18) Reference and output voltage at load change 55

Fig. (4.19) Load current under load change 56

Fig. (4.20) Reference and output voltage at reference change 56

Fig. (4.21) Reference and output voltage at voltage control 58

Fig.(4.22) Speed changed under voltage control 58

Fig. (4.23) Reference and motor speed under speed control 59

Fig. (4.24) Output voltage change under speed control 60

Fig. (4.25) Reference and motor speed under speed control 60

Fig. (4.26) Output voltage change under speed control 61

Fig. (4.27) Voltage gain versus duty ratio 63

Fig. (4.28) Maximum switch voltage stress versus voltage gain at V_{in} = 24 V. ... 63

Fig. (4.29) Maximum output diode voltage stress versus voltage gain at V_{in} = 24V. 64

Fig. (4.30) Efficiency of the proposed converter versus duty ratio 64

LIST OF TABLES:

Table (3.1) Converter parameter in CCM and DCM **15**

Table (3.2) Closed loop control parameters **29**

Table (4.1) Experimental circuit parameters **34**

Table (4.2) Components of experimental setup for the proposed converter **34**

Table (4.3) Closed loop control parameters **53**

Table (4.4) Comparing the proposed converters with other recent topologies **62**

LIST OF ABBREVIATIONS AND SYMBOLS:

AC	Alternating current
CCM	Continuous conduction mode
C_O	Output capacitor
D	Duty ratio
DC	Direct current
DCM	Discontinuous conduction mode
DSP	Digital signal processor
e_b	Back electro motive force
FACTS	Flexible AC transmission
Fs	Switching frequency
HVDC	High voltage direct current
I_a	Armature current
I_{CO}	Output capacitor current
I_{in}	Input current
I_{L1},I_{L2}	Inductor currents
I_O	Output current
J	Moment of inertia
k	Coupling coefficient of coupled inductor
kI	Integration integer
kp	Proportional integer

L_1, L_2	Inductors
L_a	Armature inductor
M	Voltage gain
n	Turns ratio of coupled inductor
PV	Photovoltaic solar panels
R_a	Armature resistance
R_{Load}	Load resistance
SEPIC	Single-ended primary inductance converter
T_{FL}	Full load torque
T_L	Load torque
T_m	Electromagnetic torque
V_a	Armature voltage
V_{CO}	Output capacitor voltage
V_{in}	Input voltage
V_{L1}, V_{L2}	Inductor voltages
VM	Voltage multiplier
V_O	Output voltage
V_{SW}	Switch voltage stress
W	Motor speed
ΔIL	Inductor current ripple
ΔVo	Output voltage ripple

CHAPTER (1)
INTRODUCTION

1.1 General Power Electronic DC/DC Converters

In recent years, power electronics became very important in industrial technology and is now used in a great variety of products, including heat controls, light controls, motor controls, power supplies, vehicle propulsion systems, flexible AC transmission systems (FACTS) and high-voltage DC systems (HVDC). The power electronics circuits can be classified into different categories: (i) AC to AC converters (AC voltage controllers); (ii) AC to DC converters (Rectifiers); (iii) DC to DC converters (DC choppers); (iv) DC to AC converters (inverters) [1].

A DC-DC converter is a very popular power converter known as DC choppers. The function of DC-DC converter is to obtain DC voltage, with variable magnitude from fixed DC voltage using for DC application. The most important DC application is photovoltaic (PV) system where the main objective of DC/DC converter ensures maximum power from PV system.

Photovoltaic solar energy has many advantages such as environmentally friendly, no noise, no moving parts, no emissions, no use of fuels and water and minimal maintenance requirements which makes it widely used in existing networks. But the output voltage of this energy has high fluctuations and a low value. So, to adjust the output voltage and convert it to high voltage level, the DC/DC converter is very important to use in these applications [3].

There are different topologies for DC/DC converter but, the main types are buck converter used to produce the output voltage less than the input. The second type is the boost converters that operate inverse the buck type where give the output voltage higher than the input. The third type is buck-boost converter provide the output voltage less than or greater than the input voltage [2]. In conventional boost converter, the switching voltage stress is equal to the output voltage and introduces large inductor current ripple. Hence it creates the large conduction loss and reverse recovery issues which affects the conversion efficiency and high voltage gain [6].

Recently, the need for high gain DC-DC converters has become one of the most viable options as they would help in integrating solar energy. The main purpose of

high gain DC/DC converters is to boost up the low voltage from the PV to high voltages which makes it feasible for connecting it to DC micro grids [4]. High gain DC/DC converters are kind of high frequency converters that convert unregulated DC voltage to regulated DC voltage with high gain at the output for many DC applications. These converters are classified into two categories, isolated and non-isolated based high step up converter.

The isolated step up converters have a transformer and by adjusting the turns ratio of the transformer, high voltage gain have been achieved. Some of those converters are flyback, push-pull, and forward type converters. These converters have drawbacks of high voltage stress due to transformer leakage inductances which reduce the efficiency. This may cause the high switching voltage stress, reverse recovery issues and reduce the high step up conversion efficiency [5]. There are suitable non isolated step-up DC/DC converters that able to overcome the drawbacks of classical boost converters. These converters can provide high voltage levels with high efficiency at output side suitable for renewable energy applications [7].

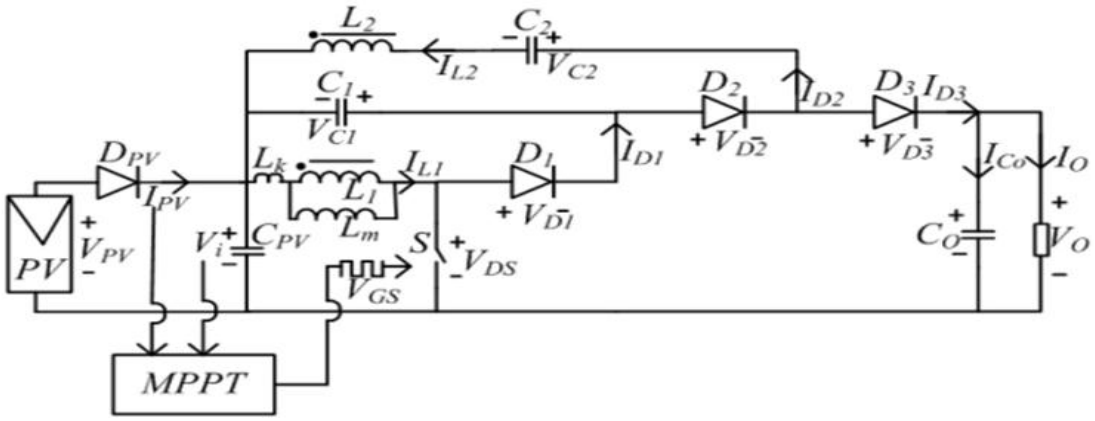

Fig. (1.1) Coupled inductor with intermediate energy storage capacitor converter

Many topologies have been introduced for this purpose [8-17] such as 1) using coupled inductor, 2) using voltage multiplier, 3) using switched capacitor, 4) using cascaded techniques, and 5) switched inductor. Coupled inductor chooses to use in high gain by increasing inductor turns ratio. But it has the following problems: large input current ripple and high switch voltage spikes because of stored energy of leakage inductance. So, clamp circuit must be used to limit this energy. However, this clamp circuit increases the conduction losses [8-11].

A topology converter that in Fig. (1.1) based on coupled inductor is presented with passive clamp circuit and intermediate energy storage capacitor used to increase the output voltage level as in [8]. But this circuit suffers from using a lot of components

that make the system expensive. Some converters consist of coupled inductors with voltage multiplier (VM) used to multiply the voltage gain presented in [9-10]. These converters provide high voltage gain with low input current ripple. However, the VM cells in DC/DC converters in Fin. (1.2) that contain coupled inductor decrease the nominal value of power semiconductors As a result of using the clamping circuit that recycles the stored energy of leakage inductance which increases the losses and reduces the overall efficiency. A topology consists of a switched inductor with double switches is described in [11] to get high gain voltage value. However, using two switches increases the circuit components and thus raises the cost of the system.

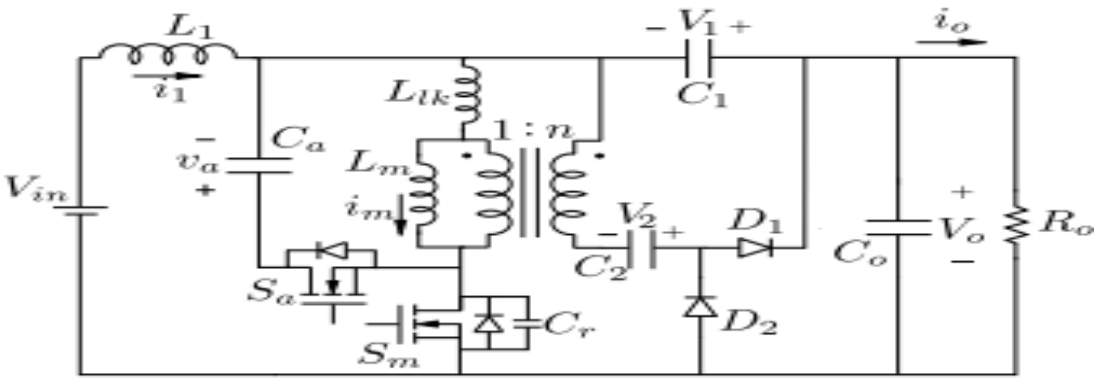

Fig. (1.2) Coupled inductor with voltage multiplier converter

A converters used a conventional cascaded boost topology based on coupled inductor and diode-capacitor cell are presented in [12, 13]. That used to suppress the switch voltage spikes resulting from leakage inductance stored energy by recycling this energy to the output side. On the other hand, using diode-capacitor cell as clamping circuit affect the system efficiency due to switching losses of this clamp as shown in Fig. (1.3).

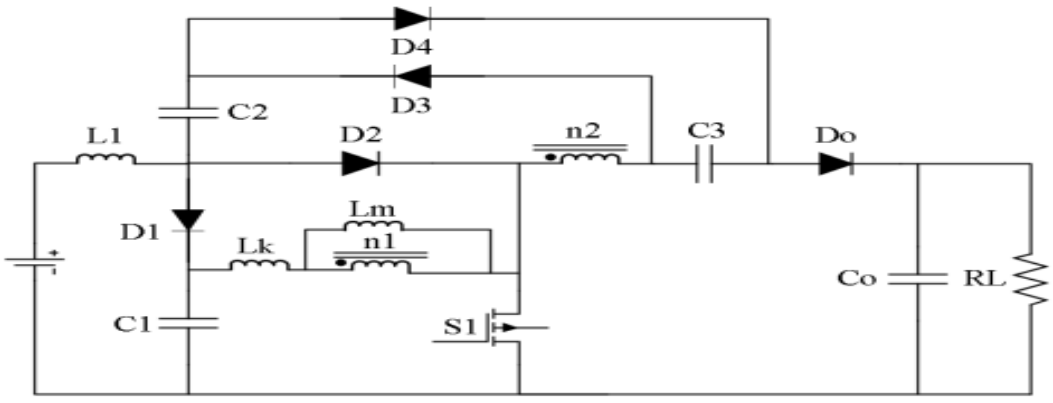

Fig. (1.3) Coupled inductor with diode capacitor converter

Converters based on the switched-capacitor principle are studied in [14, 15]. A high voltage gain is achieved, and the switch voltage stresses is reduced. However, the number of components is large, and the output diode voltage stress is high. A converter uses switched capacitor, and a coupled inductor is described in [16], where the voltage boosted by increasing the turns ratio of the coupled inductor and switched capacitor stage. This converter suffers from high transient current that has degrading effect on both efficiency and power density.

An interleaved DC/DC converter with small input current ripple for large power ranges is discussed in [17]. Also, a high step-up interleaved boost converter with switched-capacitors and switched-inductors is studied in [18]. In order to these circuits operate correctly, the duty cycles of switches should be greater than 0.5, but this led to high power losses and low efficiency. A converter based on conventional boost and single-ended primary inductance converter (SEPIC) converters as shown in Fig. (1.4) is introduced in [19, 20]. A high voltage gain and low current stresses are obtained. However, large amount of components is used in [21, 22] introduced high step-up extendable hybrid DC/DC converter based on two-phase interleaved boost converter and switched capacitor. But this converter did not suitable for high power applications due to high-level of the transient current related to switched capacitor.

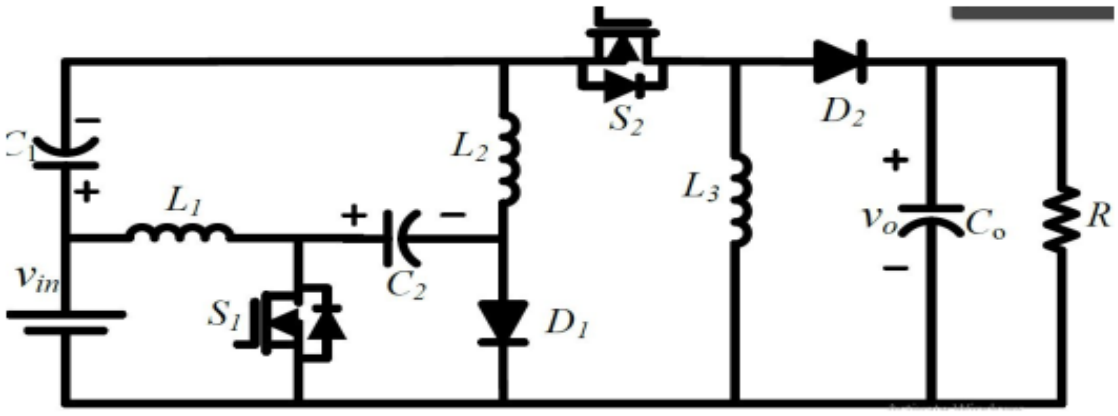

Fig. (1.4) Single-ended primary inductance (SEPIC) converter

Converter in [23] from type of non-isolated high gain DC/DC converters operate with positive output voltage and reduced current stresses but converter in [24] is about an interleaved winding coupled boost converter with passive clamp circuit that used to recycle the leakage energy to the output. These converters have switching losses due to the clamp circuit so; the overall efficiency of the converter will be decreased.

Converter in [25] explains, non-isolated full soft-switching step-up DC/DC converter with a continuous input current for renewable energy applications. The converter use of a three-winding coupled-inductor along with a voltage multiplier, to increase the gain but this system used passive clamp circuit that reduces the losses.

An ultrahigh step-up DC/DC converter is proposed in [26] with a combination of two stages boost converter, a coupled inductor, and a multiplier cell. The secondary side of the coupled inductor is unified with the multiplier cell. In addition, leakage energy of the coupled inductor is recycled and transferred to output perfectly which causes high-efficiency performance. In [27] proposes a dual-switch DC/DC converter with high-voltage gain for solar Photovoltaic (PV) systems. High-voltage gain is obtained by combining the coupled inductor and switched-capacitor voltage boosting techniques.

High step-up DC/DC converter with a continuous input current introduces in [28] which is suitable for sustainable energy systems. A three-winding coupled inductor, two power switches, three diodes, and three capacitors are utilized to perform the functions of active switched inductor and switched capacitor. This converter operates with many components that increase the system cost. A high voltage gain DC/DC boost converter with expandable diode-capacitor voltage multiplier (VM) cells in [29] is presented. The diode-capacitor VM cells and coupled inductors are employed in the presented topology to provide a higher voltage gain.

Converter in [30] employing an interleaved quadratic structure, two-winding coupled inductors, and voltage multiplier cells , the proposed converter can provide high-voltage gains, continuous input current, common ground between input and output sides, and low numbers of components. In addition, diode-capacitor lossless clamp circuits are utilized to limit the voltage stresses of the power switches. But, using coupled inductor increases voltage spikes on the switches that increase voltage stresses on the switch and therefore the losses increase which reducing the system efficiency.

Reference [31] presents high voltage gain interleaved DC/DC converter with a three-winding coupled inductor. Two interleaved and inter-coupled boost cells are connected by the input parallel and output series configuration, realizing low input current ripple and high voltage gain simultaneously. In [32] a high step-up DC/DC converter which is applied to a voltage lifts capacitor and coupled inductors to increase the voltage gain. Moreover, the interleaved structure is applied in the

converter to decrease the input ripple current. Voltage lift capacitor is used to recycling the stored energy that result from leakage inductance of the coupled inductor.

The converter in [33] is structured as an optimized integration of active switched-inductor configuration, and ladder-type voltage multiplier is merged with the regenerative-boost arrangement. Thereby, due to such an organization of structure, the proposed converter is developed the extremely high voltage-gain with comparatively fewer components. Recently, switched inductor and switched capacitor techniques in dc-dc converter are recommended to achieve high voltage by using the principle of parallel charging and series discharging of reactive elements. In [34] a modified switched inductor boost converter is proposed with reduced voltage stress across active switches. There have been many proposed topologies for high gain DC/DC converters in the literature. But topologies with higher efficiency and lesser component stress is the optimal solution. In this regard, this thesis will focus on high gain DC/DC converter based on switched inductor technique.

1.2 Thesis Objectives

There are numerous challenges and requirements for DC/DC converters. Two of them will be addressed in the thesis. The first challenge and consider the most challenging task in designing switched inductor converters is to maintain the efficiency and the number of elements at a higher voltage gain. The proposed switched inductor converter has proven its efficiency and ability to provide a high voltage gain with a smaller number of elements resulting in the proposed converter give high voltage gain with higher overall efficiency of the system.

The second challenge is clarification the closed loop control for the proposed converter to study the proposed converter with different load where the converter was tested experimentally under voltage control with resistive load. The voltage control test was investigated at different cases for input voltage change, load change and reference voltage change. Also, the converter was tested for dynamic load by using separately excited DC motor.

Simulation results for the proposed DC/DC converter are carried out using MATLAB/SIMULINK. The prototype of the proposed converter was built in the laboratory to validate the proposed converter experimentally. In order to verify the effectiveness of the proposed topology for open loop and closed loop performance.

The system of the proposed converter is implemented in real time by using digital signal processor (DSP1104). The experimental works are presented and discussed for the proposed topology.

1.3 Thesis Outlines

This thesis organized in five chapters, a list of references and appendices

Chapter (1): This chapter introduces a literature review for some pervious work, illustration some topologies of high gain DC-DC converters and objectives of this thesis.

Chapter (2): This chapter explains in detail the performance and analysis of the proposed converter in continuous conduction mode (CCM) and discontinuous conduction mode (DCM) explaining circuit description, operation modes is discussed, voltage gain equation is derived and design methodology also presented.

Chapter (3): This chapter presents the simulation results of the circuit with open loop at CCM and DCM and closed loop control system for static and dynamic loads. Closed loop system is consisting of voltage control and speed control. Different cases are studied such as input change, reference voltage change and load change. The circuit is built on MATLAB/SIMULINK program to validate it.

Chapter (4): This chapter describes the experimental setup and implementation of the circuit. A Digital Signal Processor (DSP-1104) based system is described. Experimental results were investigated for open loop at CCM and DCM and closed loop.

Chapter (5): This chapter highlights the main conclusions of the present work and the future work that can be performed on the same object.

CHAPTER (2)
DESCRIPTION AND ANALYSIS OF THE PROPOSED HIGH GAIN DC/DC CONVERTER

2.1 Summary

This chapter presents the proposed of a single switch boost converter with switched inductor in CCM and in DCM operation. In this chapter the circuit description, operation modes, mathematical modeling and parameter design are explained in CCM and DCM.

2.2 Circuit Description

The proposed converter is presented in Fig (2.1). It consists of one switch S1, two inductors L_1 and L_2, one capacitor C_o and four diodes D_1, D_2, D_3 and D_o. Both inductors L_1 and L_2 are identical.

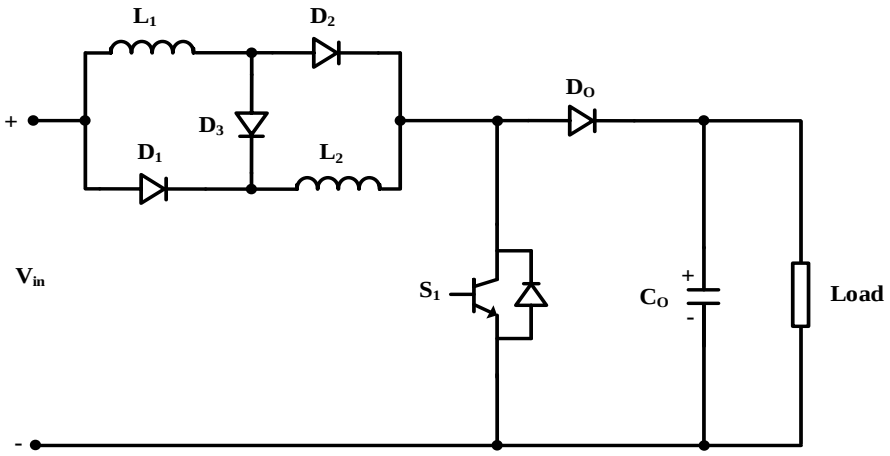

Fig (2.1) The proposed converter

2.3 Operation Modes

2.3.1 Continuous current operation modes (CCM)

The proposed converter operates in two modes in CCM and the typical key waveforms in ig. 2.5. Before describing the proposed converter in the CCM, some supposition has been considered in the CCM analysis, ideal semiconductor components, very large output capacitor

(with constant output voltage and small ripple) and in addition to the system operation in the steady-state condition.

2.3.1.1 Mode 1 (S_1 is on)

In this mode, the switch S_1 is in turned on, the diodes D_1 and D_2 are forward biased, and the diodes D_3 and D_o are revers biased. Therefore, the current follow through two inductors L_1 and L_2 and charged them in parallel path as shown in Fig.(2.2). Also, due to the inductors operate in parallel that make their voltage is equal i.e., $V_{L1}=V_{L2}$. The load is supplied by the charge on C_o. The steady-state voltage equations are as follows (assumption: $L_1 = L_2 = L$)

$$V_{L1} = V_{L2} = V_L \quad (1)$$

$$V_{L(on)} - V_{in} = 0 \quad (2)$$

For the current equations related to this mode:

$$i_{L1(on)} + i_{L2(on)} = i_{in(on)} \quad (3)$$

$$i_o = i_{co} \quad (4)$$

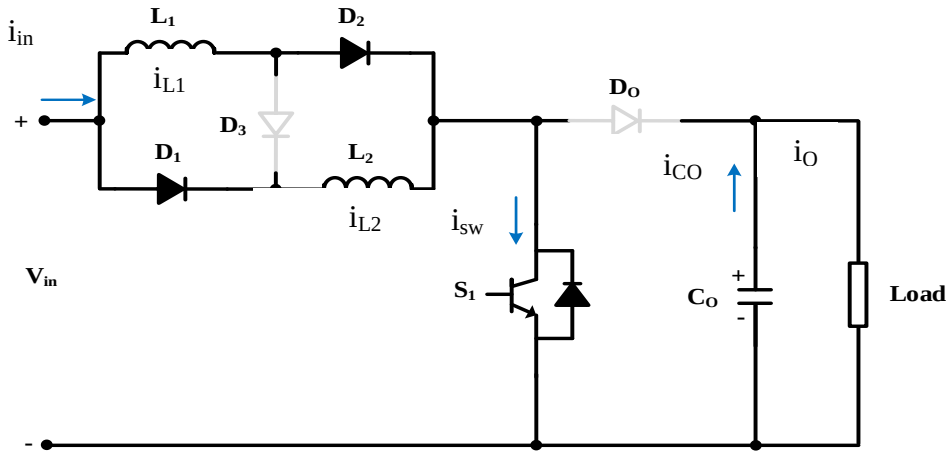

Fig. (2.2) Operating mode (1)

2.3.1.2 Mode 2(S_1 is off)

In this mode, the switch S_1 is in turned off. The diodes D_1 and D_2 become reverse biased, and the diodes D_3 and D_o are forward biased. The inductors L_1 and L_2 are connected in series and discharge their energy into the output capacitor C_o and the load as shown in Fig (2.3). The steady-state voltage equation in this mode is as follow:

$$V_o - V_{in} + 2\,V_{L(off)} = 0 \quad (5)$$

The current equations in this mode:

$i_{L1} = i_{L2} = i_{in(off)}$ (6)

$i_{L1} = i_{L2} = i_{co} + i_o$ (7)

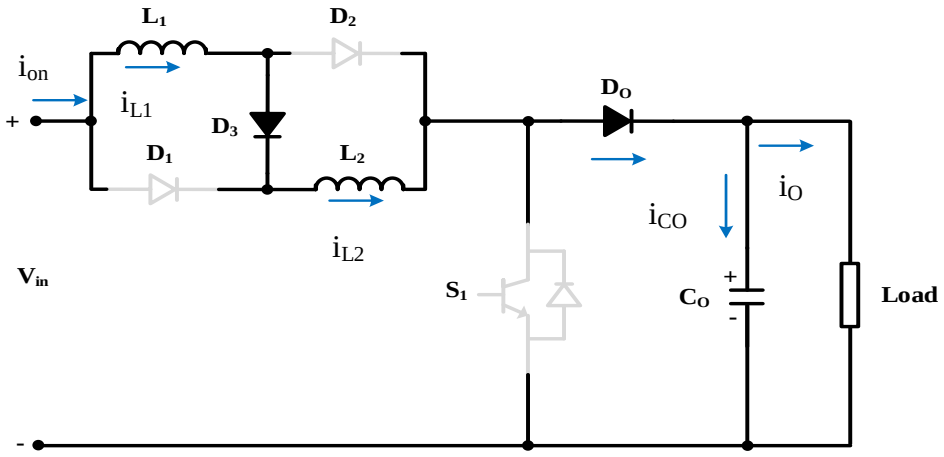

Fig. (2.3) Operating mode (2)

2.3.1.3 Voltage gain derivation in CCM

The voltage gain derivation is implemented by inductors volt-second balance method [5].

$D\ (V_{L\ (on)}) + (1 - D)\ (V_{L\ (off)}) = 0$ (8)

Substituting the value of V_L from equations (2) and (5)

$V_{L\ (on)} = V_{in}$ (9)

$V_{L\ (off)} = 0.5\ (V_{in} - V_o)$ (10)

The mathematical equation of the voltage gain becomes:

$$M = \frac{VO}{Vi} = \frac{1 + D}{1 - D}$$

The maximum switch voltage stress derived from the equation as,

$V_{sw} = V_{in} - 2\ V_{L(off)}$ (12)

By substituting from equation (8) into equation (5) and solving for finding $V_{L(off)}$, one gets;

$$V_{L(off)} = -\frac{D}{1-D} V_{in}$$ (13)

Subsequently the switch voltage stress becomes;

$$V_{sw} = \frac{1+D}{1-D} V_{in} \quad (14)$$

2.3.2 Discontinuous conduction mode operation (DCM)

The proposed converter operates in three modes for DCM operation. The operation modes and the key waveforms of the proposed converter in DCM are shown in Fig. 2.6, respectively.

2.3.2.1 Mode 1 (S_1 is off): This mode is similar to Mode 1 in CCM, as shown in Fig. (2.2).

2.3.2.2 Mode 2 (S_1 is off): This mode is similar to Mode 2 in CCM, as shown in Fig. (2.3).

2.3.2.3 Mode 3 (S_1 is still off):

In this mode, as shown in Fig. (2.4), the switch S_1 is still in OFF condition. D_1, D_2 and D_3 are still reverse biased, while D_o is not conducting. No current follows in the inductors L_1 and L_2. The load is fed by the stored energy in the capacitor C_o.

The steady state voltage equation for this mode is:

$$V_o = V_{Co} \quad (15)$$

The current equation for this mode in this mode:

$$i_o = i_{CO} \quad (16)$$

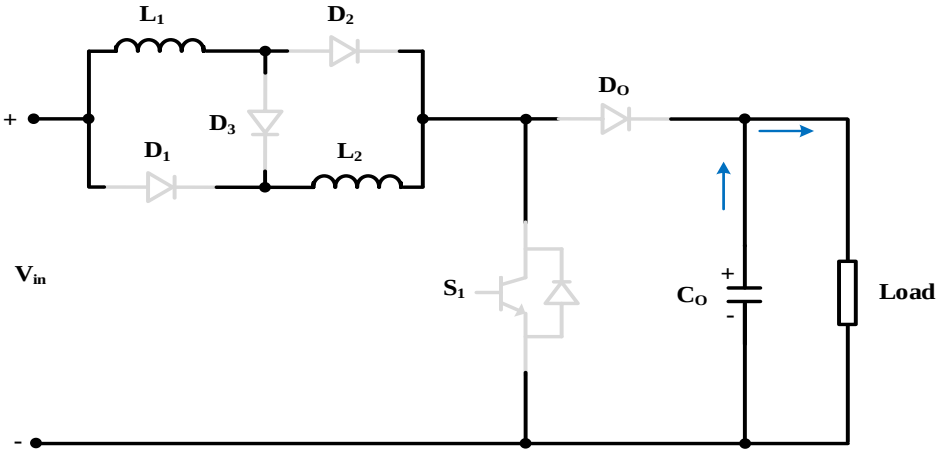

Fig. (2.4) Operating mode (3)

2.3.2.4 Voltage gain in DCM

The voltage gain derivation is implemented by inductors volt-second balance method.

$$D\,(V_{L(on)}) + 0.5\,(1 - D)\,(V_{L(off)}) = 0 \quad (17)$$

Substituting the value of $V_{L(on)}$ and $V_{L(off)}$ from equations (2) and (5), respectively.

$$V_{L(on)} = V_{in} \tag{18}$$

$$V_{L(off)} = 0.5\,(V_{in} - V_o) \tag{19}$$

Where the DCM condition operates only in half period of the OFF condition. The mathematical equation of the voltage gain becomes:

$$M = \frac{V_o}{V_{in}} = \frac{1+3D}{1-D} \tag{20}$$

The maximum switch voltage stress can be obtained from the equation;

$$V_{sw} = V_o = \frac{1+3D}{1-D} V_{in} \tag{21}$$

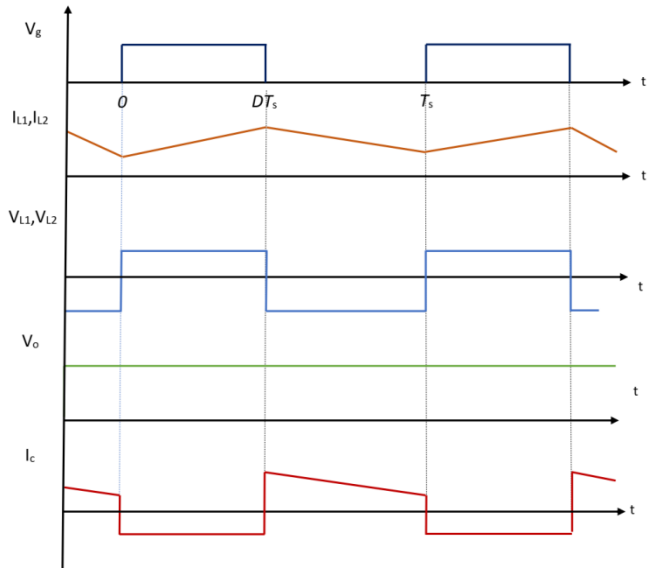

Fig. (2.5) The typical key waveforms of the proposed converter in CCM

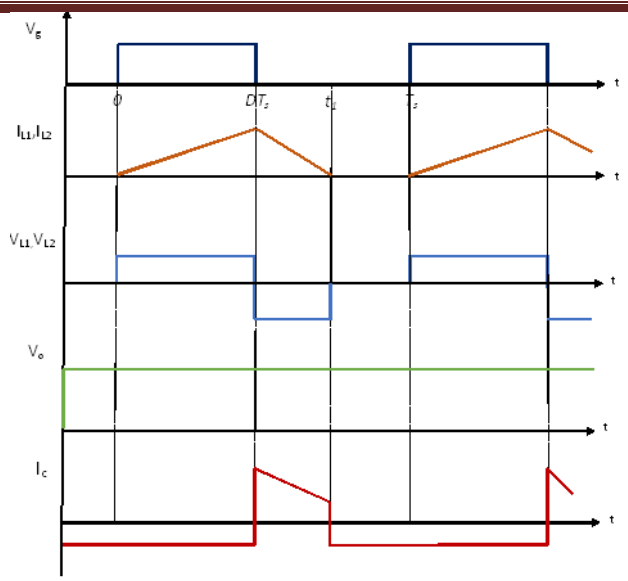

Fig. (2.6) The typical key waveforms of the proposed converter in DCM

2.4 Parameter Design

Inductors and capacitor design depend on their currents and voltages.

2.4.1 Inductor design

From the key waveforms and operation modes, the inductor can be estimated by equation:

$$V_L = L \, di/dt \tag{22}$$

By integrating equation (22), the inductor value can be calculated as in (23).

$$L = (V_L * D \; T) / (\Delta I_L) \tag{23}$$

Where ΔI_l is the inductor ripple current allowed. It's value equal to 20 to 40 percent of the output current according to IEEE standard [17].

At on state of the switch $V_L = V_{in}$, and the inductor value can be found according to equation (24);

$$L = (V_{in} * D) / (f_s * \Delta I_L) \tag{24}$$

Where f_s is the switching frequency

2.4.2 Capacitor design

The capacitor value can be found by:

$$I_o = C_o \, dv/dt \tag{25}$$

By integrating equation (25), the minimum output capacitor value (C_o) value can be determined by equation (26)

$$C_o = (I_o * D) / (f_s * \Delta V_o) \quad (26)$$

Where the output voltage ripple value as in equation (27).

$$\Delta V_o = 3.8\% \text{ to } 5\% \text{ of } V_o \quad (27)$$

As in standard the output voltage ripple equal 3.8 to 5 percent of output voltage [10].

CHAPTER (3)
PERFORMANCE EVALUATION OF HIGH GAIN DC/DC CONVERTER

3.1 Summary

In this chapter the proposed converter has been built on MATLAB/SIMULINK program and the simulation results is presented for open loop control at CCM and DCM with different values of duty ratio. The other part of this chapter discuss the simulation results for closed loop control at static load by using resistive load, in this case three conditions will be explained for closed loop of static load are input voltage change, load change and reference voltage change.

3.2 Simulation Results in CCM

To ensure the operation of the converter and to prove accuracy of theoretical relations, the simulation has been carried out by using different values of duty ratios for CCM. The parameters values used here are shown in Table (3.1).

Table (3.1) Converter parameters in CCM and DCM

Open-loop Control (CCM/DCM)	
Parameter	**Value**
Input Voltage (V_{in})	24 V
Capacitance (C_o)	330 μF
CCM	
Switching frequency (f_s)	1 KHz
Load resistance	450Ω
Inductances (L_1, L_2)	25 mH
DCM	
Switching frequency (f_s)	5KHz
Load resistance	450Ω
Inductances (L_1, L_2)	10 mH

The converter studied at different values for duty ratio equal to 30 %, 60 %, 80 %. This section explains the response of the proposed circuit. The simulation results of

input voltage, input current, inductor voltage and its current, switch voltage and its current, output voltage with input voltage and output current are discussed.

3.2.1 Steady state results at different duty ratios

Figure (3.1) shows the output voltage at different duty ratio with input voltage equal to 24 volt. The result in Fig. (3.1.a) illustrates that the output voltage at duty ratio 0.3 is 45 volt, which means that voltage gain ratio equal to 1.88. This value agrees with voltage gain equation. Also The results shown in Figf. (3.1.b) and (3.1.c) depicts the response of the circuit at duty ratio 0.6, 0.8 respectively. The output voltage at duty ratio 0.6 is 95 volt and at duty ratio 0.8 is 220 volt. These results confirm the obtained voltage gain equation

Figures (3.2.a), (3.2.b) and (3.2.c) show the output current at different duty ratio 30%, 60% and 80% respectively. As it is clear from the waveforms the output current is pure DC at D=0.3 but at D=0.6 some ripples appeared on the output current and this ripple increased with D=0.8 as shown.

Also, the input current at duty ratio 30%, 60% and 80% are shown in Figf (3.3.a), (3.3.b) and (3.3.c) respectively. The results illustrate that the input current is continuous which confirms the converter working in CCM mode. For Figf (3.4.a), (3.4.b) and (3.4.c) show the waveforms of inductor voltage and current at D=0.3, 0.6 and 0.8 where, the voltage and current for two inductors are identical where the inductor voltage is $V_{L1}=V_{L2}=V_L$ and for the inductor current $I_{L1}=I_{L2}=I_L$ so, the figure clears only one waveform for its voltage and current. Where the inductor voltage clears the two modes for CCM condition at storing energy the inductor current increasing linearly then at the instant of discharging this energy the inductor current will decrease. Also, the figure explain the peak of the current differ at each duty cycle where at 0.8 greater than D=0.6 and 0.3.

While, Figf(3.5.a), (3.5.b) and (3.5.c) illustrate the waveforms of switch voltage and current at D = 0.3, 0.6 and 0.8 respectively. Where the switch voltage stress is equal the output voltage. So, the converter efficiency is high and the losses will be reduced.

CHAPTER (3)
PERFORMANCE EVALUATION OF HIGH GAIN DC/DC CONVERTER

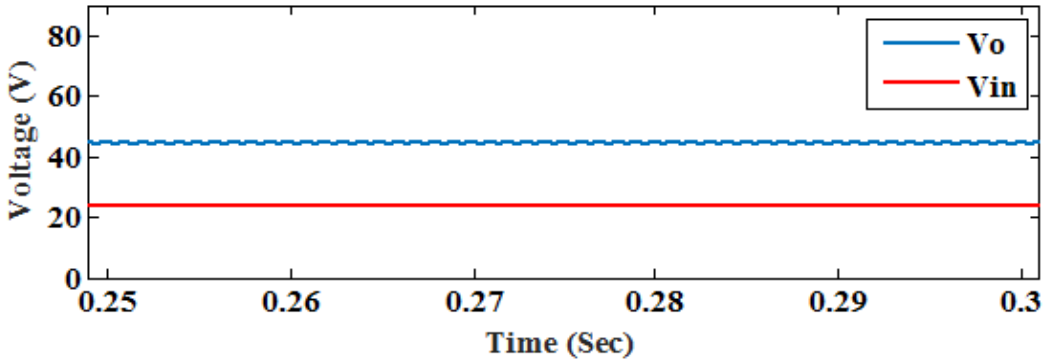

(a)

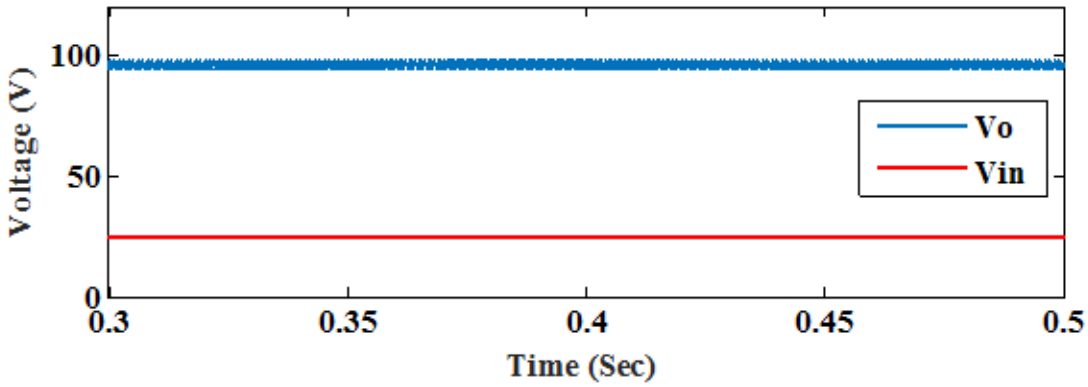

(b)

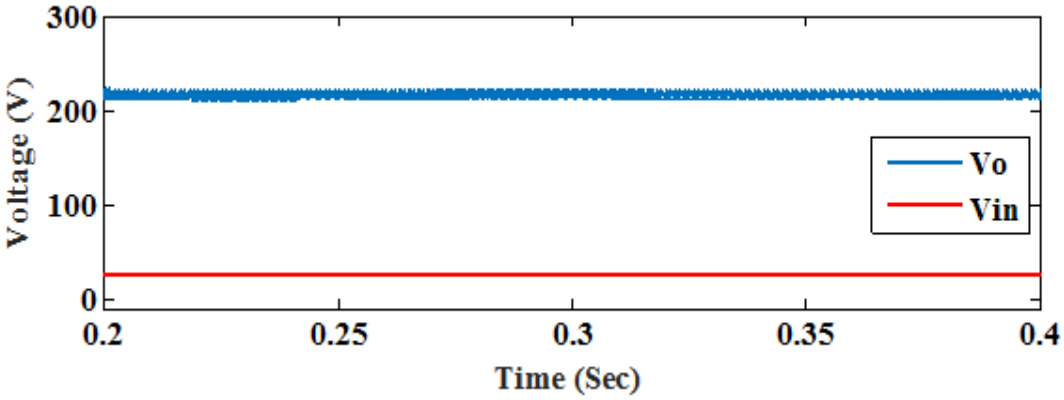

(c)

Fig. (3.1) Performance of output voltage and input voltage at different duty ratios (a) D = 0.3, (b) D = 0.6 and (c) D = 0.8 respectively

CHAPTER (3)
PERFORMANCE EVALUATION OF HIGH GAIN DC/DC CONVERTER

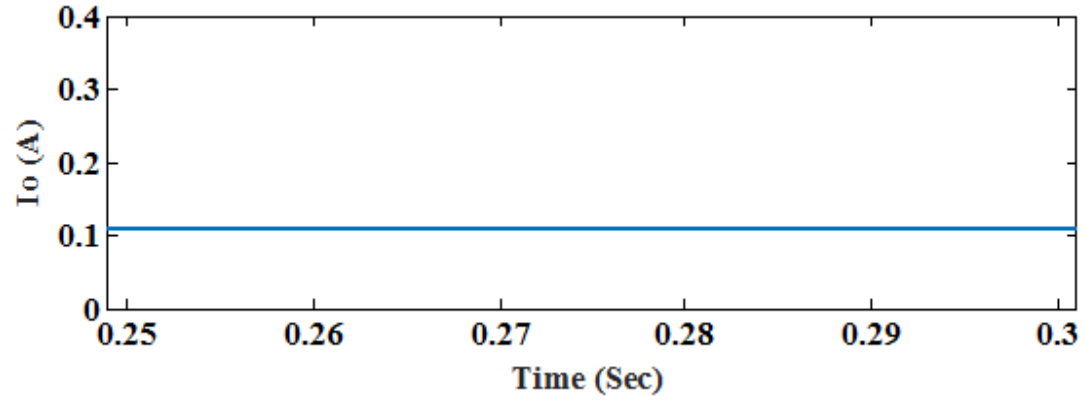

(a)

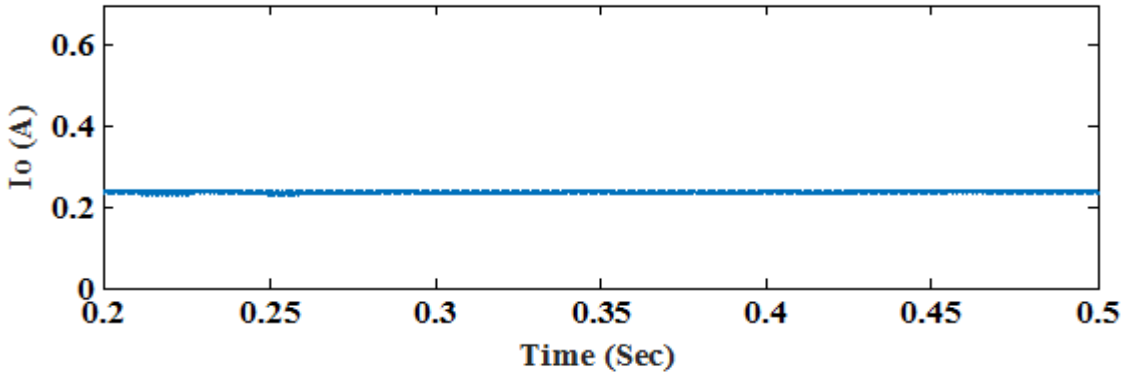

(b)

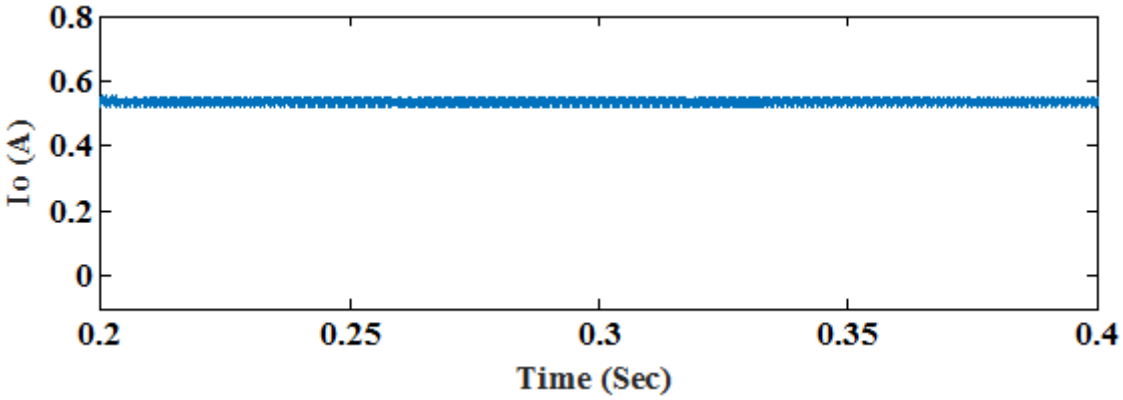

(C)

Fig.(3.2) Performance of output current at different duty ratios (a) D = 0.3, (b) D = 0.6 and (c) D = 0.8 respectively

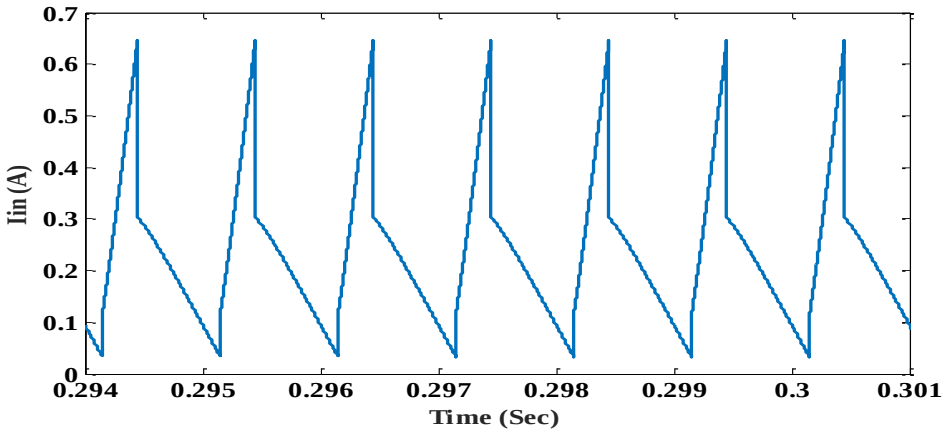

(a)

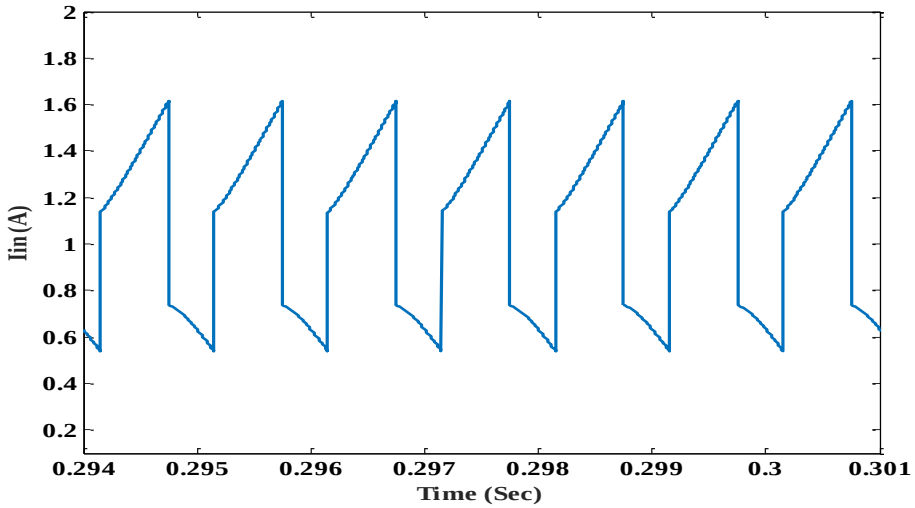

(b)

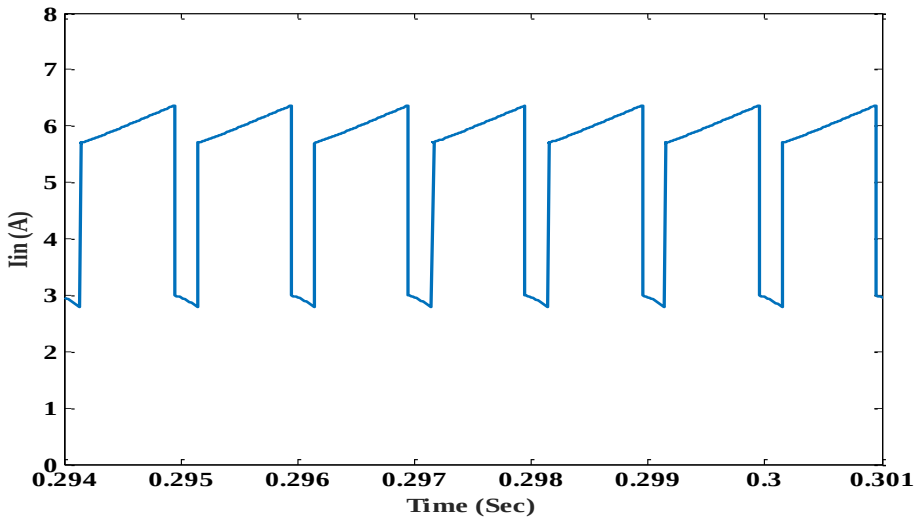

(c)

Fig. (3.3) Performance of the input current at different duty ratios (a) D = 0.3, (b) D = 0.6 and (c) D = 0.8

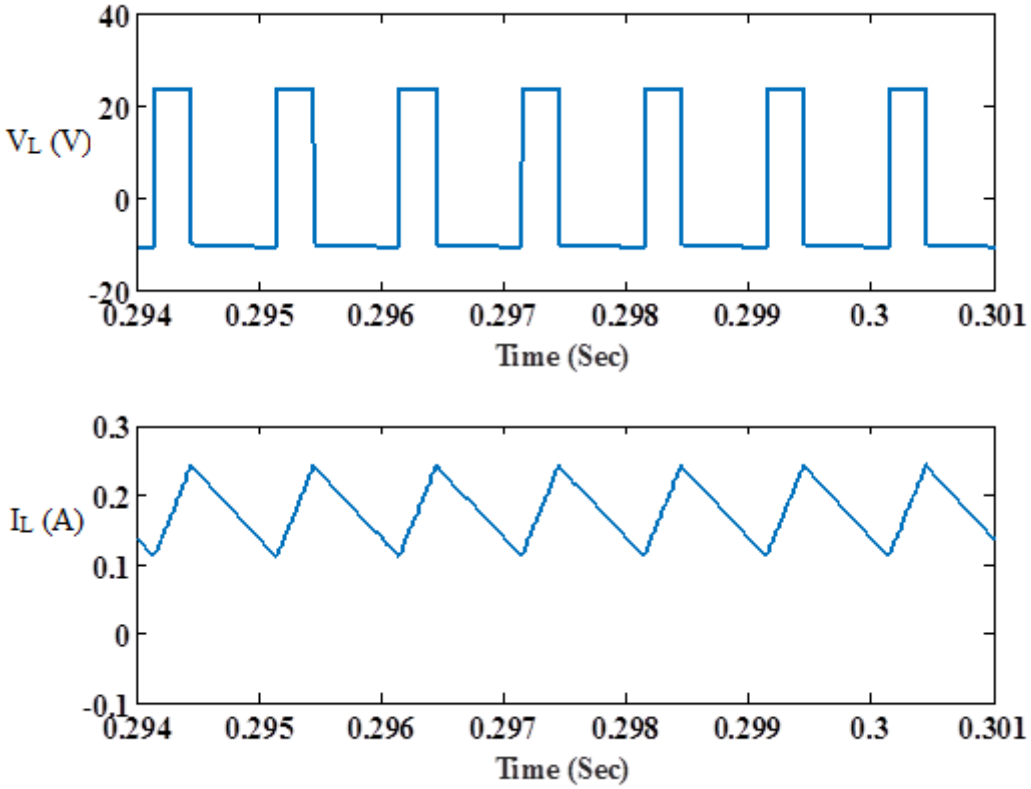
40
20
0
-20
VL (V)
0.294
0.295
0.296
0.297
0.298
0.299
0.3
0.301
Time (Sec)
0.3
0.2
0.1
0
-0.1
IL (A)
0.294
0.295
0.296
0.297
0.298
0.299
0.3
0.301
Time (Sec)

(a)

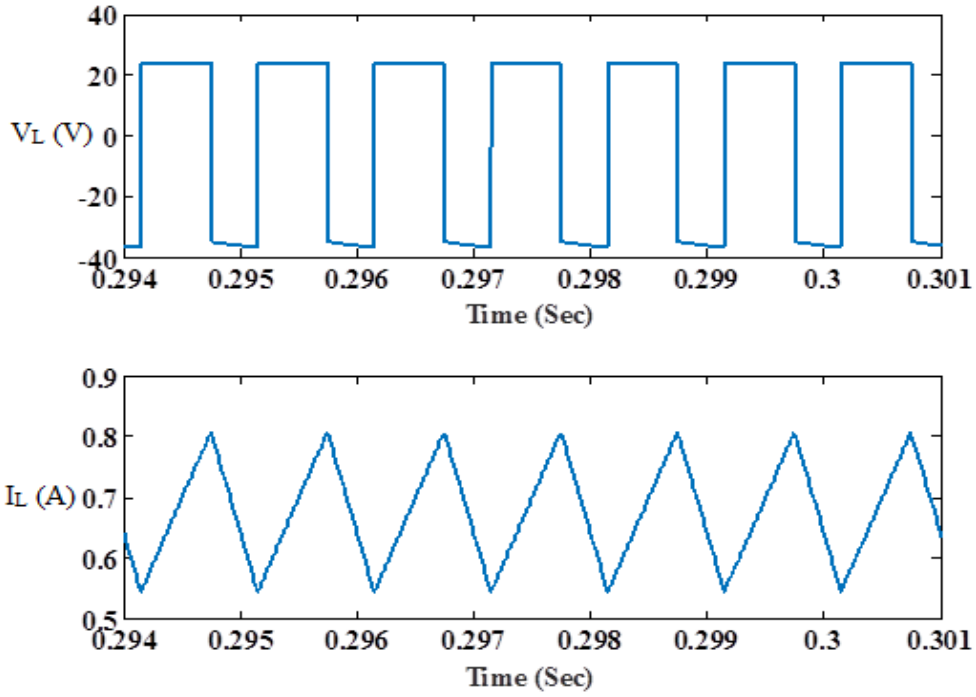
40
20
0
-20
-40
VL (V)
0.294
0.295
0.296
0.297
0.298
0.299
0.3
0.301
Time (Sec)
0.9
0.8
0.7
0.6
0.5
IL (A)
0.294
0.295
0.296
0.297
0.298
0.299
0.3
0.301
Time (Sec)

(b)

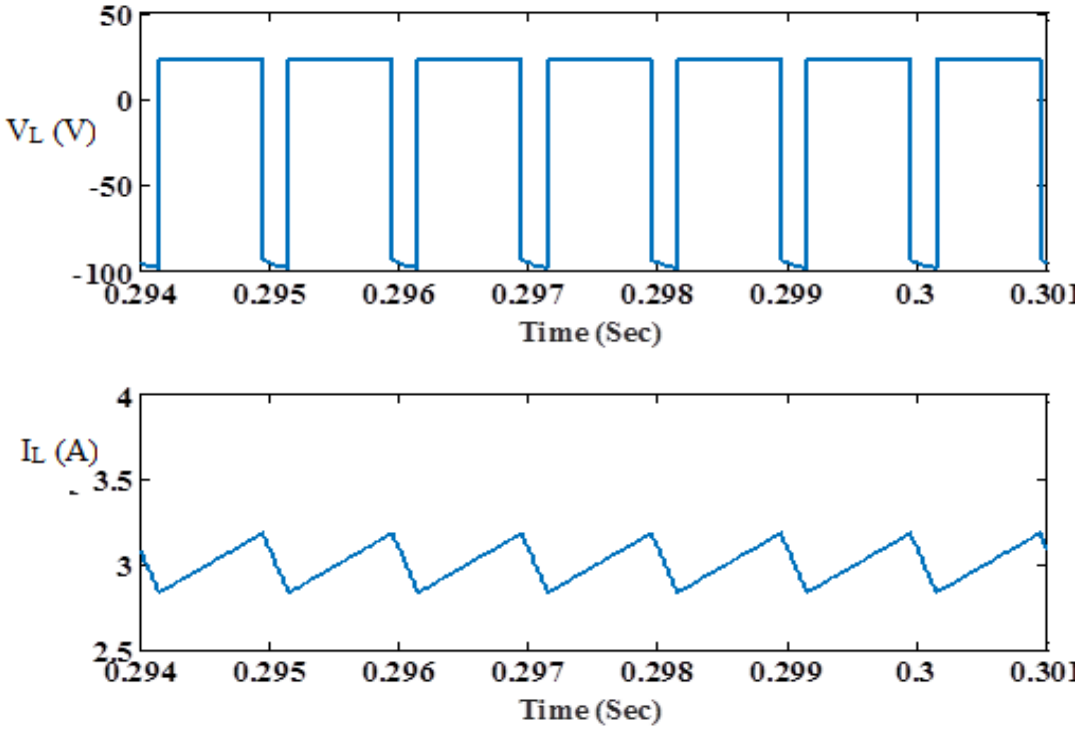

(c)

Fig. (3.4) Performance of inductor voltage and current at different duty ratios (a) D=0.3, (b) D=0.6 and (c) D=0.8

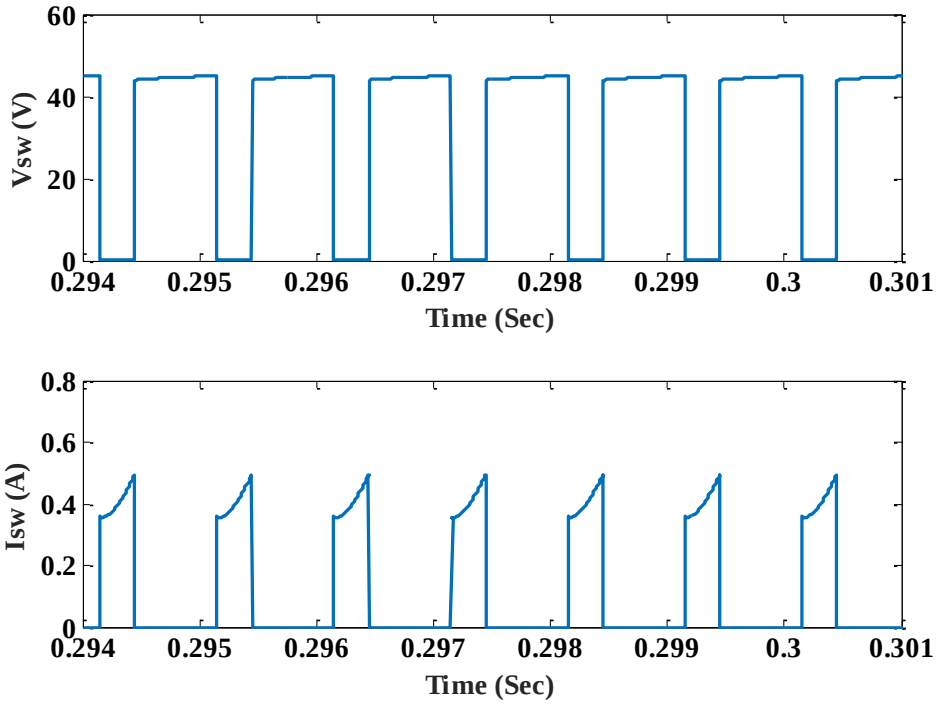

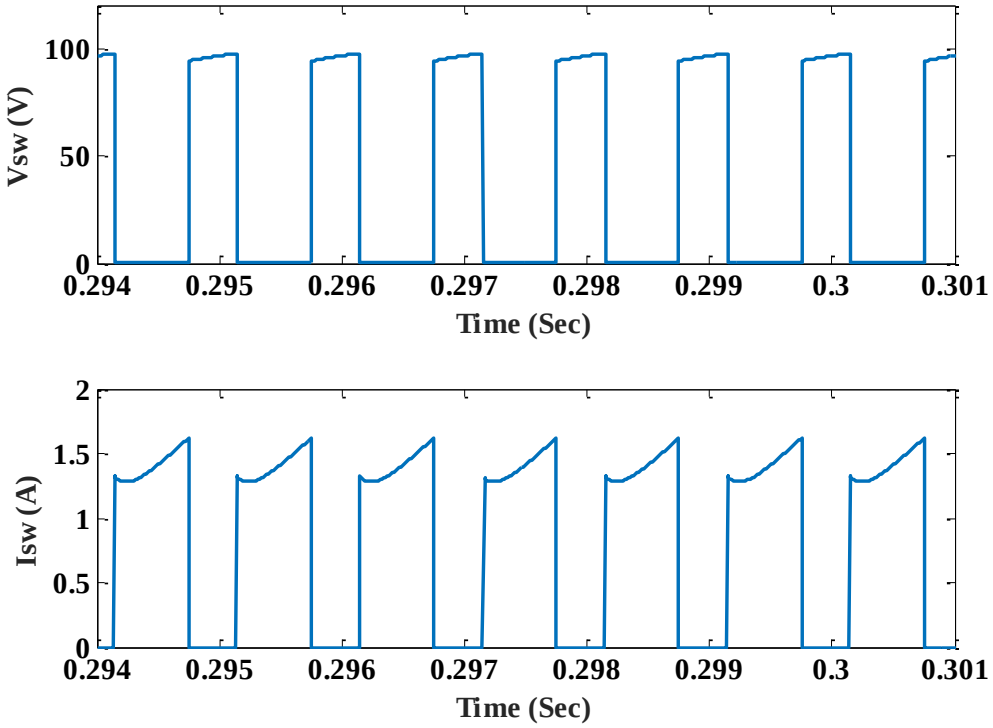

(b)

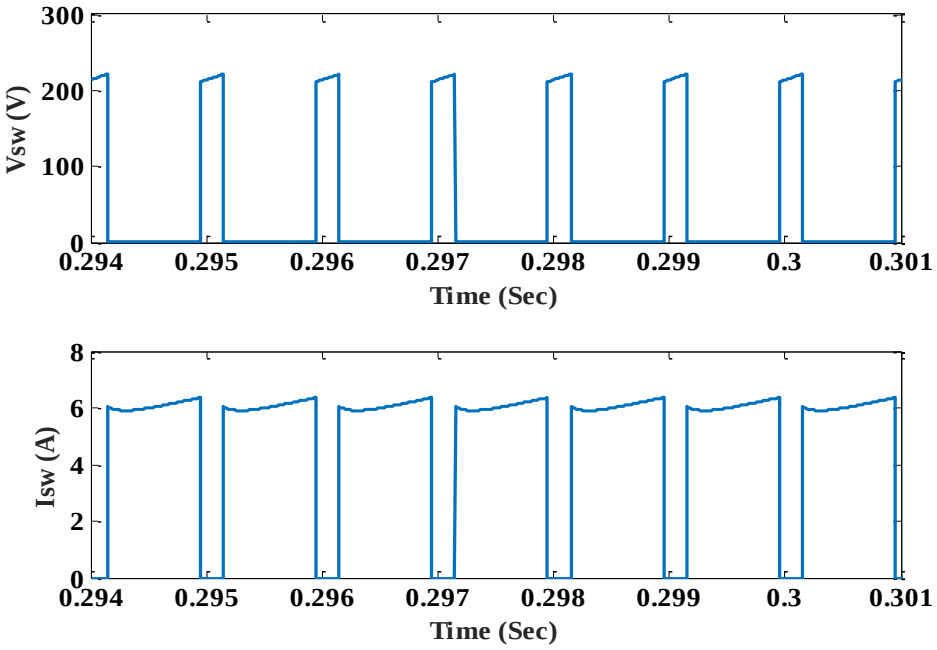

(c)

Fig. (3.5) Performance of switch voltage and current at different duty ratios (a) D = 0.3, (b) D = 0.6 and (c) D = 0.8

CHAPTER (3)
PERFORMANCE EVALUATION OF HIGH GAIN DC/DC CONVERTER

3.3 Simulation Results in DCM

In this section the simulation results of the converter will be introduced at three states for duty ratio at D=0.3, 0.5 and 0.6. to confirm the theatrical analysis with parameters as in Table (3.1). The simulation results implemented by using MATLAB/SIMULINK program. The waveforms of the output voltage, output current, input voltage, inductor voltage and current and switch voltage and its current were studied for the proposed topology at different duty cycle.

3.3.1 Simulation results at different duty ratios D = 0.3, D = 0.5 and D = 0.6

The converter here is tested at different duty ratios in terms of output voltage and current, input current, inductor voltage and current and switch voltage.

For figures (3.6.a), (3.6.b) and (3.6.c) shows the waveforms of output and input voltage at D=0.3, 0.5 and 0.6 respectively. It's clear from Fig. (3.6.a) at the input voltage = 24 V the converter gives output 73 V this means the voltage gain is 3 that matched with voltage gain derivation. For Fig. (3.6.b) and (3.6.c) at D=0.5 the output voltage 118 V with gain 4.92 that corresponds to voltage gain equation. Also at D = 0.6 with Vin = 24 give the output equal 159 with gain ratio 6.62 that very close to the inferred value from the equation.

Figures (3.7.a), (3.7.b) and (3.7.c) show the output current waveforms at duty ratios 0.3, 0.5 and 0.6. the output current appear pure DC with few ripple in permissible limit according to IEEE standard. Figf (3.8.a), (3.8.b) and (3.8.c) show the waveform of input current, it's clear from figure the current is discontinuous this achieve converter operation in DCM at D = 0.3, 0.5 and 0.6. And the duration of discontinuity is reduce whenever duty ratio increase in which after D = 0.6 the converter turn into CCM.

Figures (3.9.a), (3.9.b) and (3.9.c) shows the waveforms of inductor voltage and current at D = 0.3, 0.5 and 0.6 respectively, where the inductor voltage and current of two inductors are the same so the figure is took only for one waveform for V_L and I_L. The Fig. appears that charging and discharging of inductor energy also, the zero voltage state for the inductor voltage as mentioned before in mode (3). Where the voltage spikes on the inductor are due to the ratio of di_L/dt is increased at on state and

then decreased at off state and therefore the voltage spikes decreased on the inductors. The inductor current also achieves the discontinuity as input current.

Figures (3.10.a), (3.10.b) and (3.10.c) shows the switch voltage and current at 30%, 50% and 60% of duty cycle, it's clear that stress on switch is equal the output voltage this improves the overall efficiency of the converter. For switch current also discontinuous as input and inductor current.

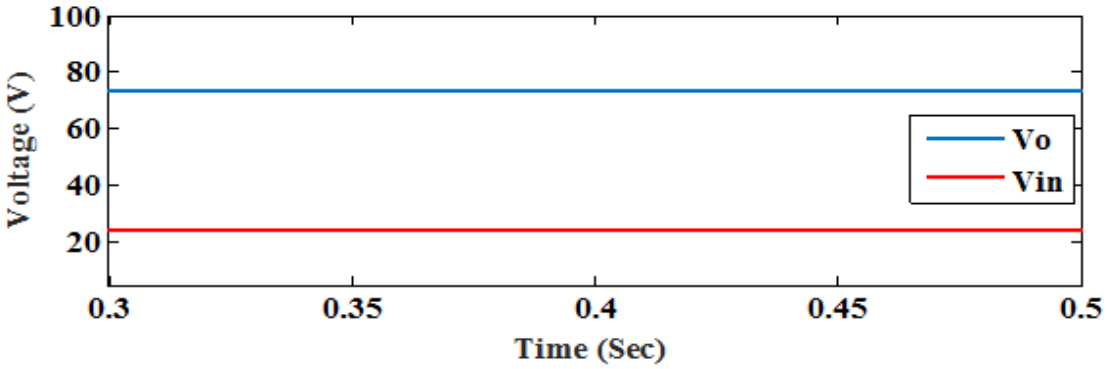

(a)

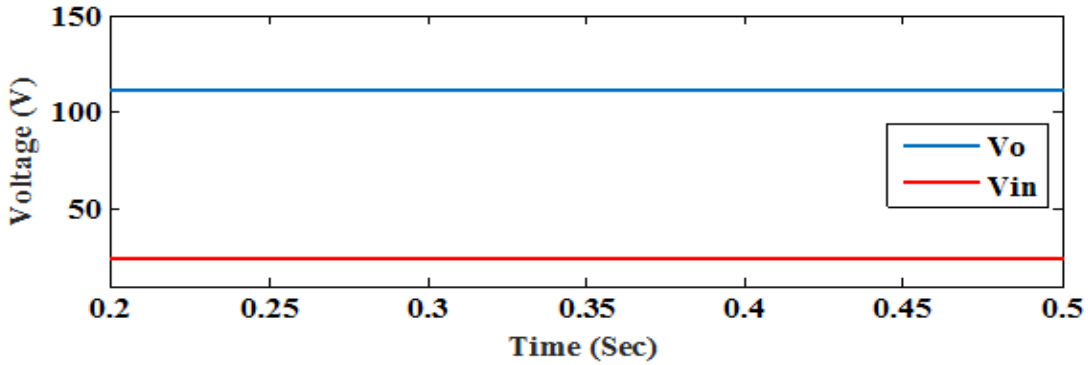

(b)

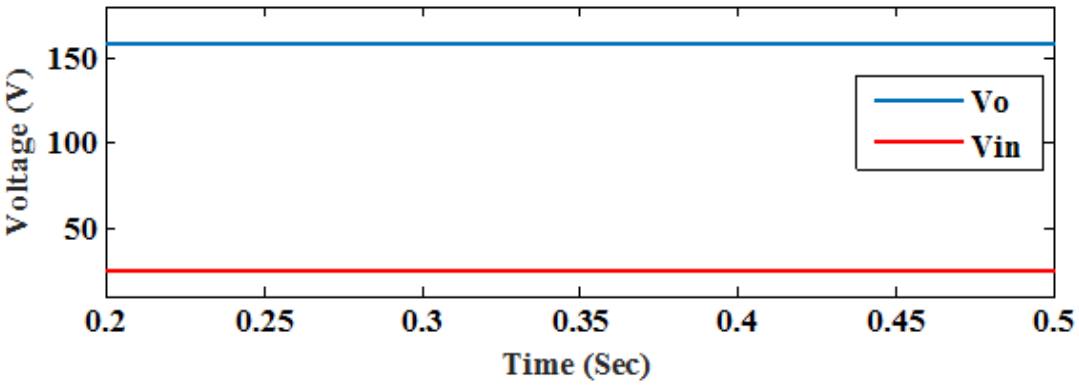

(c)

Fig. (3.6) Performance of output voltage and current at different duty ratios (a) D = 0.3, (b) D = 0.5 and (c) D = 0.6

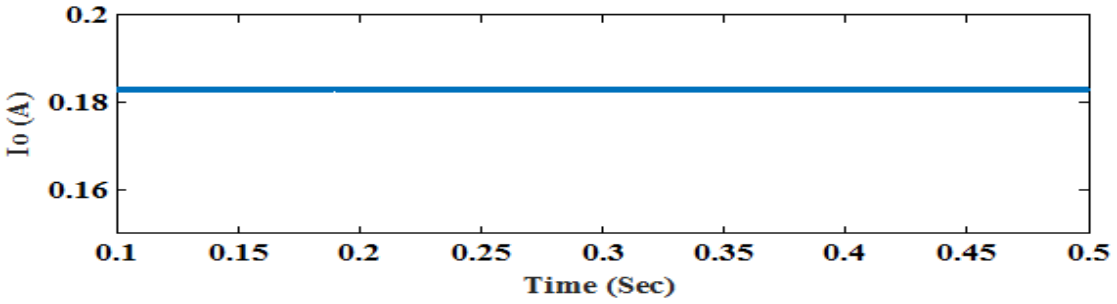

(a)

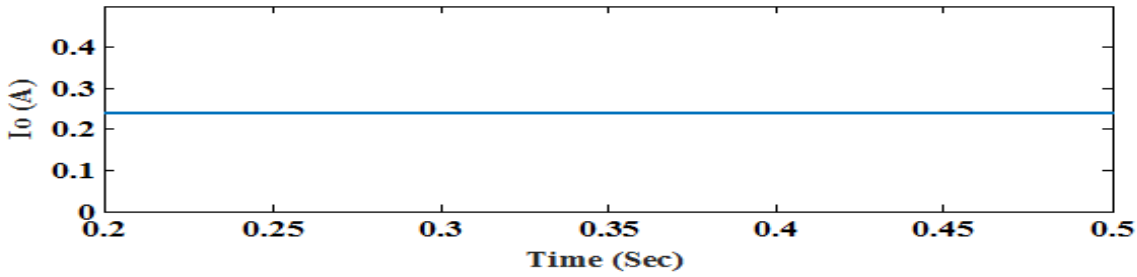

(b)

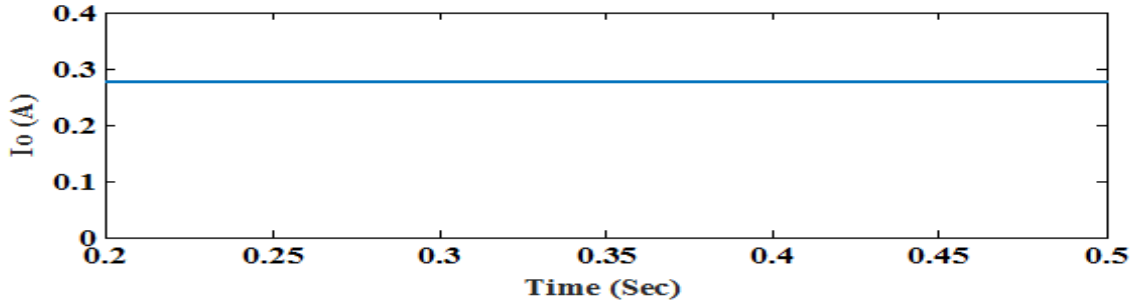

(c)

Fig. (3.7) Performance of output voltage and current at different duty ratios (a) D = 0.3, (b) D = 0.5 and (c) D = 0.6

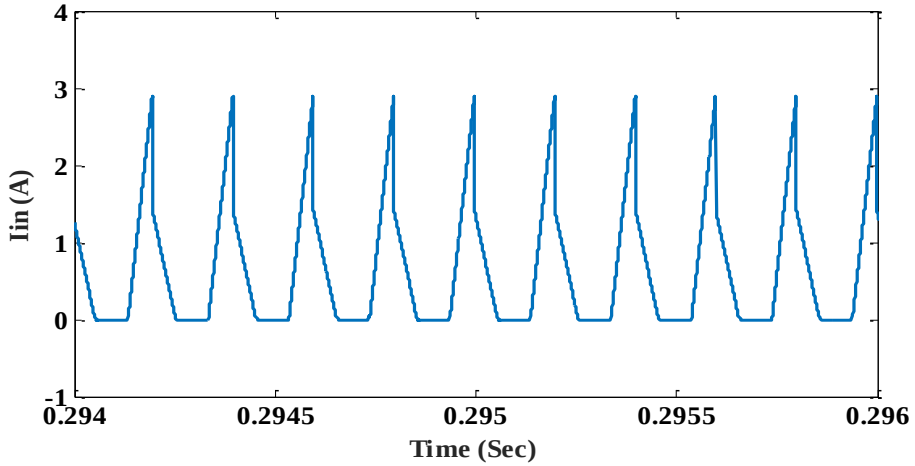

(a)

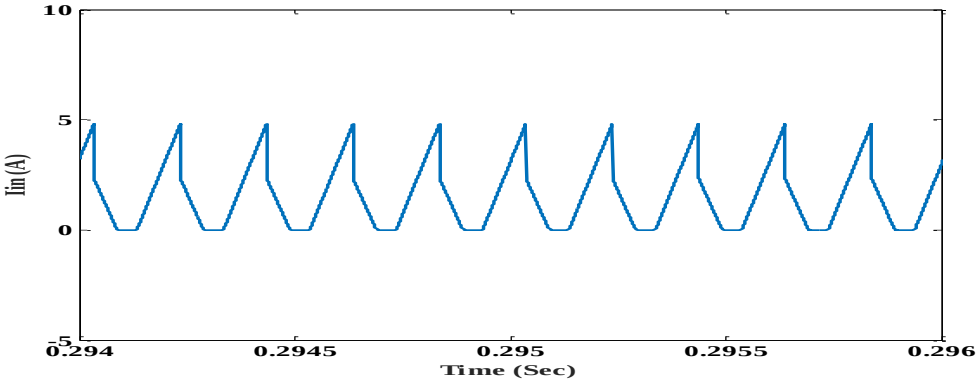

(b)

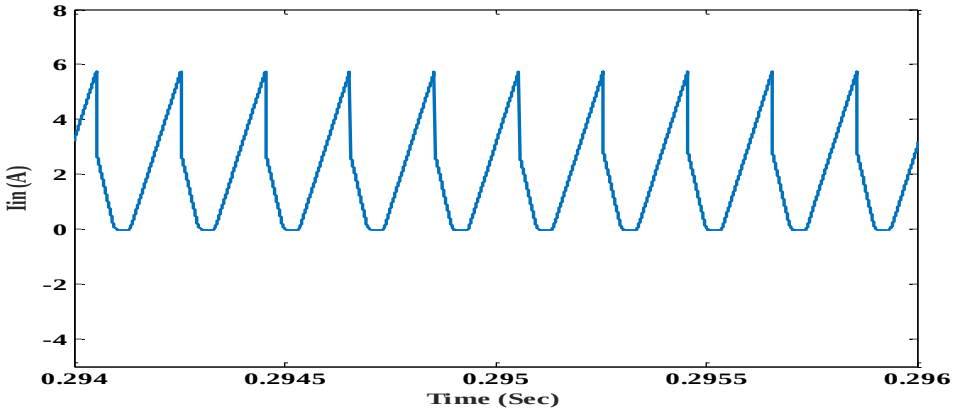

(c)

Fig. (3.8) Performance of input current at different duty ratios (a) D = 0.3, (b) D = 0.5 and (c) D = 0.6

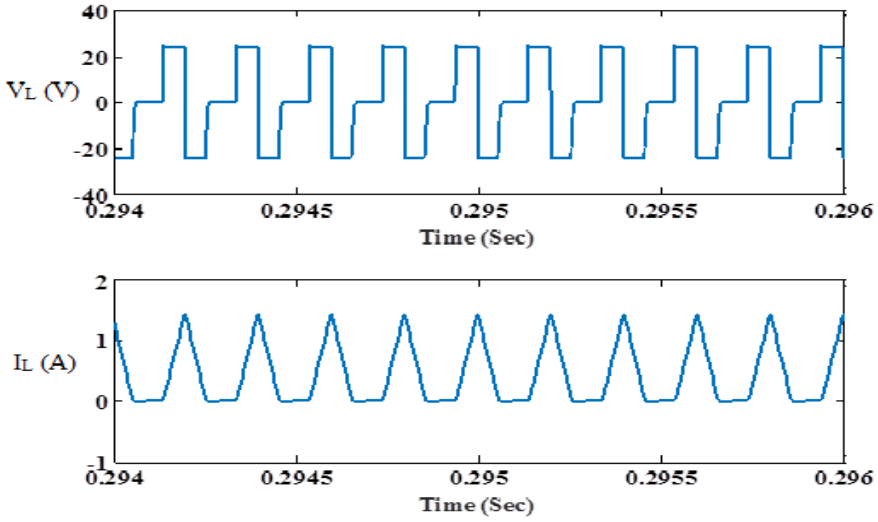

(a)

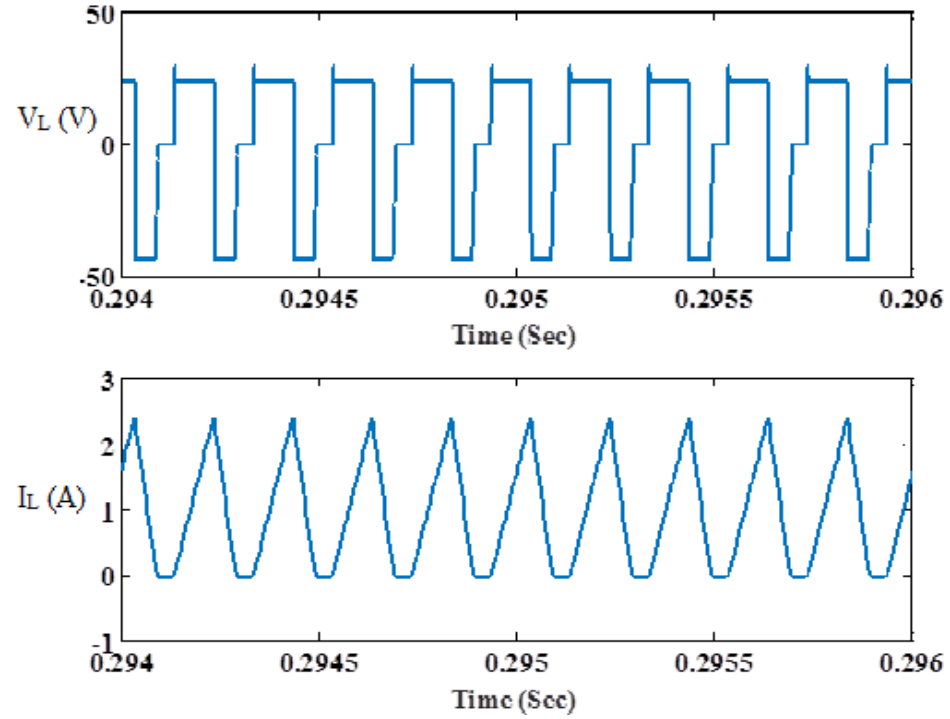

(b)

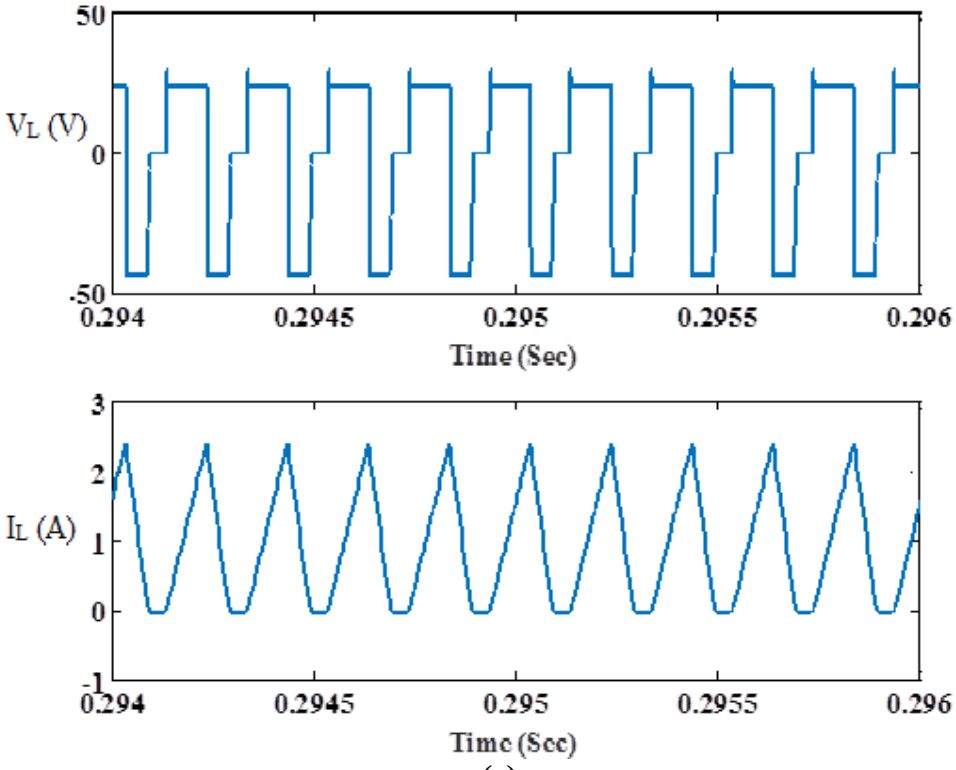

(c)

Fig. (3.9) Performance of inductor voltage and its current at different duty ratios (a) D = 0.3, (b) D = 0.5 and (c) D = 0.6

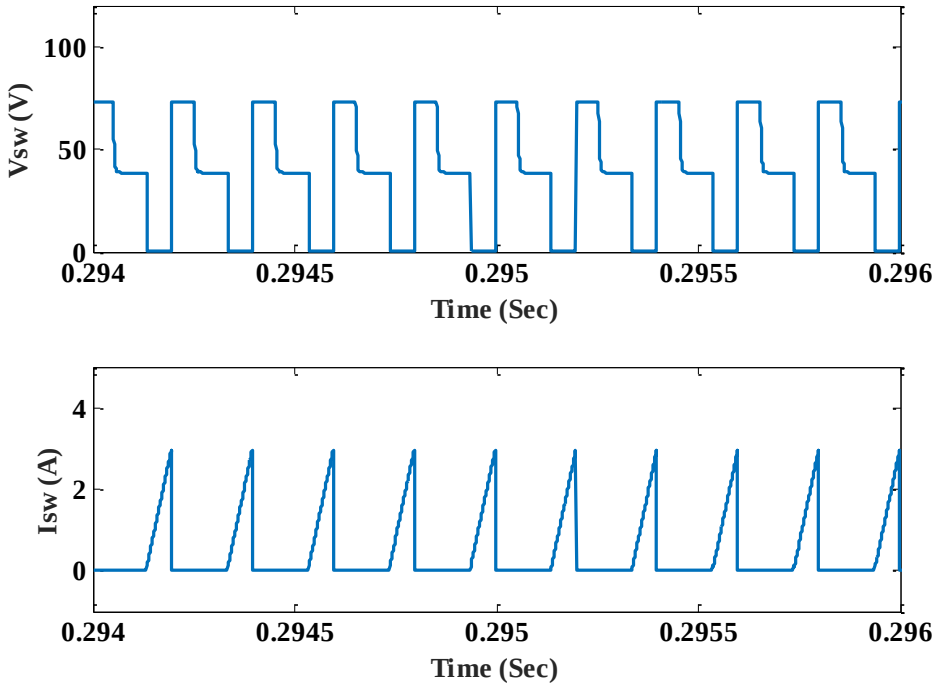
100
50
0
Vsw (V)
0.294
0.2945
0.295
0.2955
0.296
Time (Sec)
4
2
0
Isw (A)
0.294
0.2945
0.295
0.2955
0.296
Time (Sec)

(a)

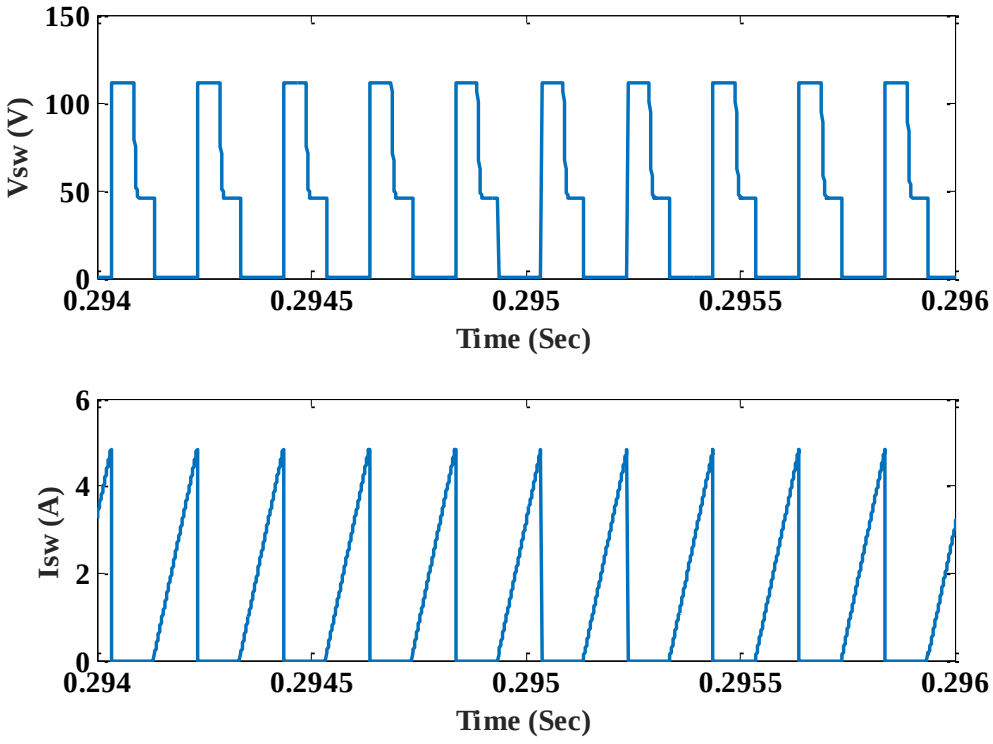
150
100
50
0
Vsw (V)
0.294
0.2945
0.295
0.2955
0.296
Time (Sec)
6
4
2
0
Isw (A)
0.294
0.2945
0.295
0.2955
0.296
Time (Sec)

(b)

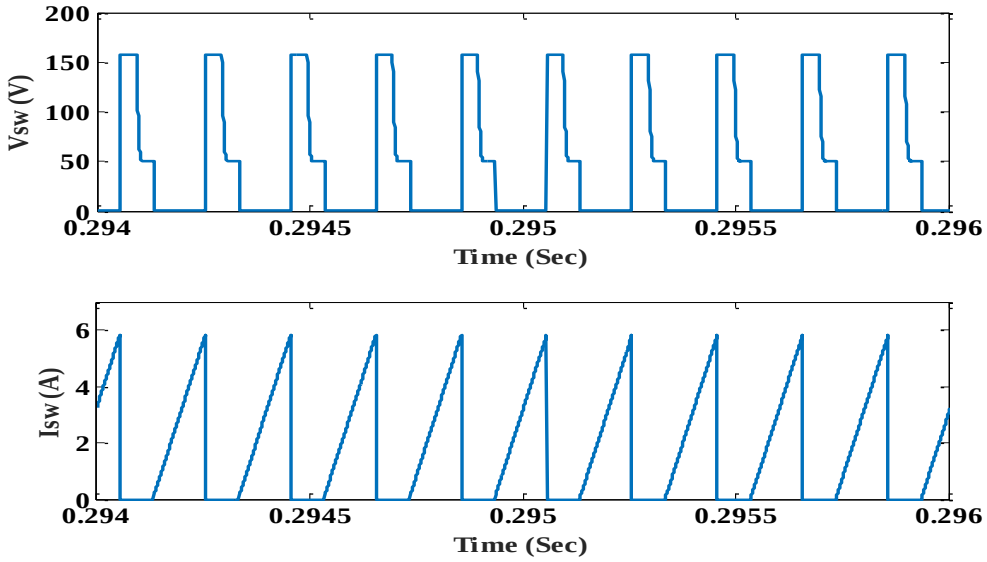

(c)

Fig. (3.10) Performance switch voltage and current at different duty ratios (a) D = 0.3, (b) D = 0.5 and (c) D = 0.6.

3.4 Simulation Results of Closed Loop Control at Static Load Performance

In this section the simulation results of closed loop control will be explained at static load with three states are of input change, load change and reference voltage change at parameters as shown in Table (3.2).

Table (3.2) Closed loop control parameters

Closed-loop Control	
Parameter	**Value**
Inductances (L_1, L_2)	10 mH
Capacitance (C_o)	330μF
Switching frequency(F_S)	1 K HZ
Static Load	
Proportional gain (K_P)	100
Integral gain (K_i)	200
Dynamic Load	
Proportional gain (K_P)	98.6
Integral gain (K_i)	215
Armature voltage	50V
Armature current	1A

3.4.1 Input voltage change

For closed loop control under input change, a simple PI controller is used. The parameters for the PI are *Kp* =100 and *Ki* = 200. The proposed converter tested for supply voltage change experimentally at L_1=L_2=10 mH and R_{load}=450Ω as in Table (3.2). By changing supply voltage from 35V to 22V at reference voltage 50V, the output voltage and output current will be constant as shown in Fig. (3.12) and (3.13).Fig. (3.11) shows the supply voltage that change decreasing from 35V to 22V.

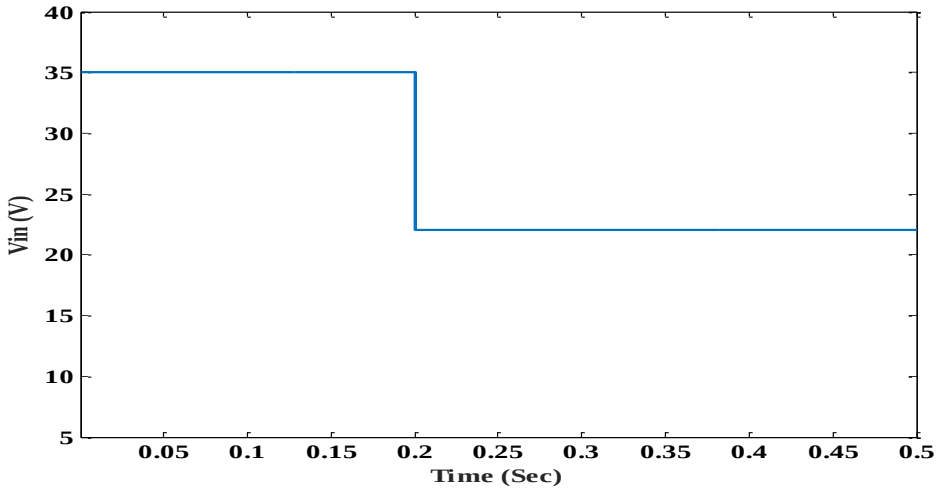

Fig. (3.11) Input voltage at input change

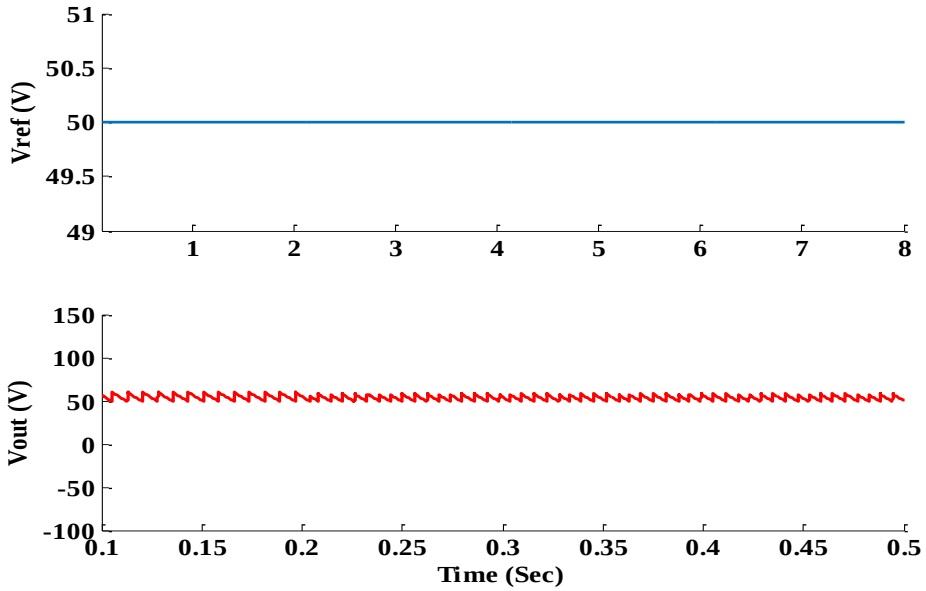

Fig. (3.12) Reference and output voltage under input change

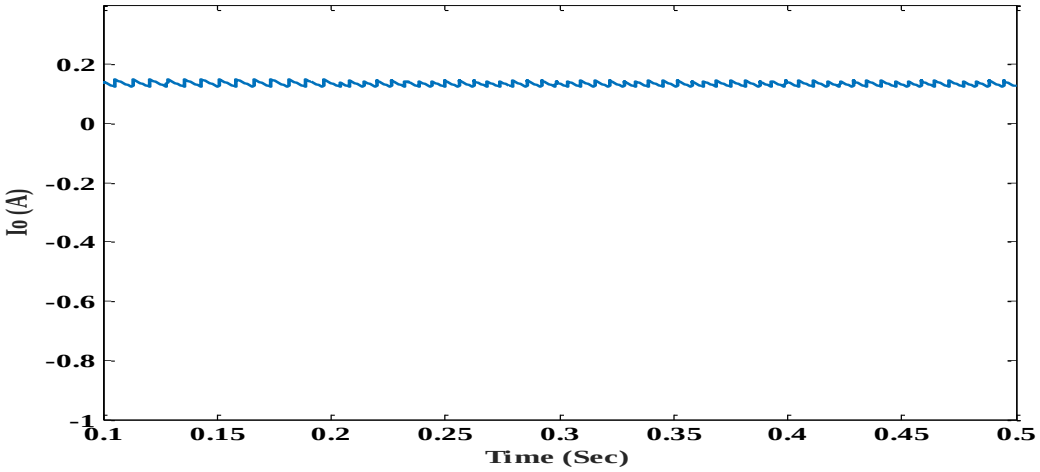

Fig. (3.13) Output current under input change

3.4.2 Load change

For closed loop control under load change, a simple PI controller is used. The waveforms of reference and output voltages, and load current during changing of the load are shown in Figf (3.14) and (3.15) respectively. With the reference voltage equal to 50 V, two load step changes are introduced. At the instant t = 0.21 sec, the load increased and at the instant t = 0.34sec, the load decreased again. And then the output voltage not changed.

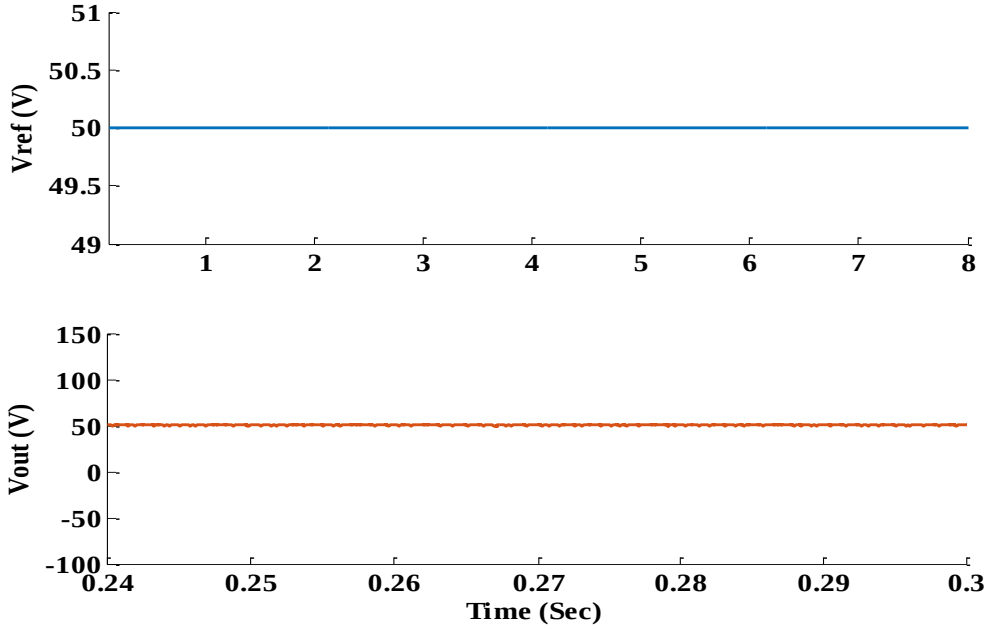

Fig. (3.14) Reference and output voltage under load change

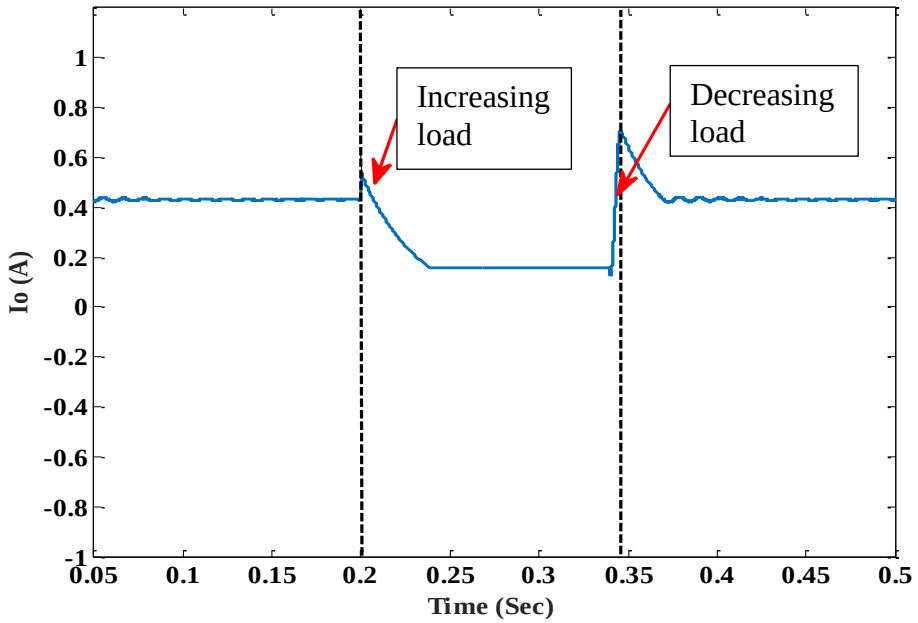

Fig. (3.15) Load current change

3.4.3 Reference voltage change

For closed loop control under load change, a simple PI controller is used. The waveforms of reference and output voltages during changing of the reference voltage are shown in Fig (3.16). The reference voltage will be change from 70V to 40V as in figure and the output voltage respond to this change.

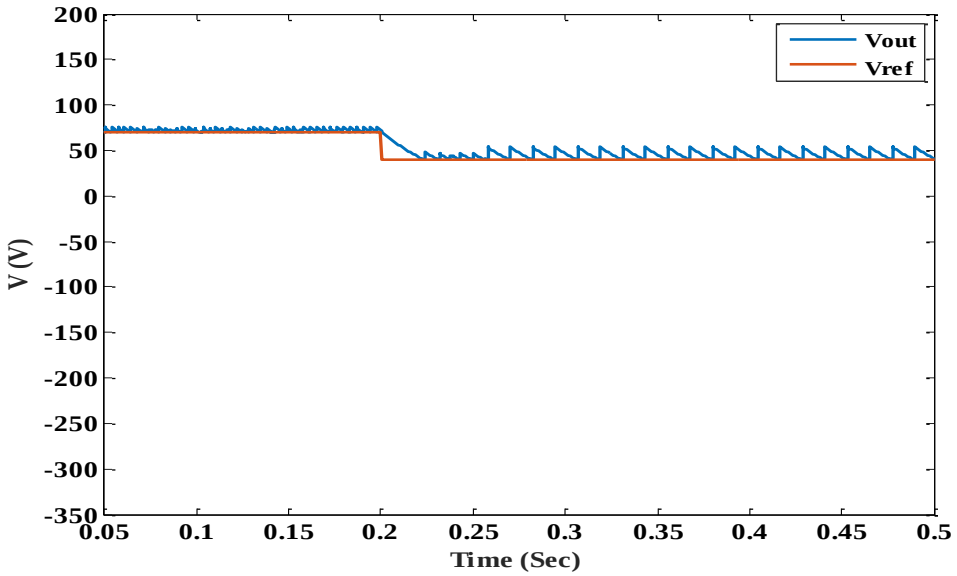

Fig. (3.16) Reference and output voltage under reference change

CHAPTER (4)
EXPERIMENTAL SETUP OF HIGH GAIN DC/DC CONVERTER

4.1 Summary

In this chapter the experimental set up has been built on to verify the effectiveness of the proposed DC/DC converter. Experimental results were investigated for open loop for CCM and DCM. And experimental results introduces for closed loop at static load by using resistive load to discuss input voltage change, load change and reference voltage change. The closed loop control results at dynamic load also explained by using separately excited DC motor as a load. To test the proposed converter at voltage control and speed control. Digital signal processor (DSP) controller board (DSP1104) was used to implement and test the proposed converter experimentally.

4.2 Experimental Setup Description for Open Loop Control System

The prototype of the proposed converter has been implemented and tested in the laboratory. To confirm the simulation results the converter, is validated experimentally and the results are taken into oscilloscope device. The proposed converter is tested at open loop with the same duty ratios as in simulation part with D=0.3, 0.6 and 0.8 for CCM and duty equal 0.3, 0.5 and 0.6 for DCM. This system is fully controlled in real time using DSP controller board (DSP1104).

The DSP board is placed in the PCI slot on the main board of PC, with uninterrupted communication through dual port memory. Fig. (4.1) shows the real view of the complete system in the laboratory. The experimental circuit parameters explained in Table (4.1) and the main parts of the system which labeled are listed in table (4.2). The following sections describe the main components of the system in detail.

CHAPTER (4)
EXPERMENTAL SETUP OF HIGH GAIN DC/DC CONVERTER

Table (4.1) Experimental circuit parameters

Open-loop Control (CCM/DCM)	
Parameter	**Value**
Input Voltage (V_{in})	24 V
Capacitance (C_o)	330 μF
Switching frequency (f_s)	1 KHz
CCM	
Load resistance	450Ω
Inductances (L_1, L_2)	25 mH
DCM	
Load resistance	450Ω
Inductances (L_1, L_2)	10 mH

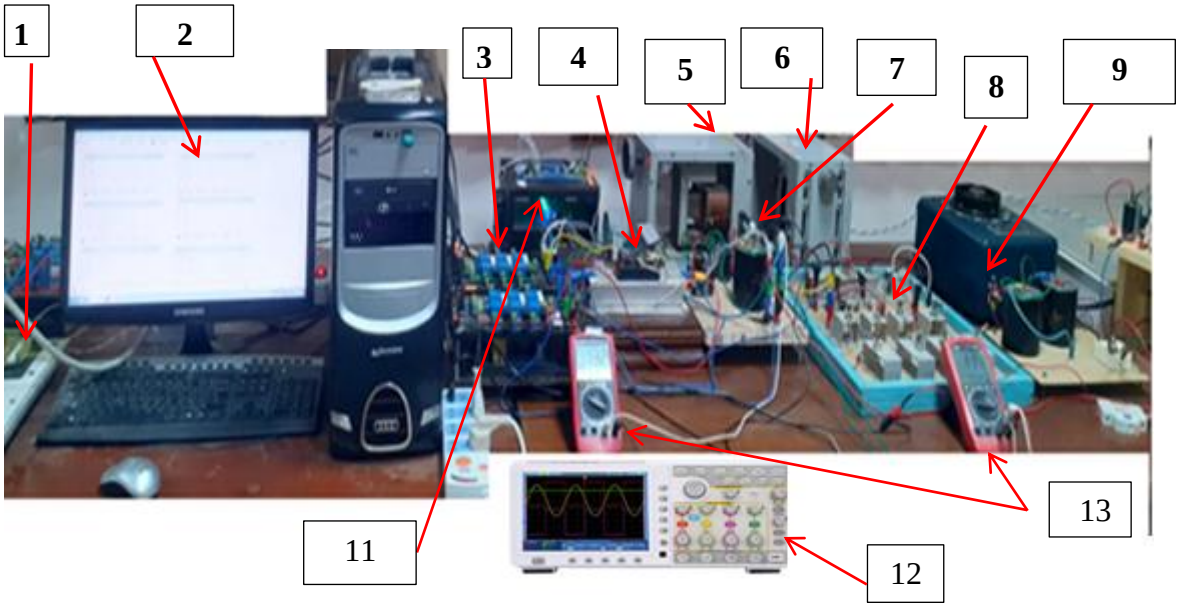

Fig. (4.1) Experimental setup for the proposed converter

Table (4.2) Components of experimental setup for the proposed converter

Label	Component	Label	Component
1	DSP platform	5	Switched Inductor (L_1)
2	Personal computer	6	Switched Inductor (L_2)
3	Voltage and current transducers	8	Diodes (D1, D2, D3 and Do)
4	Main switch (S_1)	9	Input DC source
7	Output capacitor	11	Drive circuit
12	Oscilloscope	13	Measurements

4.2.1 Main power circuit

A single phase transformer with rectifier circuit have been used to supply the system with a DC voltage at value 24. Isolated Gate Bipolar transistor (IGBT's) [type: CM100DY-24H] is used as a switch in the circuit. One IGBT are used in the proposed converter. The IGBT is controlled by signals generated by the controller board. More information about IGBT's is given in Appendix B.

4.2.2 Isolating and base driving circuit

For operating IGBT as a switch, the gate voltage must be appropriate so that the IGBT are into the saturation for low on-state voltage and cut-off for off-state. The main function of the base drive circuit is to generate pulse having proper voltage level for the IGBT. The outputs of the digital I/O subsystem of the DSP board (DSP1104) are pulses having magnitude of 5 V, which is not sufficient for the gate drive of IGBT. Moreover, isolation is needed between the controller board and the IGBT because the logic signal should be applied between the gate and the emitter. Thus a base drive circuit is essential for the IGBT, to provide an isolation and appropriate voltage to the IGBT.

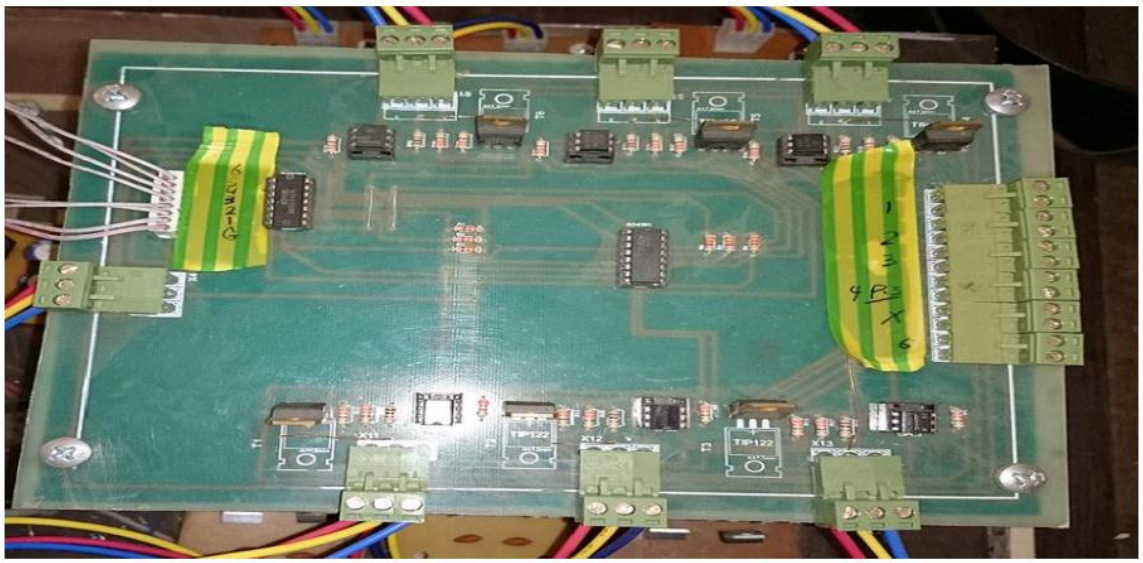

Fig (4.2) The real view of driving circuit

4.2.3 Voltage and current transducers

In order to obtain feedback current and voltage control from the power circuit, the load current and the output voltage should be measured on-line and supplied to the

controller via its A/D converters. For voltage transducer the actual voltage is measured using voltage sensor, which is a transducer for electronic measurement of DC and AC voltages with galvanic isolation between the primary circuit (high power) and the secondary circuit (electronic circuit). These transducers providing electrical isolation between the power circuit and the controller. Each current transducer was designed to measure a maximum of 25 A with a sensitivity of 100 mV/A. The output current signal of this sensor is converted to a voltage by connecting a resistor between output of the sensor and ground. Output voltage can be scaled by selecting various resistor values, and fed to the DSP board through the A/D converter. Fig. 4.2 presents a circuit of voltage transducer, current sensor circuit and real view of both current and voltage transducers (3-LA 25-NP and 3 LV 25-P).

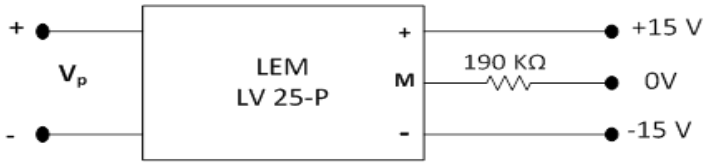

a

b

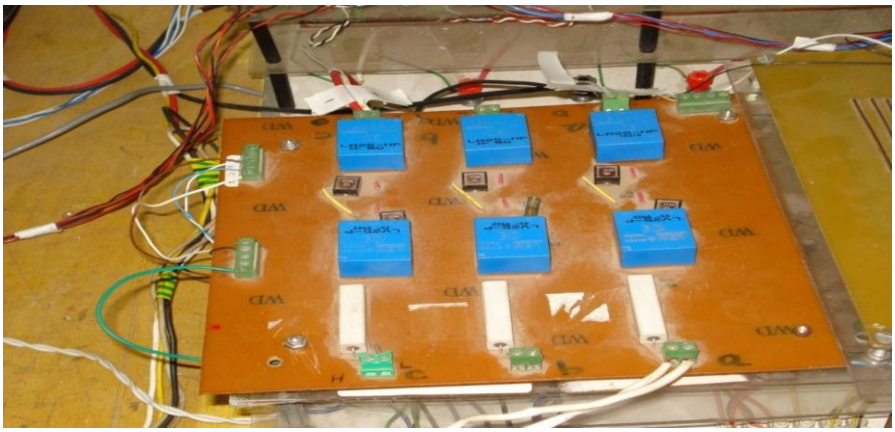

C

Fig. (4.3) a- The voltage transducer, b- Current transducer and c- Real view of current and voltage transducer

4.2.4 DSP1104 controller board

The DS1104 digital signal processing (DSP) controller board from dSPACE provides the interface between the controller and the system. DS1104 Controller Board is placed in the PCI slot on the main board of PC. The DS1104 contains a main processor and a slave Digital Signal Processor (DSP). The main processor is a 603 PowerPC, running at 250MHz with 32 MB of SDRAM, and the slave DSP is a TMS320F240, Texas Instrument floating-point DSP, 20MHz CPU clock. It contains four 16-bit analog-to-digital (A/D) channels, four 12-bit A/D channels, eight 16-bit digital-to-analog (D/A) channels, and other input/output interfaces. The provided Control Desk Developer along with "Matlab/Simulink" provides user-friendly interface to system control and observation.

There are three different ways to connect external devices to the DS1104. To access the I/O units of the master PPC and the slave DSP, connect external devices:

To the 100-pin I/O connector P1 of the DS1104, or

To the two 50-pin Sub-D connectors P1A and P1B, those are included in the DS1104 hardware package, or

To the optional connector panel CP1104 or the optional combined connector /LED panel CLP1104, which provides an additional array of LEDs indicating the states of the digital signals.

To make the interconnection of both input signals (current/ voltage transducers and incremental encoder), and output signals (pulse to IGBT switch) with the DS1104 board simple and easy, a connection port of DSP is extended through an interface board that is shown in Fig. (4.4).

We can arrange the current & voltage transducer circuit, the interface circuit (IR), the power supply (5, 15, 20) and the DSP port connection in a stand.

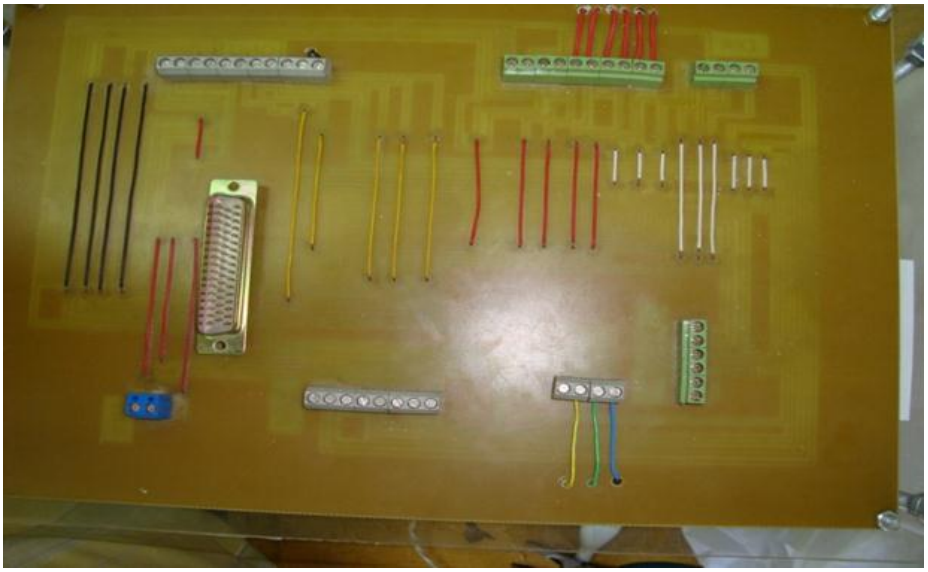

Fig. (4.4) DSP port connection.

4.3 Experimental Results for CCM

In this section the converter waveforms of input voltage, output voltage, input current, gate signal, switch voltage and inductor voltage and its current are explained to validate the converter at D = 0.3, 0.6 and 0.8 respectively. For Figf.(4.5.a), (4.5.b) and (4.5.c) show the waveforms of input and output voltage, where at input voltage =24V the converter given 45V with gain 1.875 at output for D = 0.3, and 94V for D = 0.6 in this case the voltage gain is 3.92 and at D = 0.8 the output voltage equal 200V and its gain equal 8.33 these values validated the simulation results at the same duty ratios.

Figures (4.6.a), (4.6.b) and (4.6.c) shows the waveform of input current of the converter at different duty ratios D = 0.3, 0.6 and 0.8 respectively. Its clears from figure the input current is continuous that ensure the converter works in CCM. The average value of the input current increase with increasing of duty ratio but this value within limit range for the input current.

Figures (4.7.a), (4.7.b) and (4.7.c) shows the experimental waveforms of gate signal and switch voltage the waveforms appear that at gate signal voltage with various duty ratios at D = 0.3, 0.6 and 0.8 the switch voltage is equal to the output voltage. This means the switch voltage stress is reduced also, the switching losses decreased and therefore the overall system efficiency increased.

Figures (4.8.a), (4.8.b) and (4.8.c) shows the waveforms of inductor voltage and current for one inductor only due to two inductors are identical in their voltage and currents. Its clears from figure the converter operate effectively in continuous current mode because the inductor current also continuous.

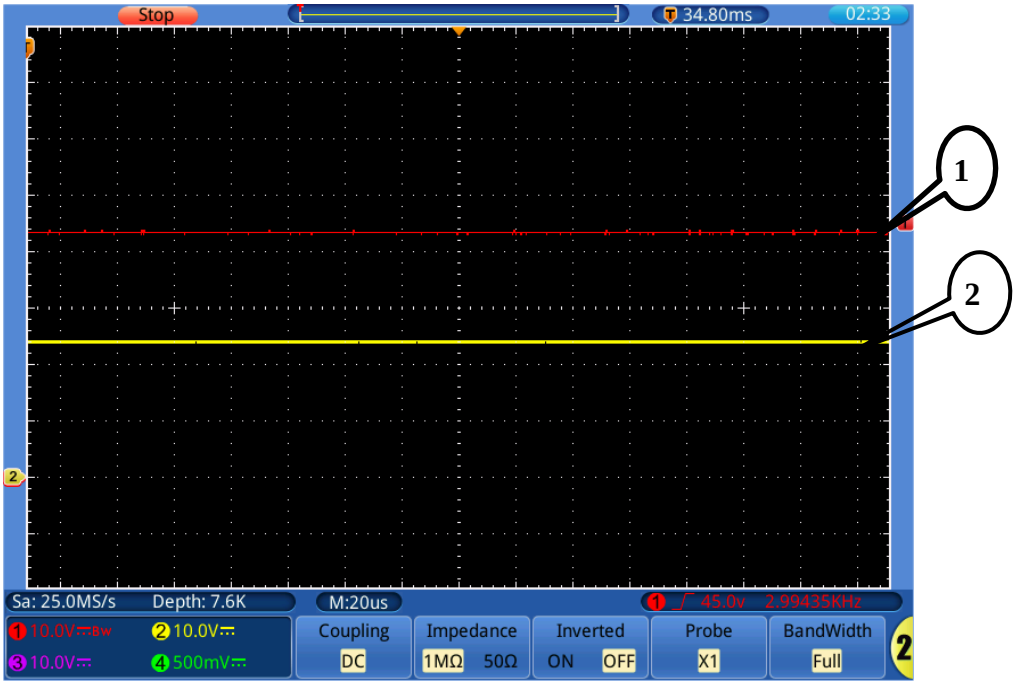

(a)

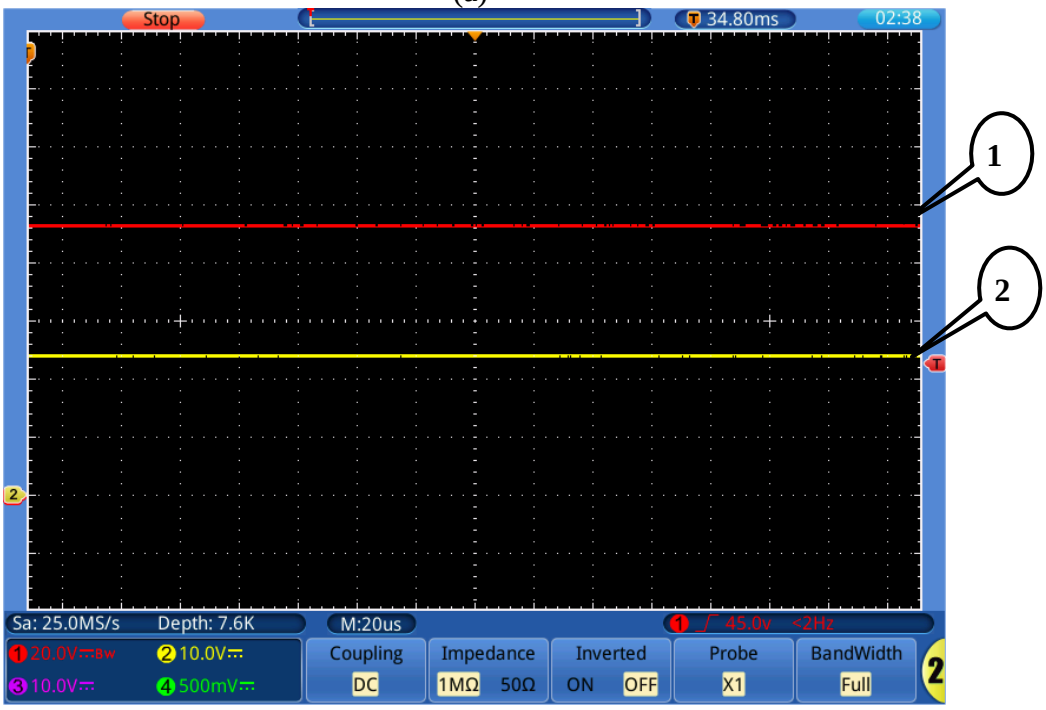

(b)

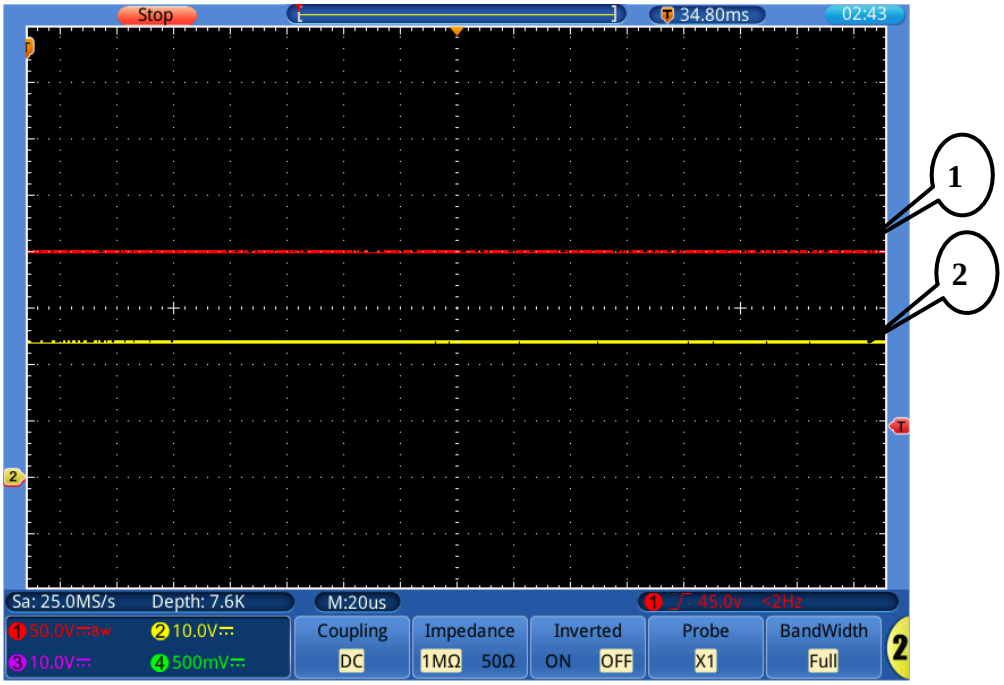

(C)

1- Output voltage 2- Input voltage

Fig. (4.5) Performance waveforms of output and input voltage at different duty ratios (a) D = 0.3, (b) D = 0.6 and (c) D = 0.8

(a)

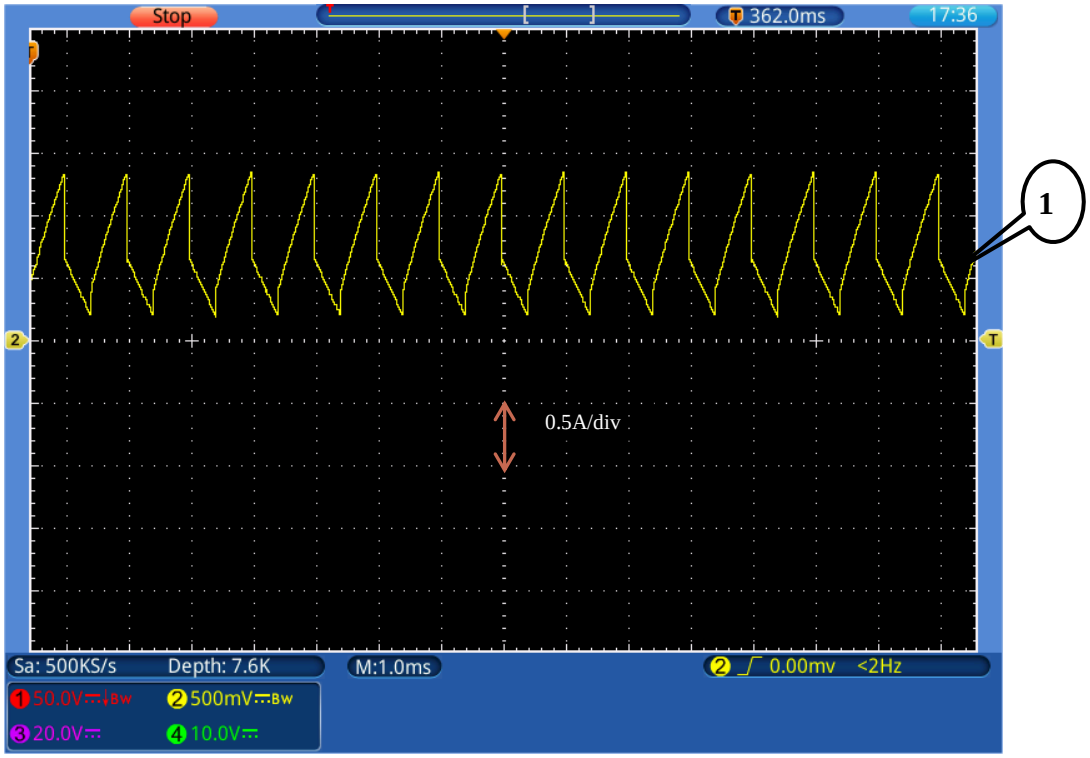

(b)

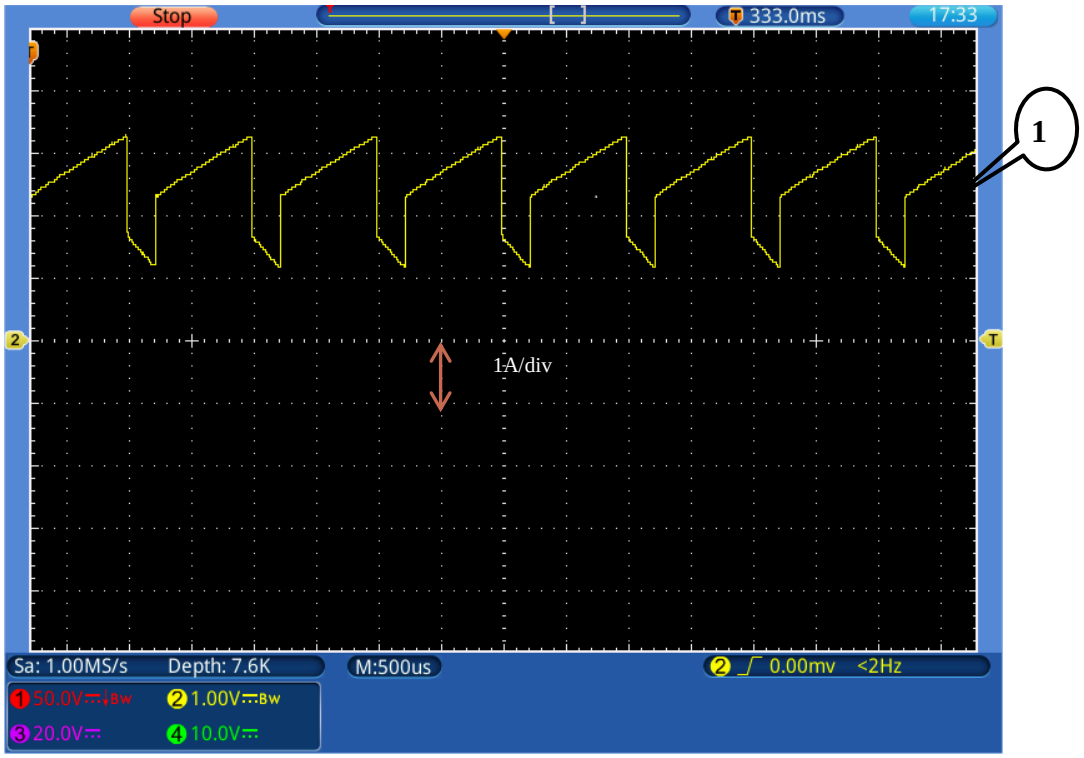

(c)

1- Input current

Fig. (4.6) Performance waveforms of input current at different duty ratios (a) D = 0.3, (b) D = 0.6 and (c)D = 0.8

CHAPTER (4)
EXPERMENTAL SETUP OF HIGH GAIN DC/DC CONVERTER

(a)

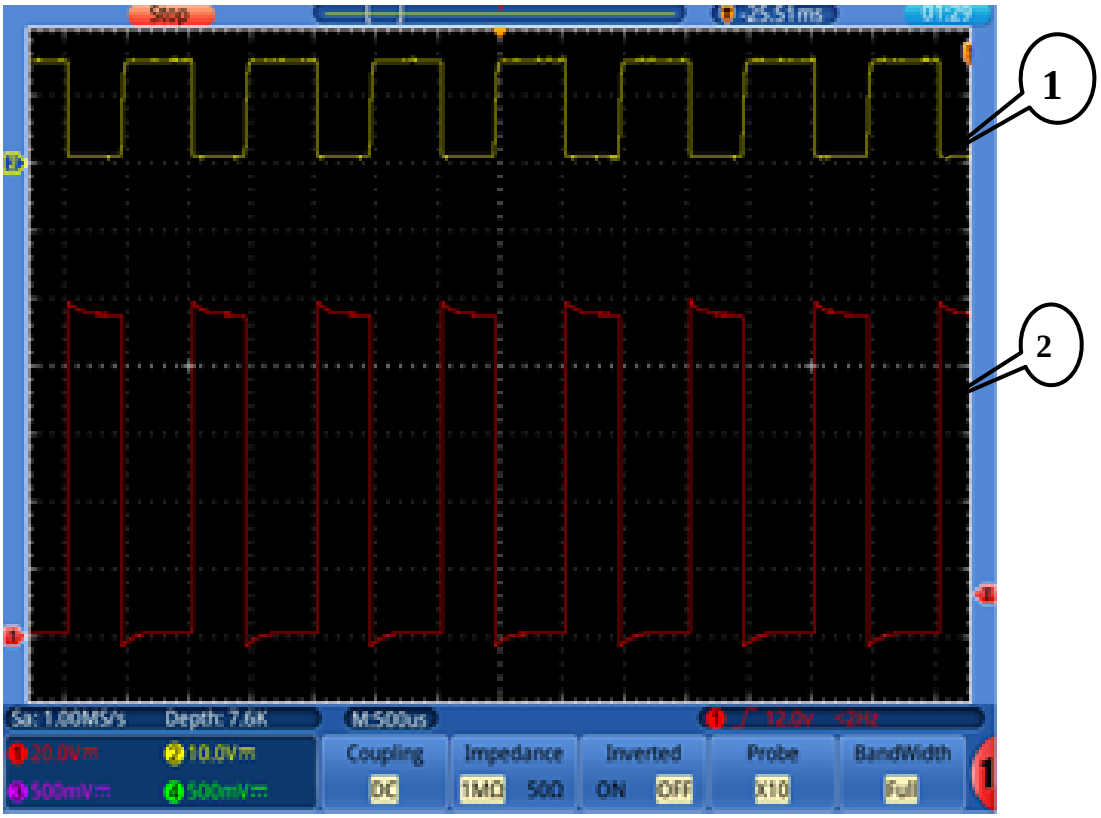

(b)

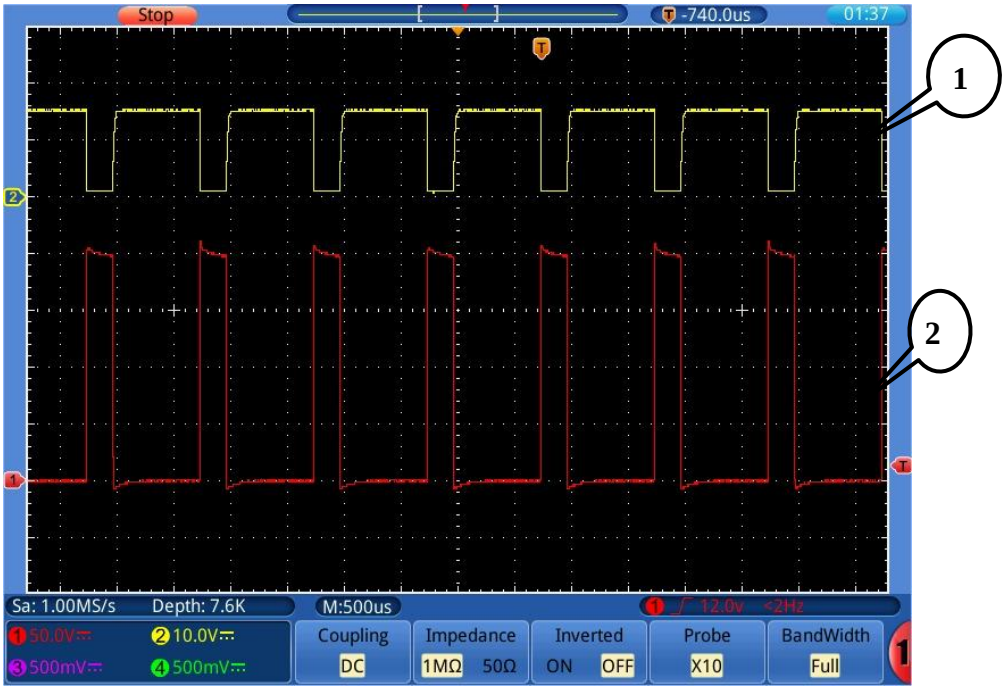

(c)

1- Gate signal pulse 2- Switch voltage

Fig. (4.7) Performance waveforms of gate signal, switch voltage at different duty ratios (a) D = 0.3, (b)D = 0.6 and (c) D = 0.8

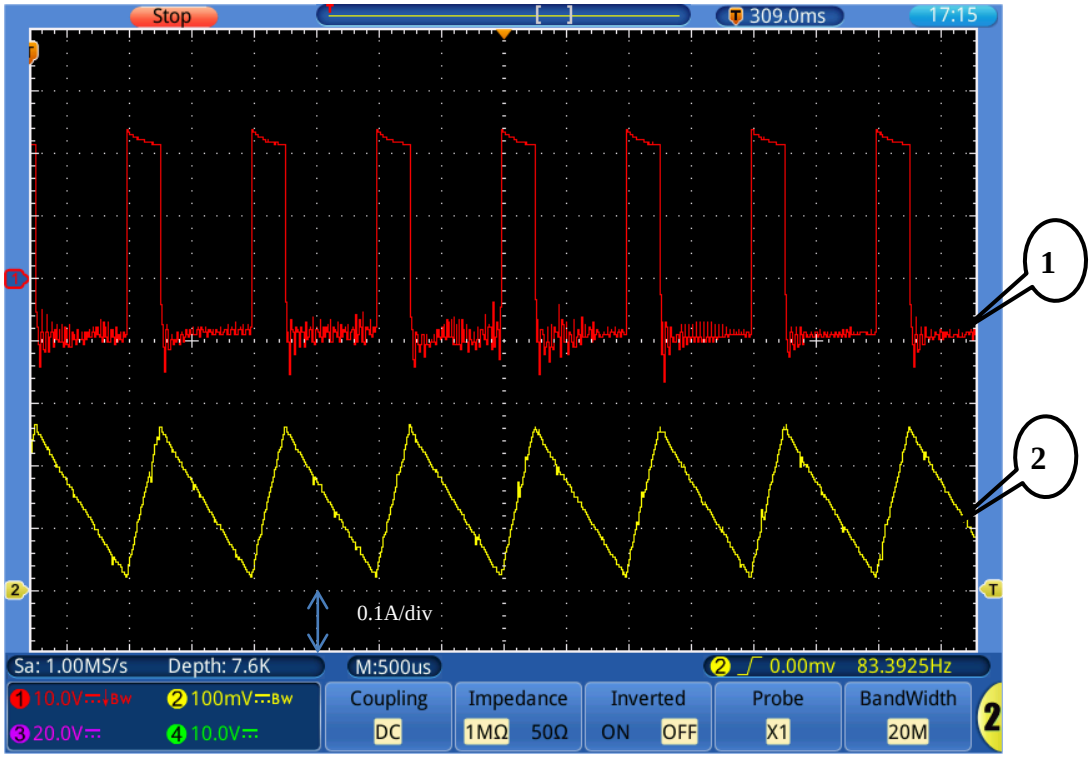

(a)

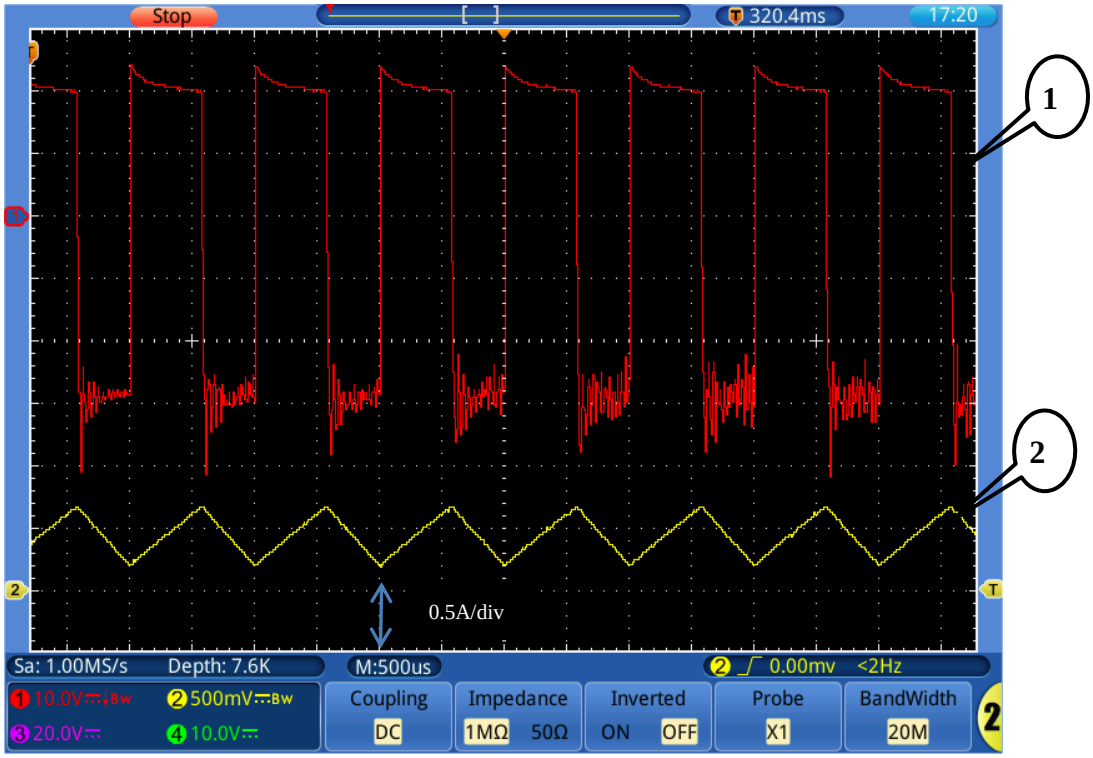

(b)

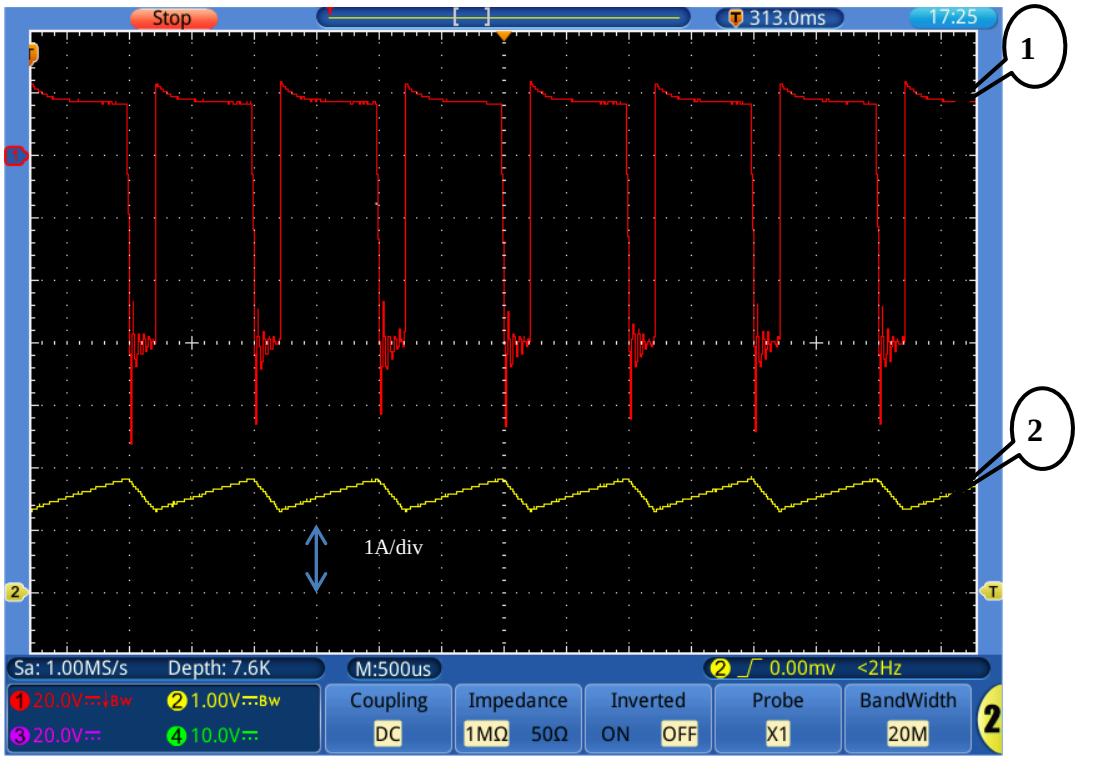

(c)

1- Inductor voltage 2- Inductor current

Fig. (4.8) Performance waveforms of inductor voltage and current at different duty ratios (a)D = 0.3, (b) D = 0.6 and (c) D = 0.8

4.4 Voltage Gain with Duty Ratio in CCM

The relation between voltage gain and duty ratio in continuous conduction mode at experimental and mathematical results is shown as below in figure (4.9). It's observed from figure there is a high convergence between two values for voltage gain (M) at each duty ratio (D) in CCM.

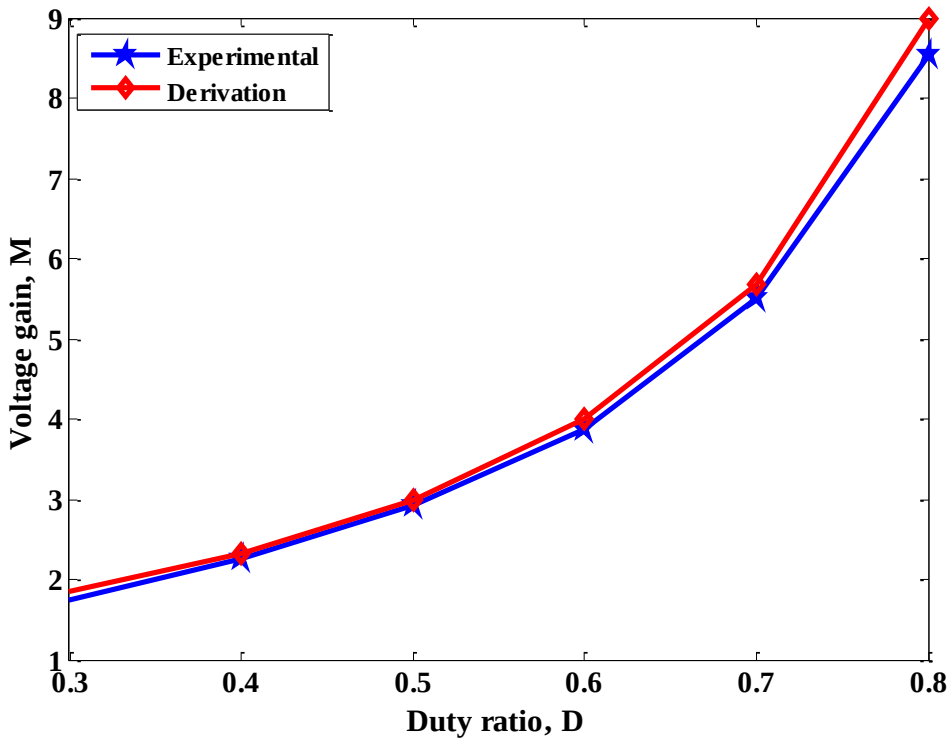

Fig. (4.9) Voltage gain versus duty ratio

4.5 Experimental Results at DCM Performance

To validate the simulation results that introduced in previous chapter for DCM, the converter practically tested at the same three cases of duty ratio in simulation section at D=0.3, 0.5, 0.6. To prove the simulation and experimental results very close to each other at any value for duty ratio.

4.5.1 Experimental results at different duty ratios

The experimental waveforms that introduces in this subsection at D=0.3, 0.5 and 0.6 are output and input voltage, input current, inductor voltage and its current and gate signal and switch voltage to analyze the converter in this case.

Figures (4.10.a), (4.10.b) and (4.10.c) shows the waveforms of output and input voltage, the figure clear that at input voltage 24V the converter gives output equal 66

V at D = 0.3 hence the voltage experimentally equal 2.75 and mathematically equal 2.71. And for D = 0.5 the output equal 116V where the experimentally gain is 4.83 and by equation equal 5. In case of D = 0.6 the output voltage is 155V then the voltage gain is 6.46 and mathematically is 7. These values mean presence a high convergence between two values.

Figures (4.11.a), (4.11.b) and (4.11.c) shows the waveform of input current at duty ratios D=0.3, 0.5 and 0.6 respectively. Where the figure explain the converter is suitable for DCM application because the input current is discontinuous.

Figures (4.12.a), (4.12.b) and (4.12.c) show the waveforms of inductor voltage and its current for D=0.3, 0.5 and 0.6. The inductor voltage and current in figure like the simulation waveform of inductor voltage which means the converter achieves the DCM in both simulation and experimental results. Due to two inductor are identical in their voltage and current so, one waveform is taken for them.

Figures (4.13.a), (4.13.b) and (4.13.c) show the gate signal and switch voltage. The figure explain at gate signal with duty ratio D=0.3, 0.5 and 0.6. The switch voltage stress is reduced that make the efficiency increased and switching losses decreased.

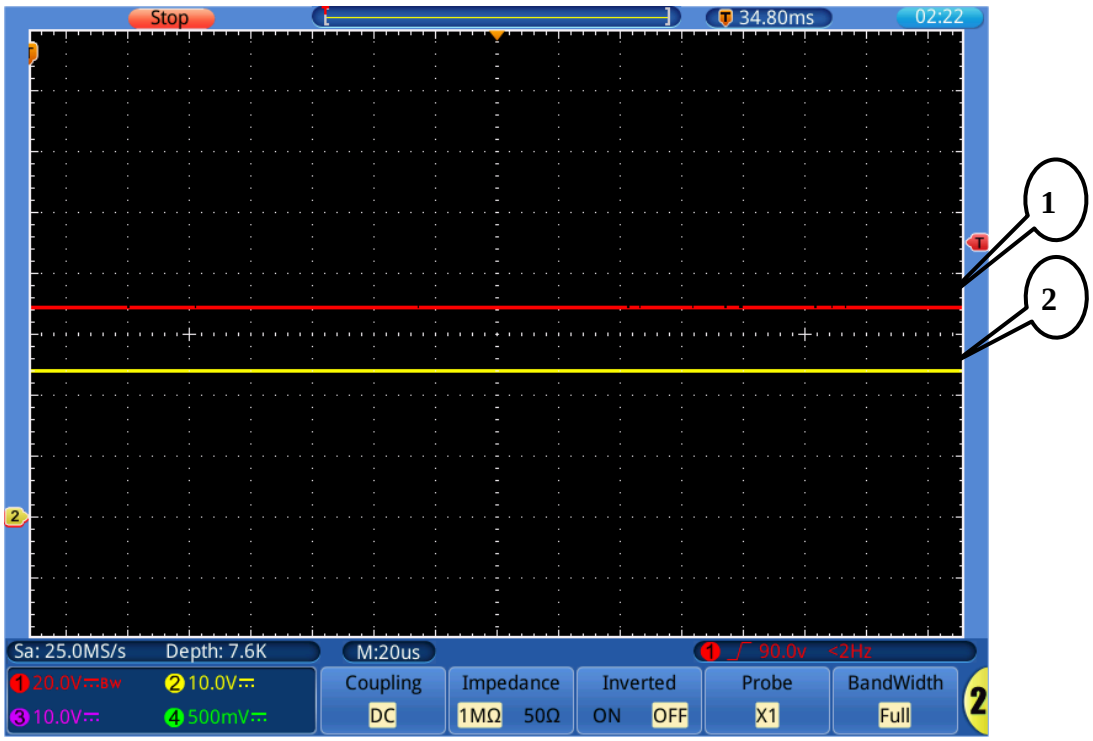

(a)

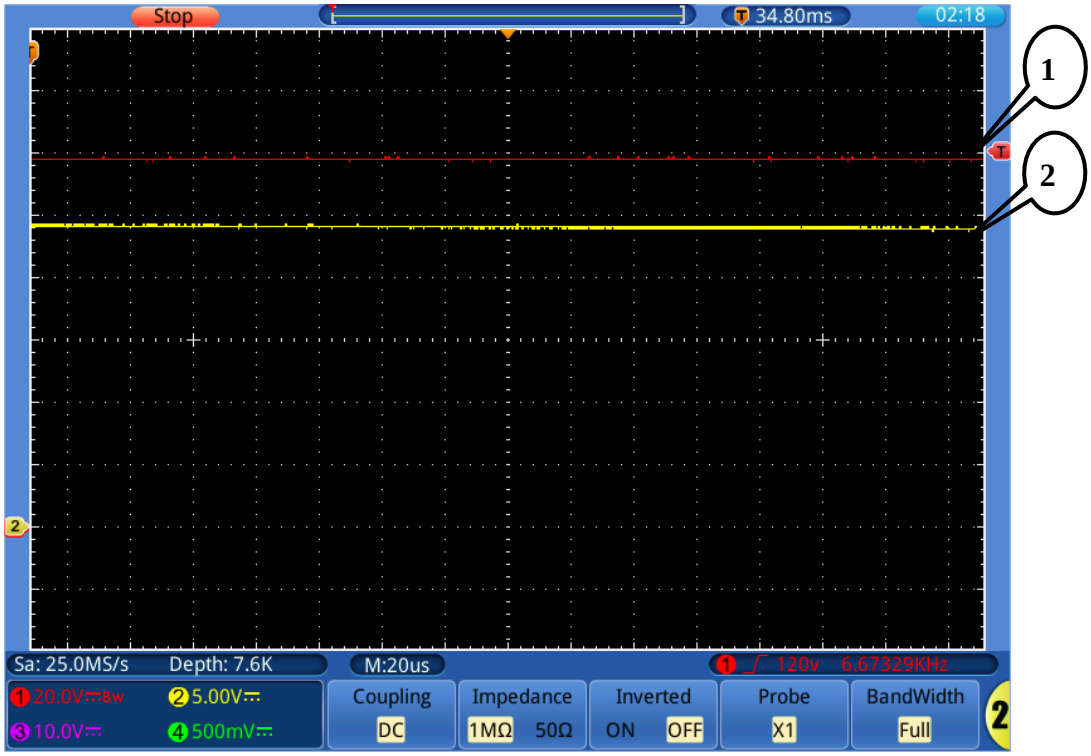

(b)

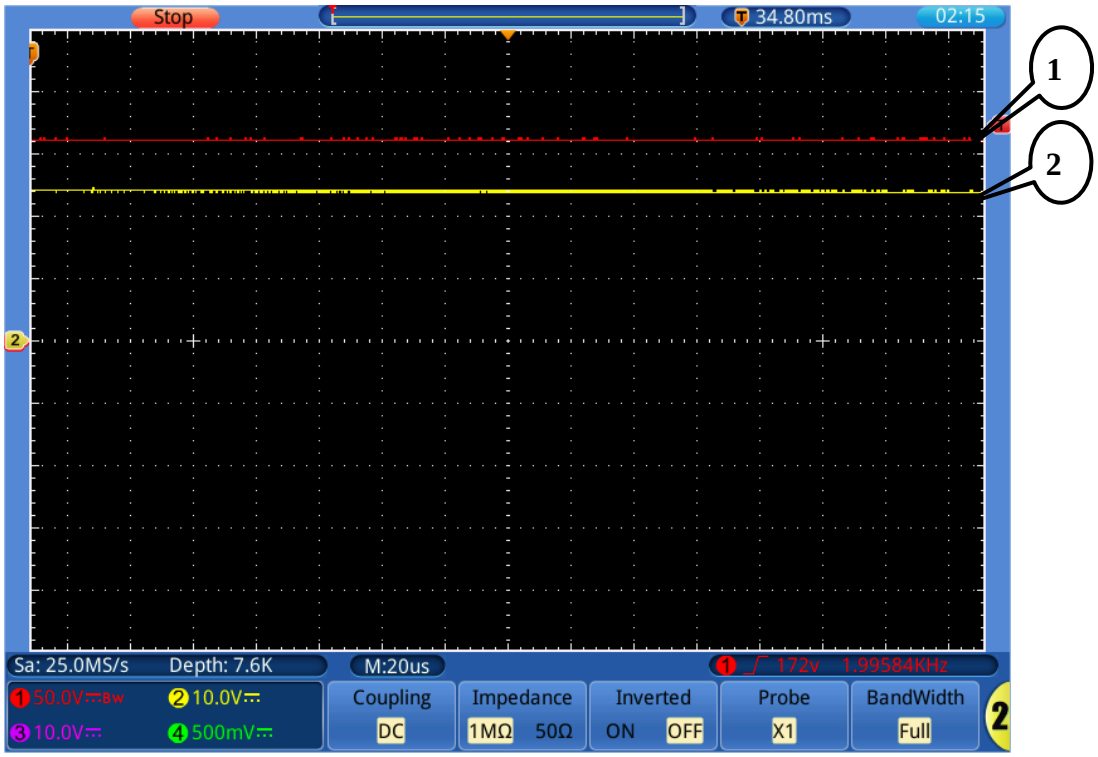

(c)

1- Output voltage 2- Input voltage

Fig. (4.10) Performance waveforms of output and input voltage at various duty ratios (a) D = 0.3, (b) D = 0.5 and (c) D = 0.6

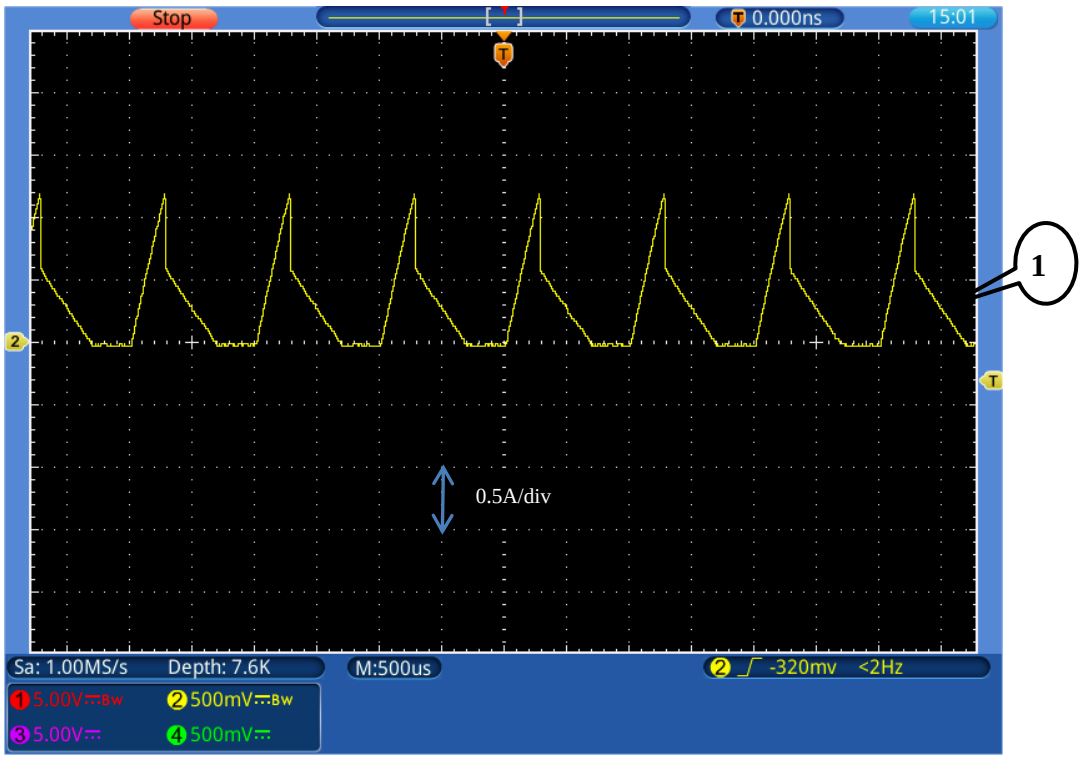
Stop
0.000ns
15:01
1
0.5A/div
Sa: 1.00MS/s
Depth: 7.6K
M:500us
-320mv
<2Hz
5.00V
500mV
5.00V
500mV

(a)

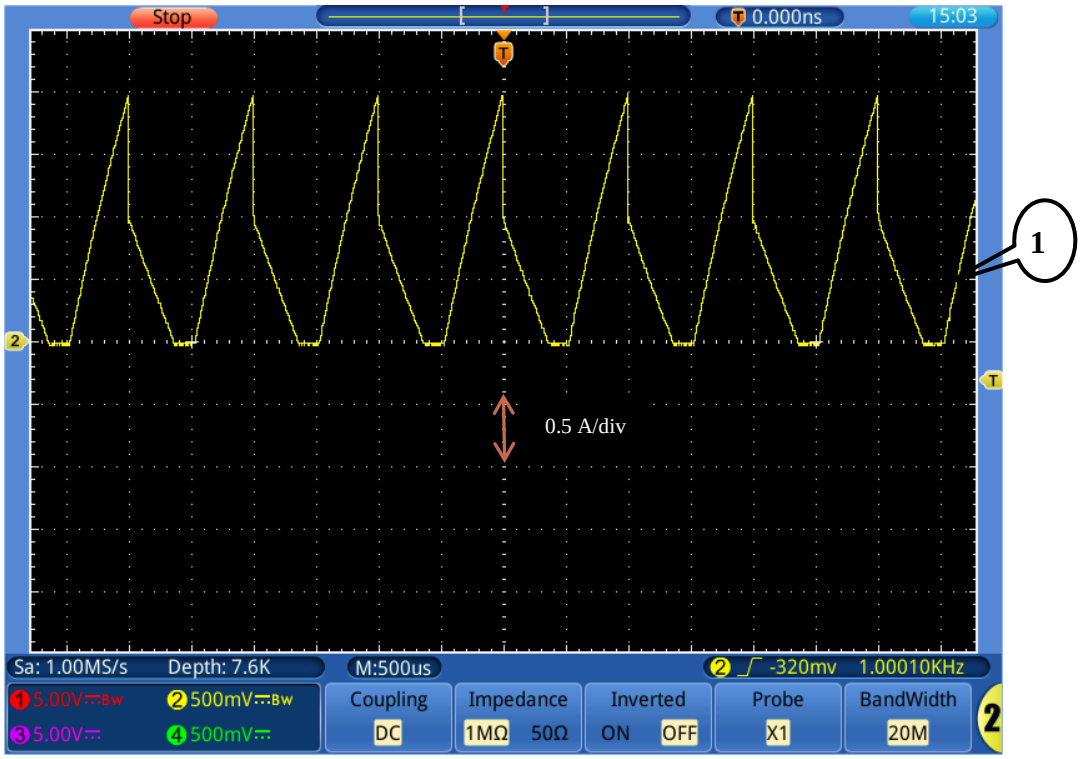
Stop
0.000ns
15:03
1
0.5 A/div
Sa: 1.00MS/s
Depth: 7.6K
M:500us
-320mv
1.00010KHz
5.00V
500mV
5.00V
500mV
Coupling
DC
Impedance
1MΩ
50Ω
Inverted
ON
OFF
Probe
X1
BandWidth
20M

(b)

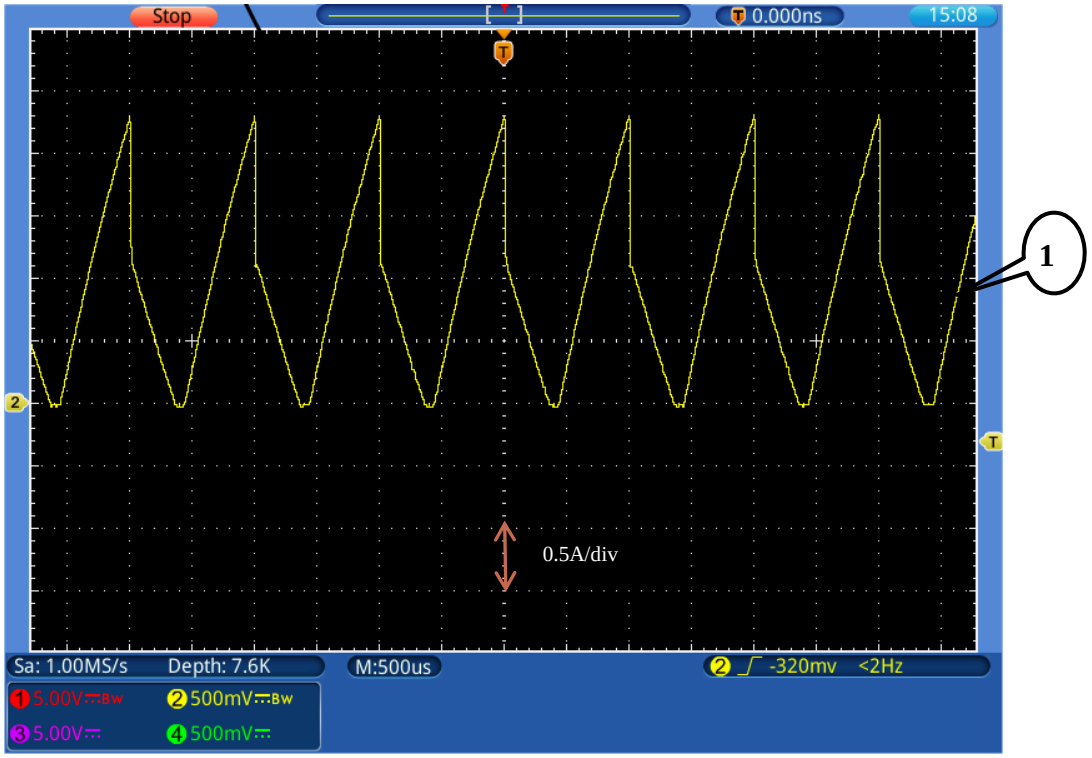

(c)
1- Input current
Fig. (4.11) Performance waveforms of input current at various duty ratios (a) D = 0.3, (b) D = 0.5 and (c) D = 0.6

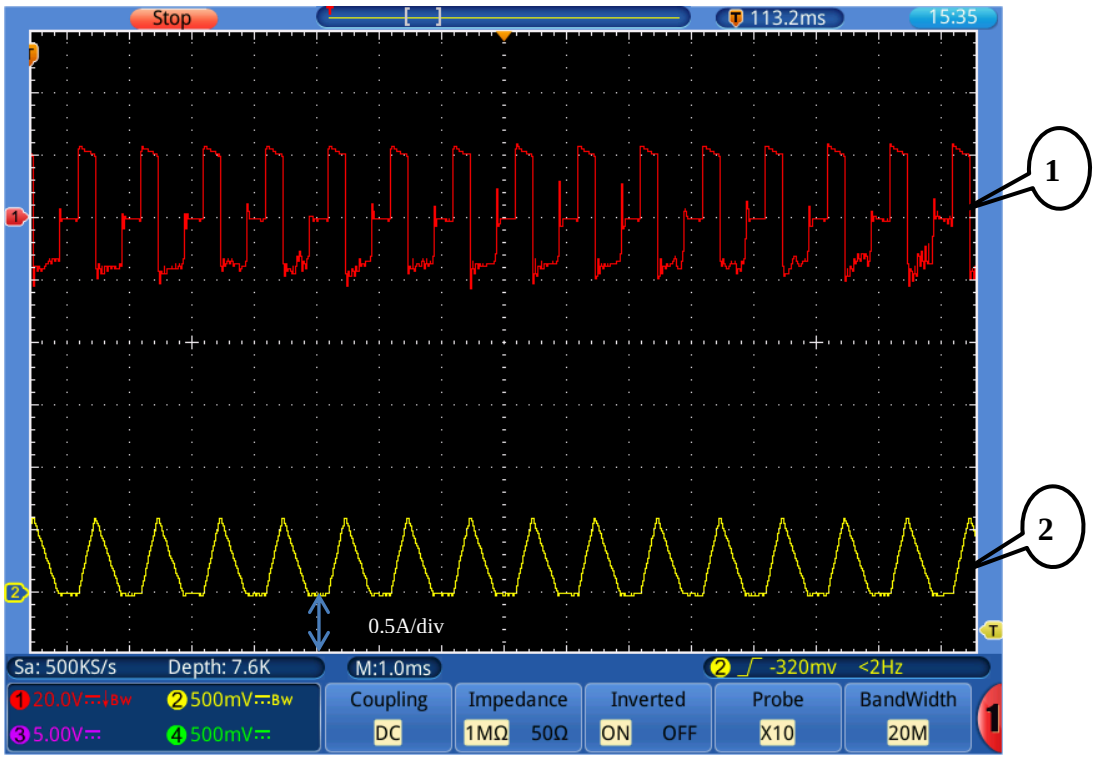

(a)

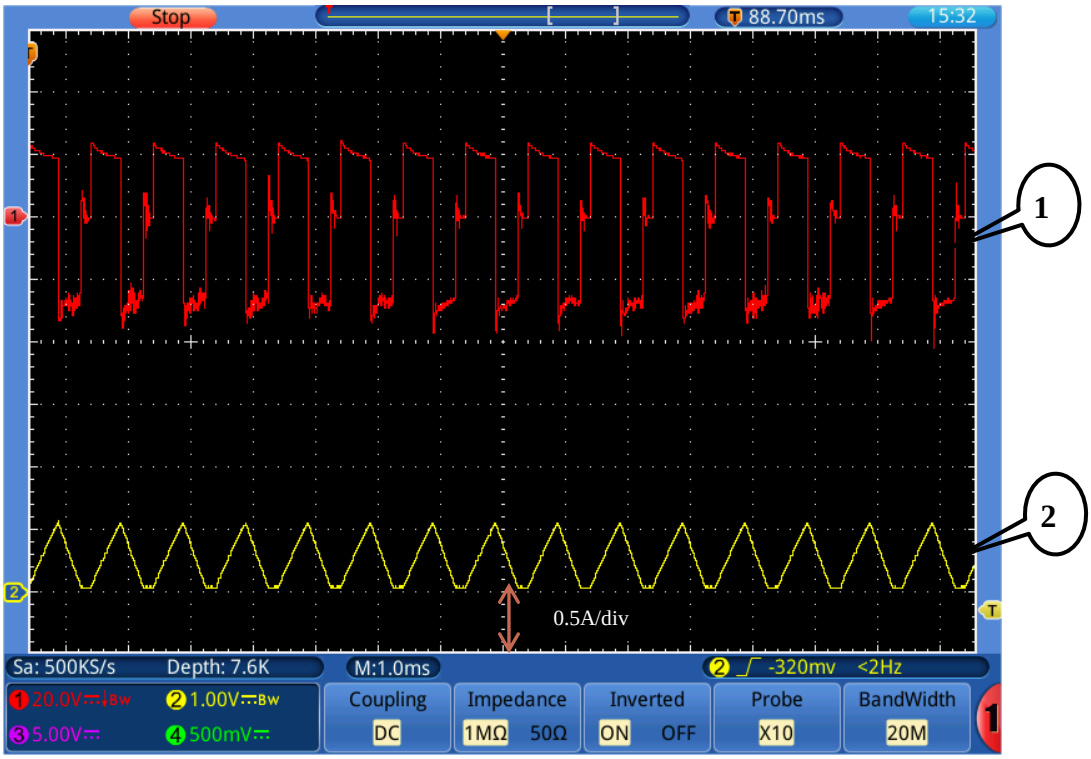

(b)

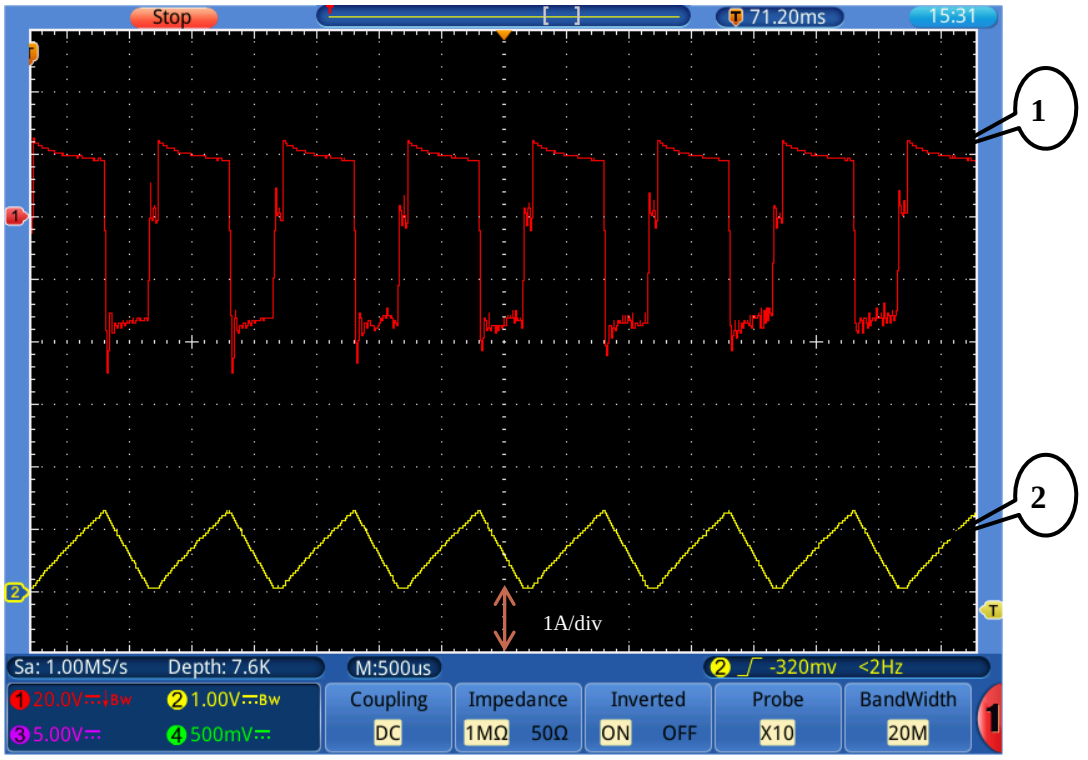

(c)

1- Inductor voltage 2- Inductor current

Fig. (4.12) Performance waveforms of inductor voltage and it's at various duty ratios (a) D = 0.3, (b) D = 0.5 and (c) D = 0.6

CHAPTER (4)
EXPERMENTAL SETUP OF HIGH GAIN DC/DC CONVERTER

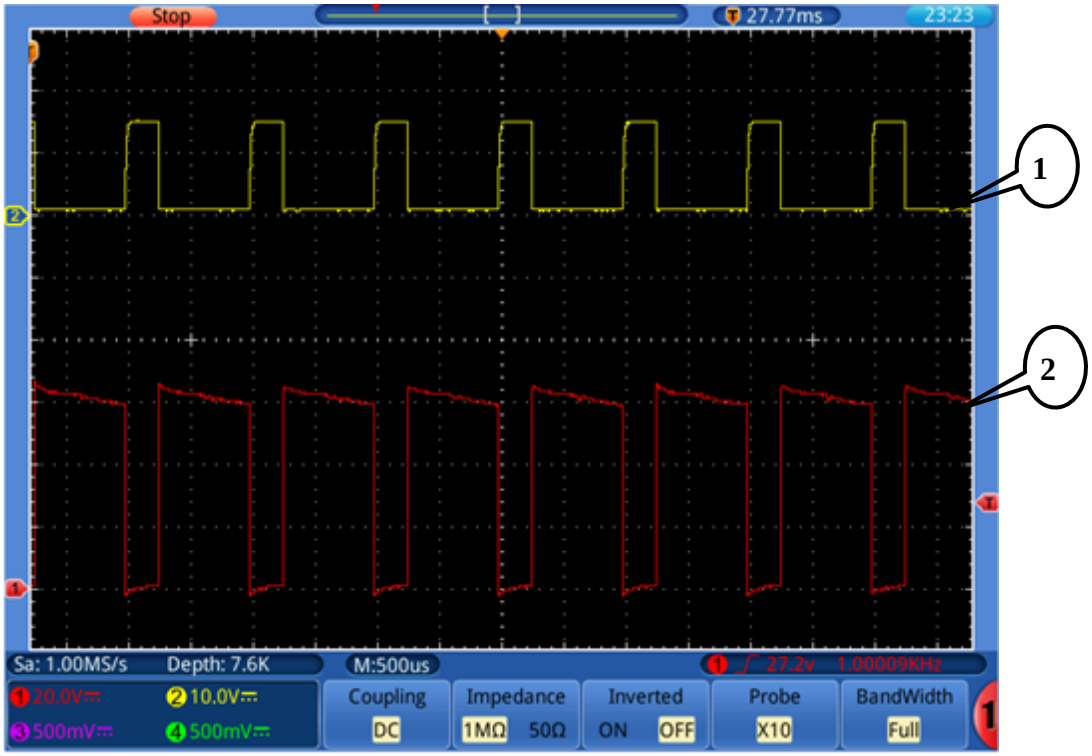

(a)

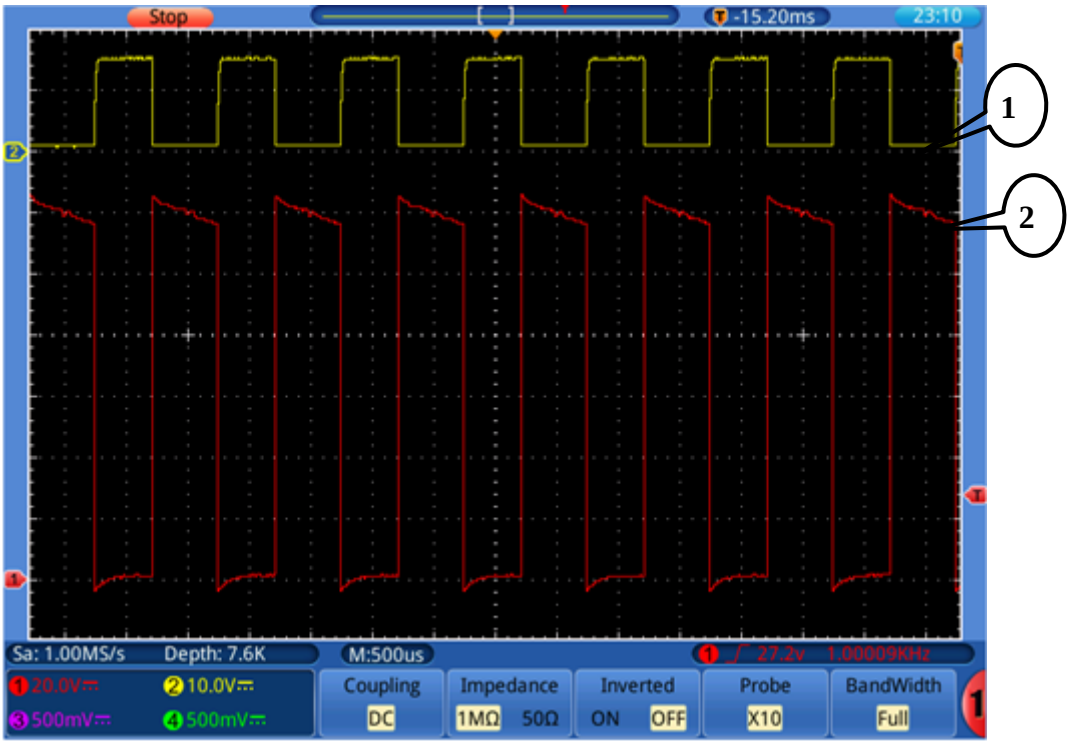

(b)

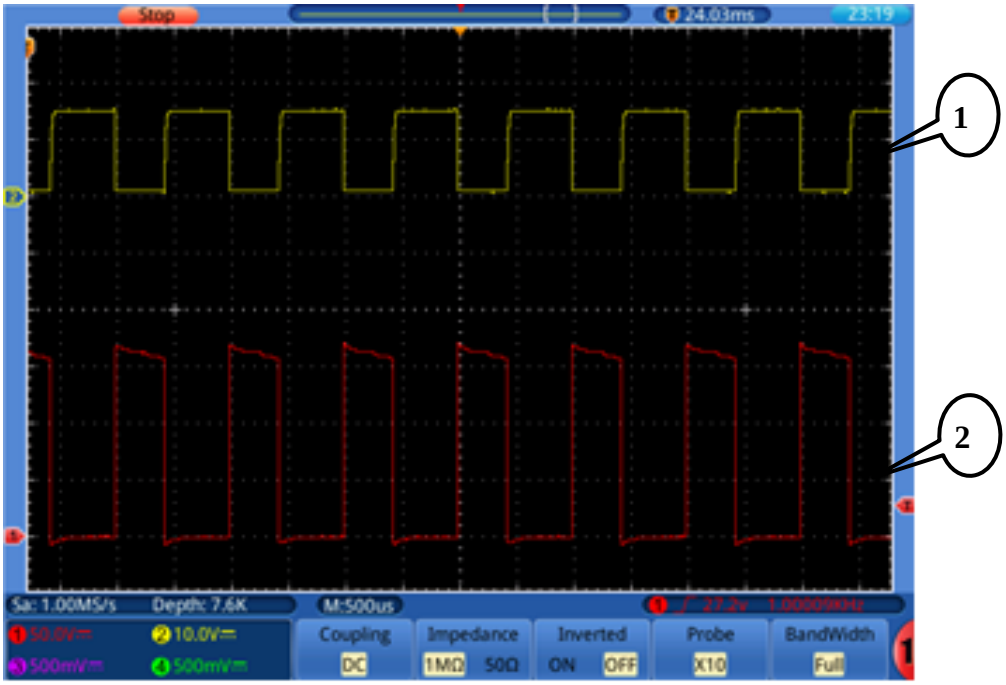

(c)

1- Gate signal pulse 2- Switch voltage

Fig. (4.13) Performance waveforms of gate signal pulse and switch voltage at various duty ratios (a) D = 0.3, (b) D = 0.5 and (c) D = 0.6

4.6 Voltage Gain with Duty Ratio in DCM

The relation between voltage gain and duty ratio in discontinuous conduction mode at experimental and mathematical results is shown as below in Fig. (4.14). It's observed from figure there is a high convergence between two values for voltage gain (M) at each duty ratio (D).

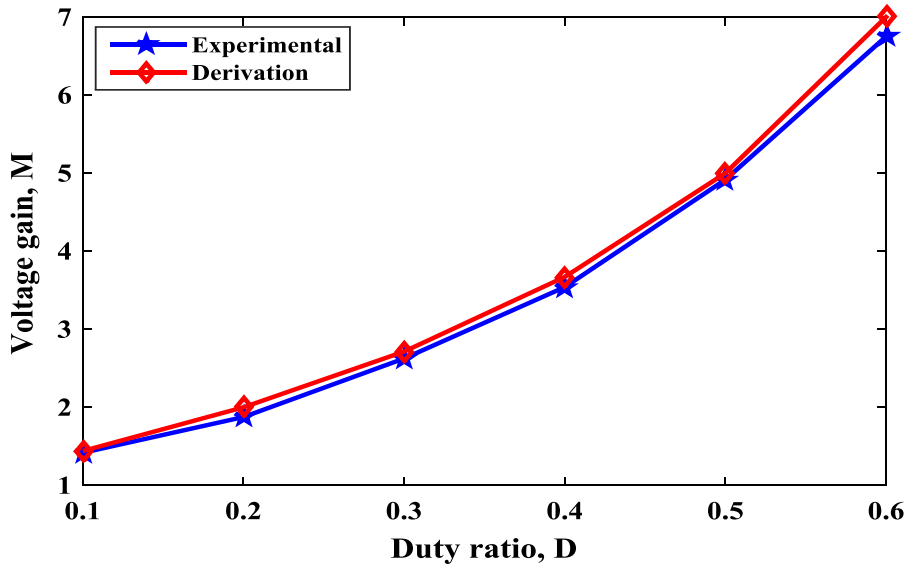

Fig. (4.14) Voltage gain versus duty ratio at experimental and mathematical results

4.7 Experimental Results of Closed Loop Control at Static Load

In this section the experimental results of closed loop control will be explained at static load. For voltage control with three states are of input voltage change, load change and reference voltage change with parameters as shown in Table (4.3).

Table (4.3) Closed loop control parameters

Closed-loop Control	
Parameter	**Value**
Inductances ($\boldsymbol{L_1}$, $\boldsymbol{L_2}$)	10 mH
Capacitance ($\boldsymbol{C_o}$)	330μF
Switching frequency (F_S)	1 KHZ
Static Load	
Proportional gain ($\boldsymbol{K_P}$)	100
Integral gain ($\boldsymbol{K_i}$)	200
Load resistance (R_L)	450Ω
Dynamic Load	
Proportional gain ($\boldsymbol{K_P}$)	98.6
Integral gain ($\boldsymbol{K_i}$)	215
Armature voltage (V_a)	50V
Armature current (I_a)	1A

4.7.1 Input voltage change

For closed loop control under input change, a simple PI controller is used. The parameters for the PI for *Kp* and *Ki* as in Table (4.3) . The proposed converter tested for supply voltage change experimentally at L_1=L_2=10 mH and R_{load}=450Ω. By changing supply voltage by decreasing from 35V to 22V as shown in Fig. (4.15) at reference voltage 50V, the output voltage and output current will be constant as shown in Figf (4.16) and (4.17). This means that the converter not affect with changing in input voltage at any value by increasing or decreasing. Where the output voltage and current waveforms not changed with this control, that voltage and the output current still constant and robustness against these variations.

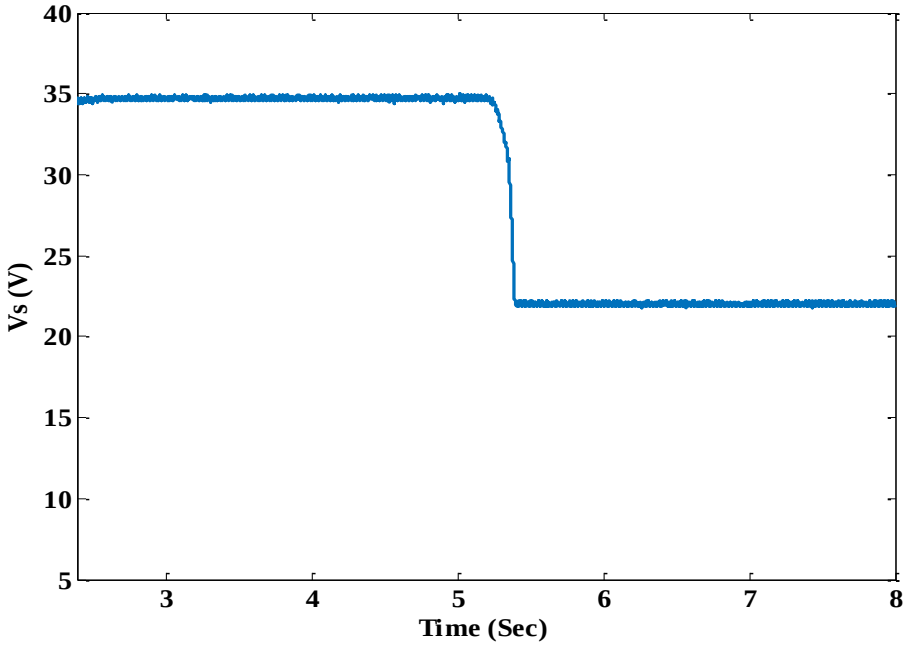

Fig. (4.15) Input voltage change

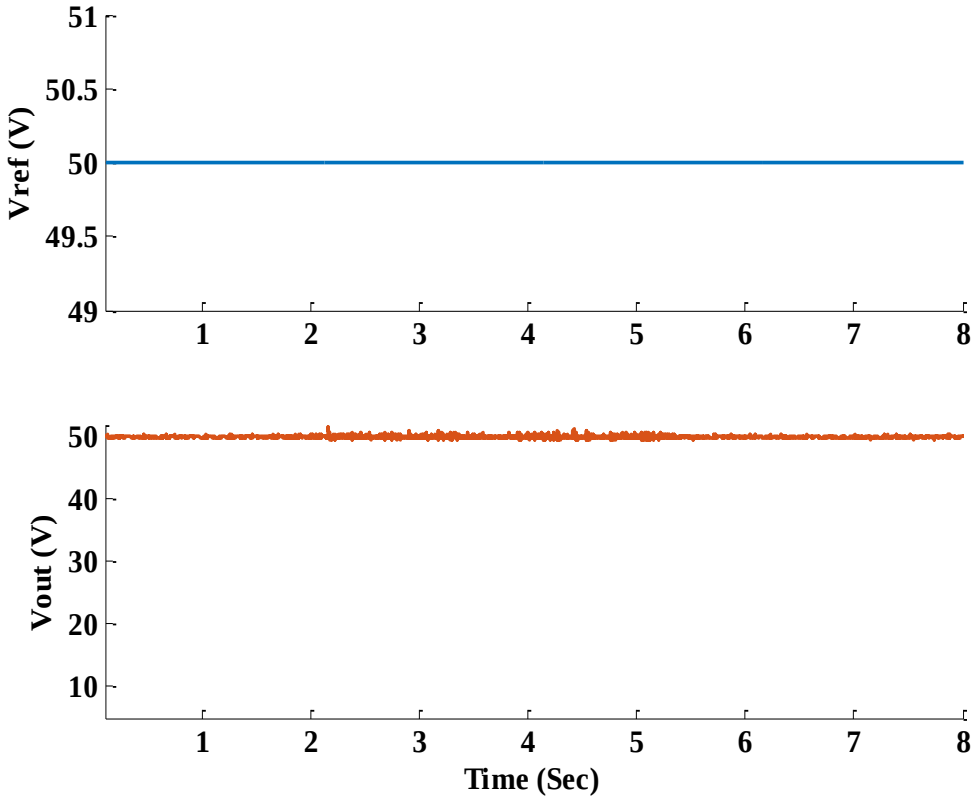

Fig. (4.16) Reference and output voltage under input change

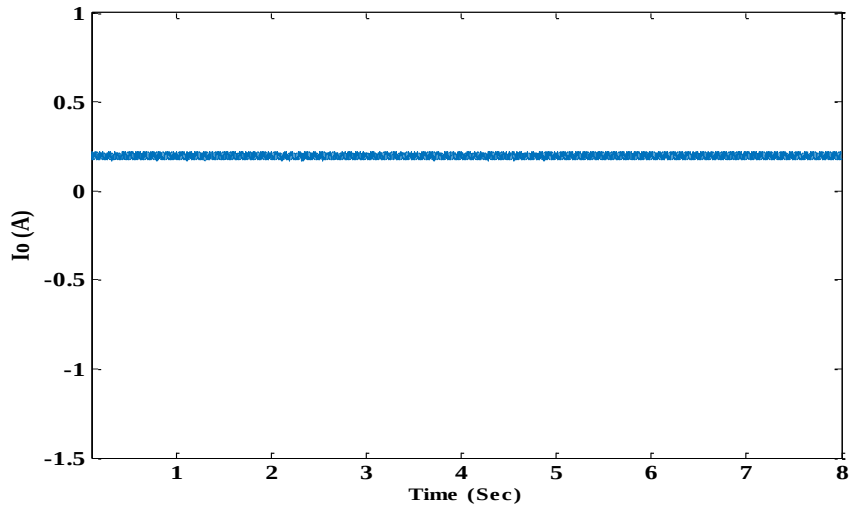

Fig. (4.17) Output current under input change

4.7.2 Load change

For closed loop control under load change, a simple PI controller is used. The waveforms of reference and output voltages, and load current during changing of the load are shown in Figf (4.18) and (4.19) respectively. With the reference voltage equal to 50 V, two load step changes are introduced. At the instant t = 1.248 sec, the load increased from about 25% of the rated load to the rated load. At the instant t = 3.75748 sec, the load decreased from the rated load to about 25% of the rated load again.

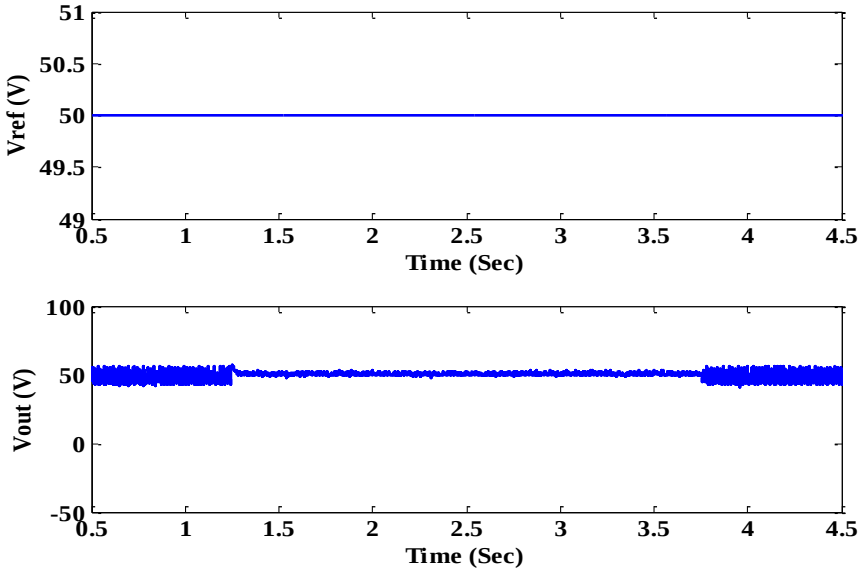

Fig. (4.18) Reference and output voltage at load change

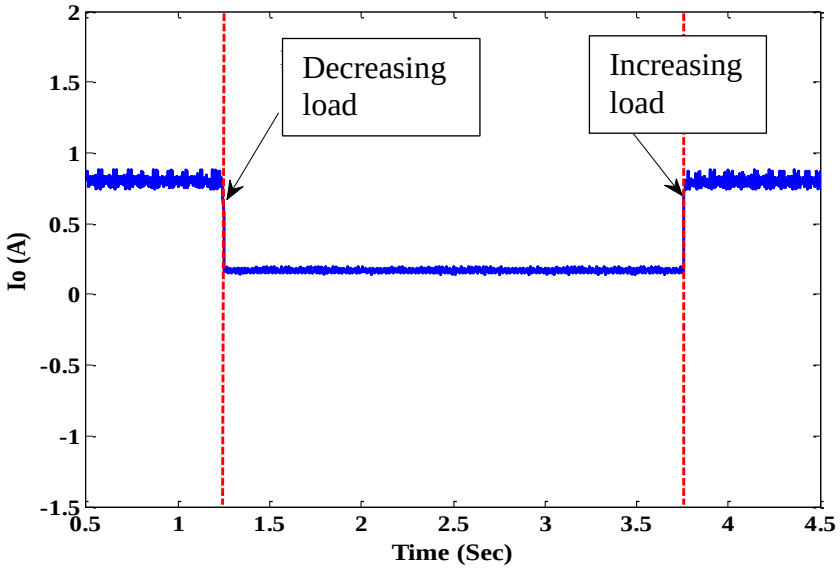

Fig. (4.19) Load current under load change

4.7.3 Reference voltage change

For closed loop control under load change, a simple PI controller is used. The waveforms of reference and output voltages during changing of the reference voltage are shown in Fig. (4.20). At the instant t = 1.266 sec, the reference voltage decreased from 100 V to 70 V then at the instant t = 2.67 sec, the reference voltage increased to 100 V again. Also, the output voltage respond to this change as shown in Fig..

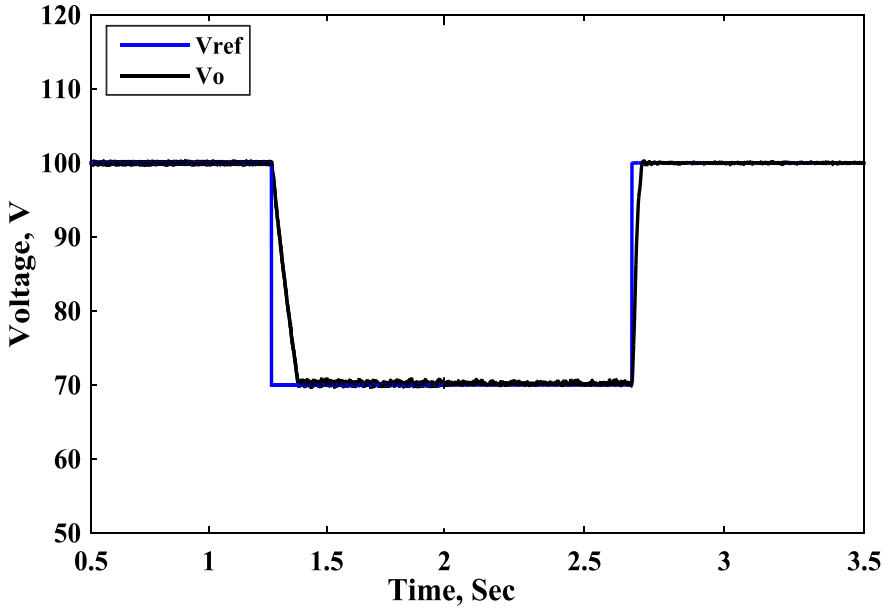

Fig. (4.20) Reference and output voltage at reference change

4.8 Experimental Results of Closed Loop at Dynamic Load Performance

For closed loop control at dynamic load using a simple PI controller with parameter K_P=98.6 and K_I=215 as in Table (4.3). The converter loaded by separately excited dc motor with field winding voltage V_{field} =25V. The armature winding is supplied from the proposed converter. Hence the differential equation that explain the dynamic behavior of the separately excited DC motor are given as

$$\mathrm{Va(t)} = Raia(t) + La\frac{dia(t)}{dt} + \mathrm{eb(t)}$$

$$eb(t) = Kw(t)$$

$$Tm(t) = Kia(t)$$

$$\frac{dw(t)}{dt} = \frac{Tm(t) - TL(t)}{J}$$

Where V_a(t),Ia(t) are the armature voltage and current respectively, e_b(t) is back electromotive force, w(t) is the speed, T_m(t) and T_l(t) are electromagnetic and load torque, R_a and L_a are armature resistance and inductance and J is the moment of inertia.

4.8.1 Voltage control

To show the effectiveness of the proposed converter to drive the motor effectively, the results shown in Figf. (4.21) and (4.22) are presented. With a load torque equal to 50% of the motor torque, the motor operates at armature voltage equal 35 V and speed equal to 1300 rpm. At the instant t = 2.3 sec, a step change in the reference armature voltage from 35 V to 40 V is introduced so, the motor speed responds to this change and increases to 1500 rpm. Then when a step change in the reference armature voltage from 40 V to 35 V is introduced at the instant t = 5.92 sec, the motor speed responds to this change and decreases to 1300 rpm. The converter is tested for voltage control with separately excited DC motor as dynamic load. Where, the reference voltage is changed from 35V to 40V and load torque is 50% from full load torque. Its observed from Fig. (4.21) the output voltage responds to change in reference voltage, also the

speed changed from 1300rpm to 1500rpm with the change in the voltage as shown from Fig. (4.22).

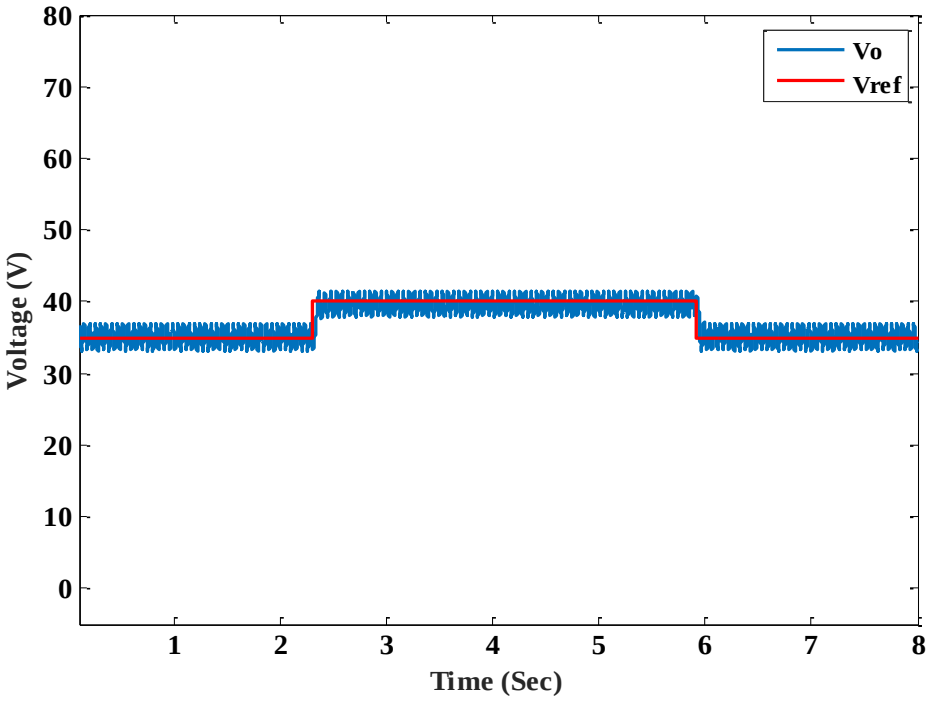

Fig. (4.21) Reference and output voltage at voltage control

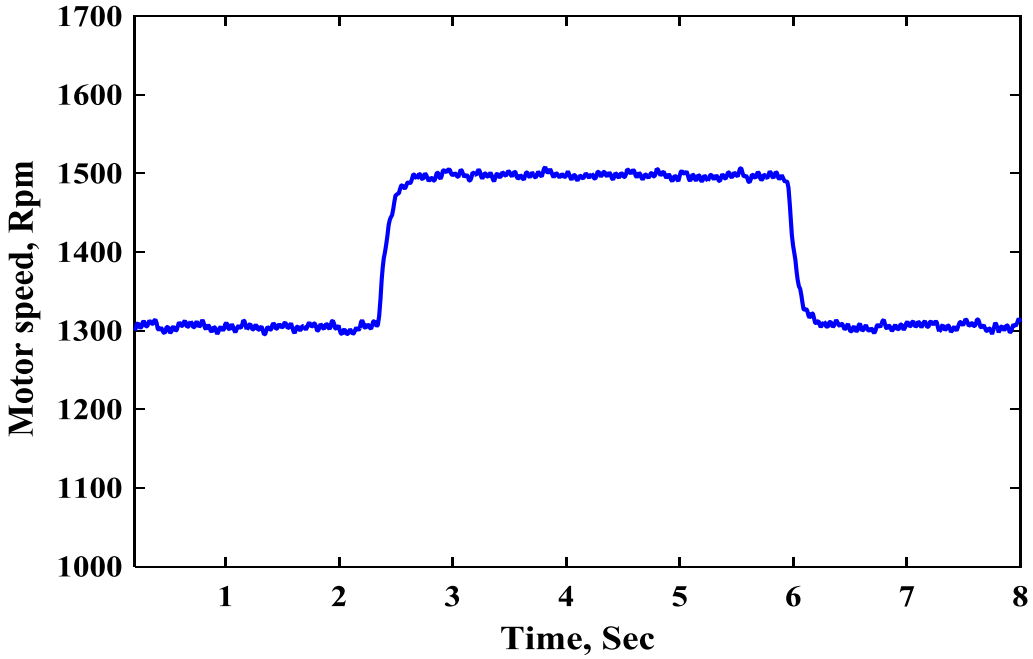

Fig.(4.22) Speed changed under voltage control

4.8.2 Speed control

The converter tested for speed control at two cases at load torque (T_L) changed from 40% to 60% from full load torque (T_{FL}) and at T_L changed from 60% to 40% with reference speed equal 1800 rpm.

Figure (4.23) shows the reference speed and motor speed at changing in T_L from 40% to 60% of T_{FL}. The figure explains the motor speed is constant under torque changing. Fig. (4.24) shows the output voltage changed by increasing value under speed control by load torque changing from 40% to 60% of $T_{FL.}$ Fig. (4.25) shows the reference speed and motor speed at changing in T_L from 60% to 40% of T_{FL}. The figure explains the motor speed is constant under torque changing. Fig. (4.26) shows the output voltage changed by decreasing value under speed control by load torque changing from 60% to 40% of T_{FL}

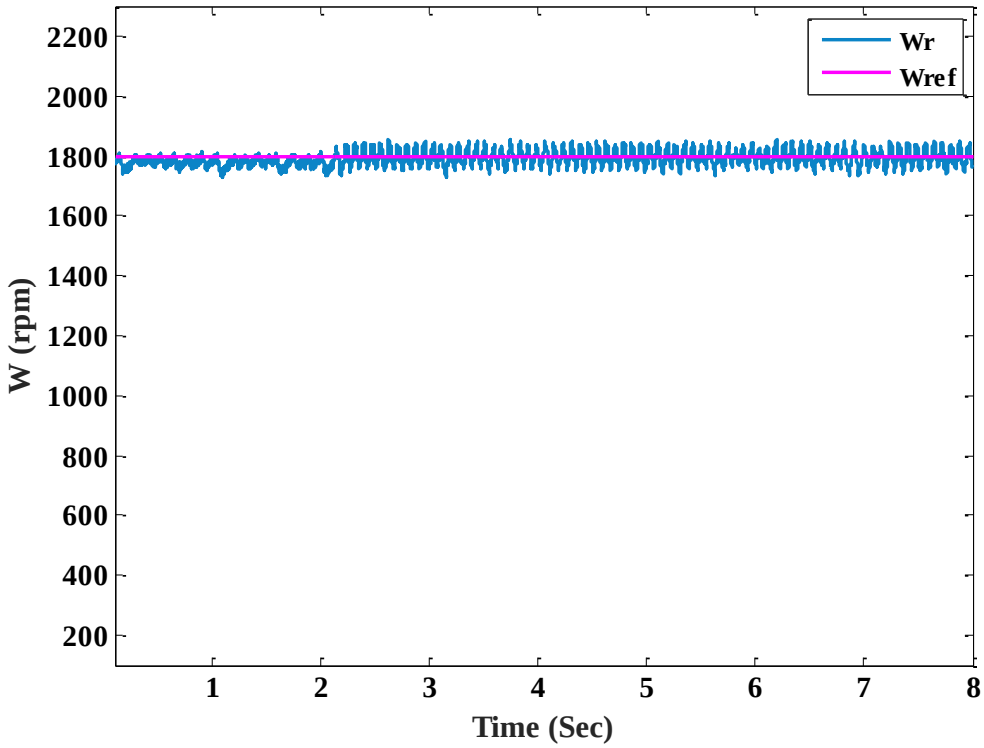

Fig. (4.23) Reference and motor speed under speed control

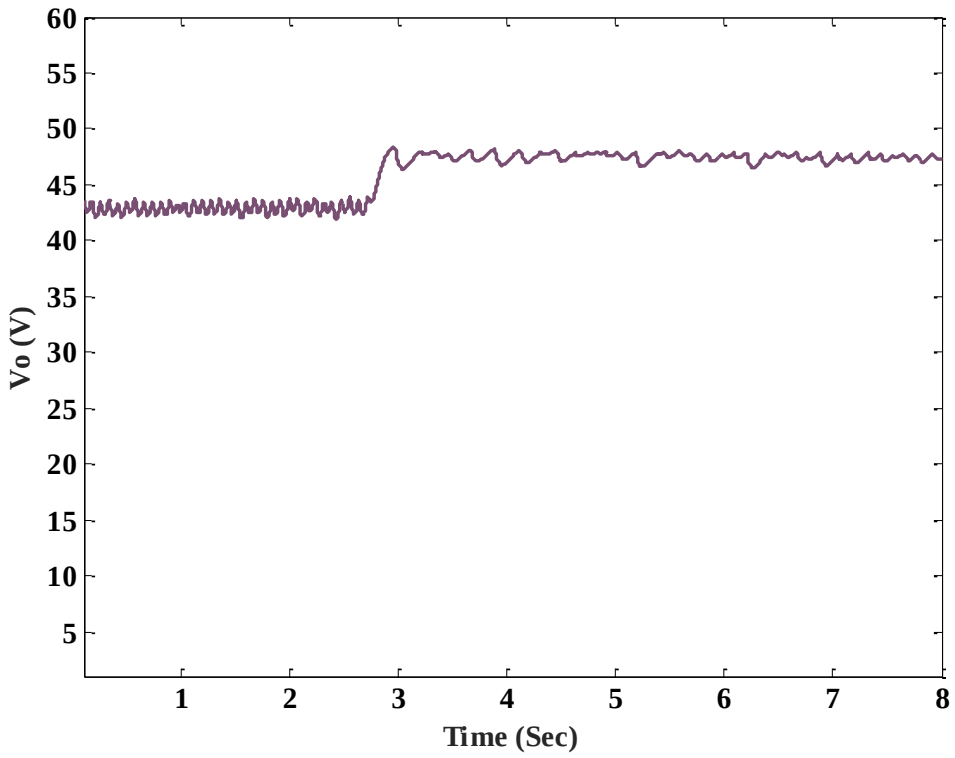

Fig. (4.24) Output voltage change under speed control

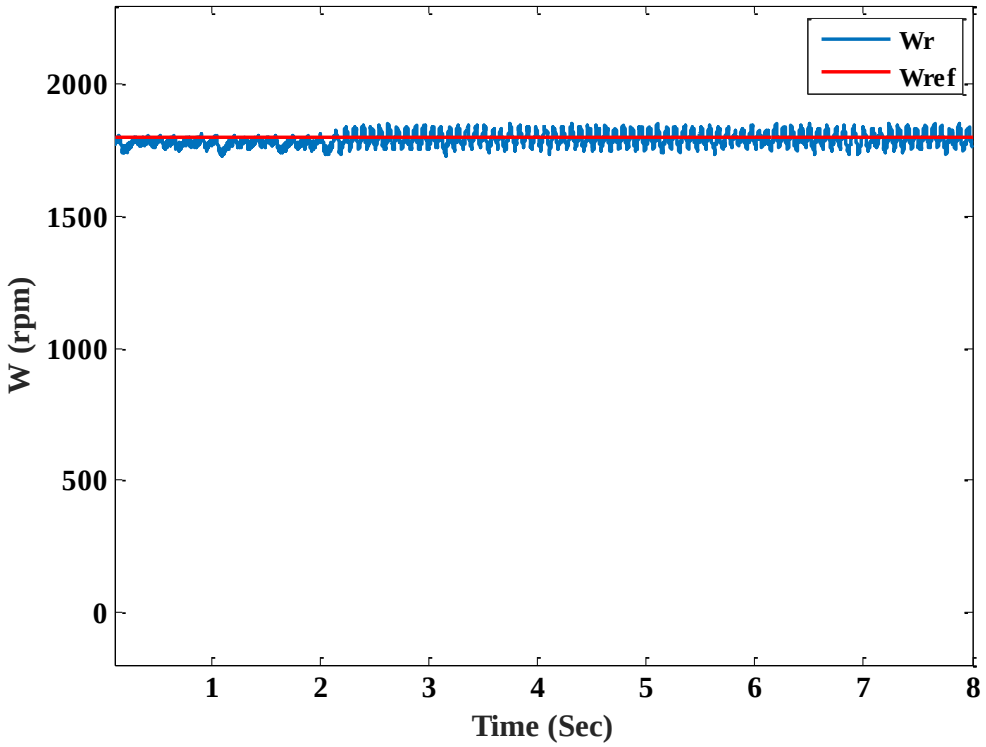

Fig. (4.25) Reference and motor speed under speed control

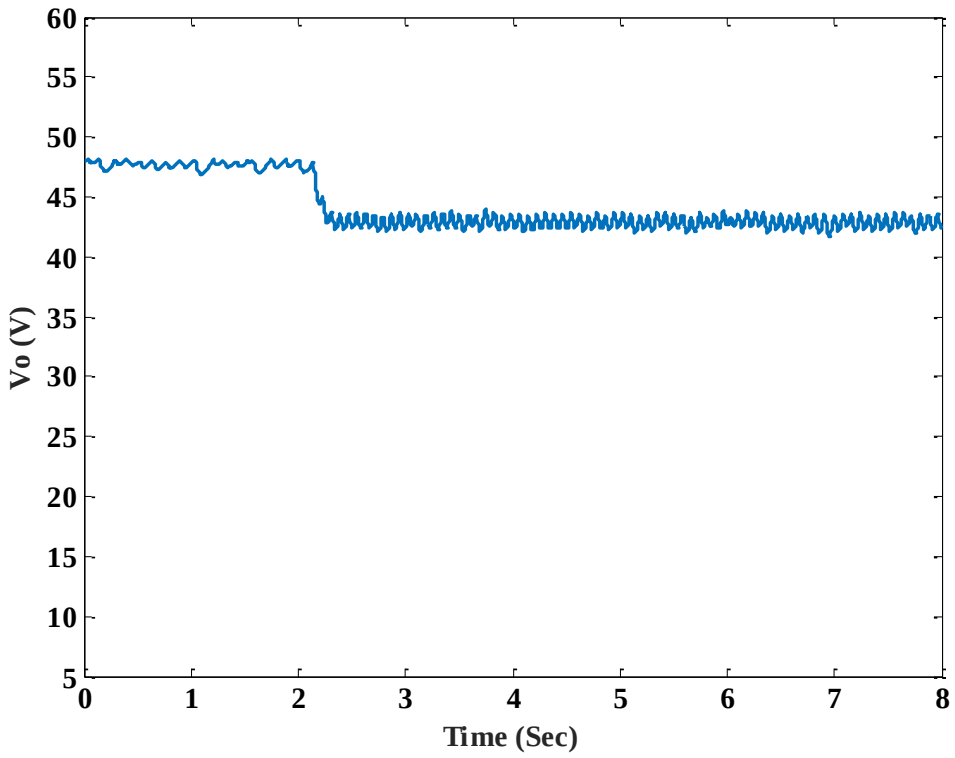

Fig. (4.26) Output voltage change under speed control

4.9 Comparisons of the Proposed Converter with Previous Work

In this section the proposed converter compared with other recent converters in terms of number of switches, number of inductors, number of capacitors, number of diodes, voltage gain equation, and switch and output diode voltage stresses as in Table (4.4). As described in Table (4.4), the proposed converter has the least components count compared to the other converters in [5], [8], [10] and [17]. Also, for the modest duty ratios the proposed converter has the larger gain compared with the conventional, conv. [5], conv. [8], and conv. [17] except conv. [10] that has the largest voltage gain as shown in Fig. (4.27). However, conv. [10] needs high output capacitor value that increases the volume and cost of the converter.

The maximum voltage stresses across power switches of the converters are compared as shown in Fig. (4.28). the maximum switch voltage stresses of the conventional, conv. [8], and proposed are equal. The maximum switch voltage stresses of the proposed is lower than conv. [17], but it higher than conv. [5] and conv. [10]. The maximum output diode voltage stresses of the converters are

displayed in Fig. (4.29). Conv. [17] has the highest value, while conv. [5] has the lowest value. The maximum output diode voltage stress of the proposed converter is equal to the conventional and conv. [8]. Based on these comparisons, the proposed converter has good performance.

Table (4.4) Comparing the proposed converters with other recent topologies

Converter Type	**Conventional boost**	**Conv. [5]**	**Conv. [8]**	**Conv. [10]**	**Conv. [17]**	**Proposed**
No. of switches	1	1	2	1	2	1
No. of inductors	1	2	4	3	3	2
No. of capacitors	1	3	4	4	3	1
No. of diodes	1	3	2	5	2	4
Voltage gain equation	$\frac{1}{1-D}$	$\frac{2}{1-D}$ $n=1, k=1$	$\frac{1}{1-D}$ $n=1, k=1$	$\frac{2(1+D)}{(1-D)^2}$ $n=1$	$\frac{D}{(1-D)^2}$	$\frac{1+3D}{1-D}$ in DCM $\frac{1+D}{1-D}$ in CCM
Switch voltage stress	V_o	$\frac{V_o}{2}$	V_o	$\frac{V_o}{2(1+D)}$	$\frac{V_o}{D}$	V_o
Output diode (D_o) voltage stress	V_o	$\frac{V_o}{2}$	V_o	$\frac{V_o}{(1+D)}$	$\frac{V_o}{D}$	V_o
Output capacitor (C_o) voltage stress	V_o	V_o	V_o	V_o	V_o	V_o

*n and k are the turns ratio, and the coupling coefficient of the coupled inductor, respectively.

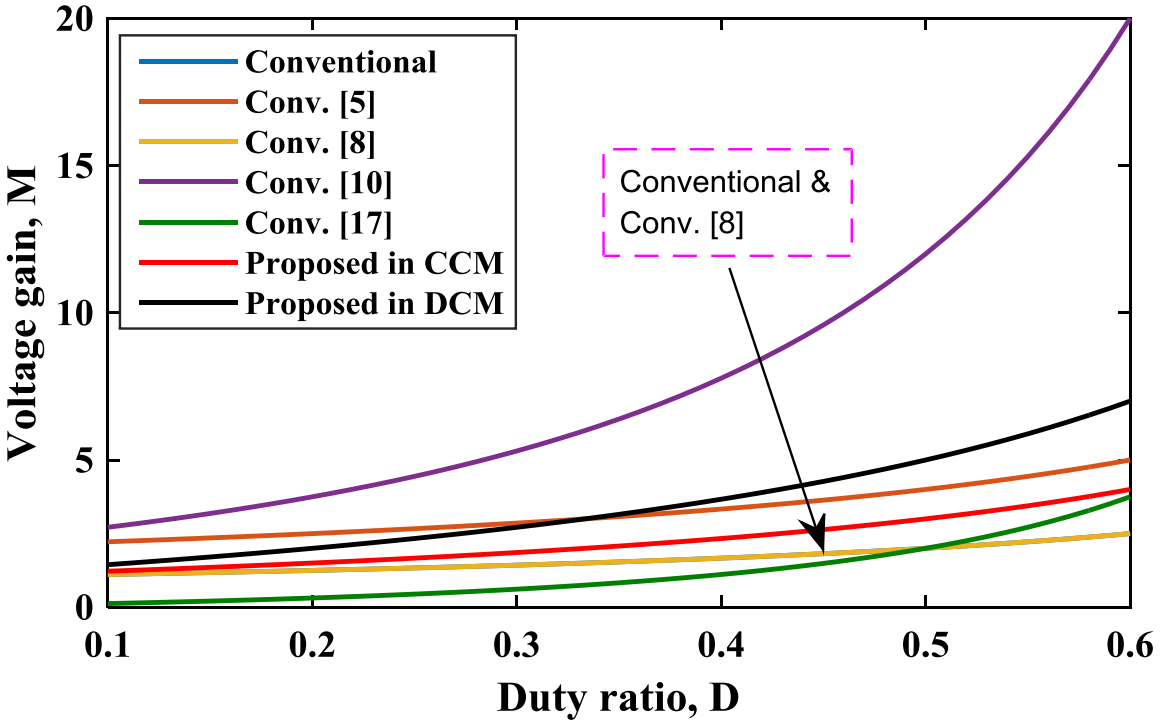

Fig. (4.27) Voltage gain versus duty ratio

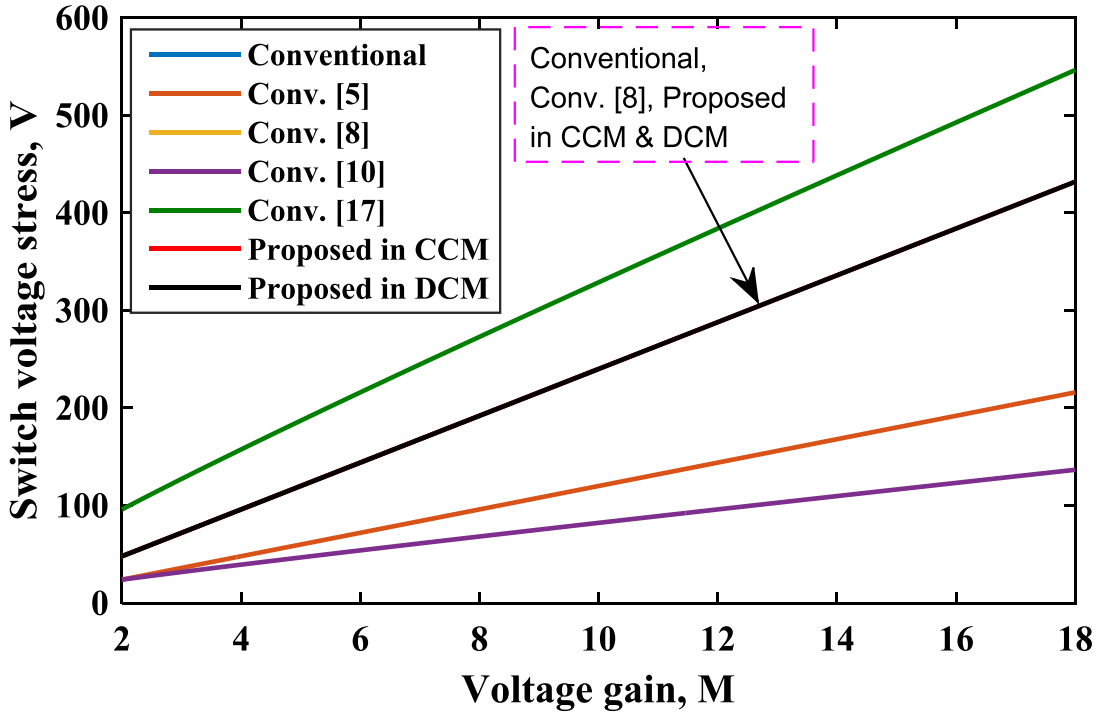

Fig. (4.28) Maximum switch voltage stress versus voltage gain at V_{in} = 24 V.

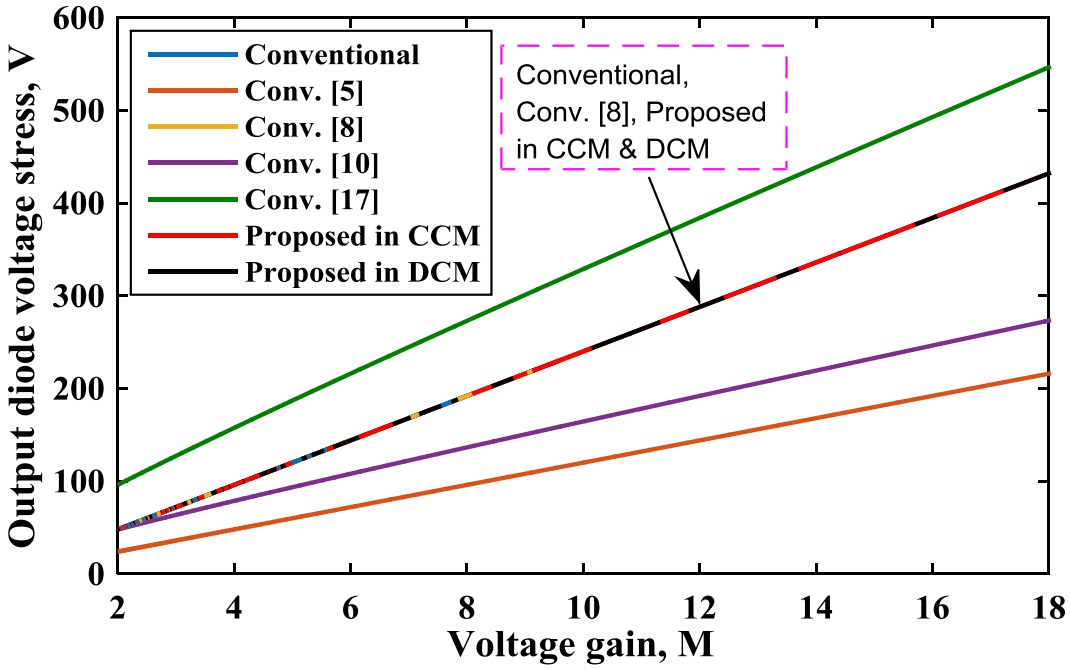

Fig. (4.29) Maximum output diode voltage stress versus voltage gain at V_{in} = 24V.

4.10 Converter Efficiency

The converter efficiency is measured at different duty ratios and the result is shown in Fig. (4.30). the efficiency is higher when the converter operates in DCM. The maximum efficiency that the converter reaches is 93 % at D = 0.6.

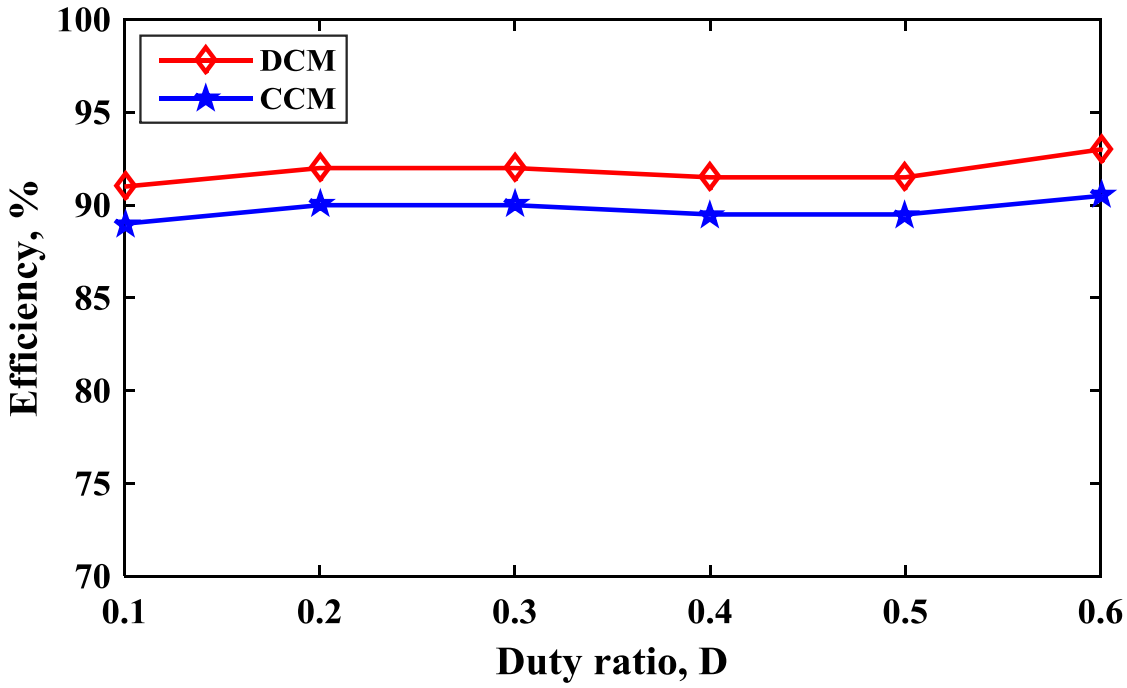

Fig. (4.30) Efficiency of the proposed converter versus duty ratio

CHAPTER (5)
CONCLUSIONS AND FUTURE WORK

5.1 Conclusions

Nowadays the demand for renewable energy sources as PV solar panel is increasing due to many advantages of these sources, but to use them its required using high gain DC-DC converter with them to increase the output voltage. In this thesis a literature reviews about many topologies that used with PV application was introduced but the switched inductor converters have promised to be alternative converter for the traditional DC-DC converters. The reason for switched inductor converters are more using for PV application because they achieve continuous input current necessary for use with solar panels. This thesis discussed the proposed topology using single switch with switched inductor to use for PV application. This proposed demonstrated desirable attributes necessary for a solar converter. This can achieve output voltage with high gain and high efficiency. Also, its input current is continuous is the important requirements for PV solar panel. From the study of the proposed converter for PV application the following conclusions are drawn in this thesis:

In chapter (2) the proposed converter was analyzed in details in continuous conduction mode (CCM) and discontinuous conduction mode (DCM), from this analysis the proposed converter has many merits such as simple structure, use few components and using one switch that reduced the switching losses and using fewer components reduce the cost of the system and due to these merits the overall efficiency is increased. In this chapter the converter was described an operation modes was introduced.

In chapter (3) the simulation studies have been done using **MATLAB/SIMULINK** program. Also, in this chapter the simulation results for open loop were introduced for CCM and DCM at different level of duty ratio. In addition to the simulation results for static load case of closed loop control system were explained at input voltage change, load change and reference voltage change.

In chapter (4) the proposed converter has been demonstrated for experimental results for (CCM) and (DCM). Experimental studies are confirmed by implementing a laboratory platform. Also, this chapter shows the experimental analysis of closed loop

control for the proposed converter at static load performance under three tests input change, load change and reference voltage change. In addition to this chapter presented the closed loop control analysis at dynamic performance by using separately excited DC motor at voltage control and speed control to prove the converter able to operate with dynamic load as static load. This chapter also, introduced a comparison analysis to the proposed converter with other recent converters in terms of number of using components, voltage gain and switch voltage stress to ensure that the proposed has higher voltage gain and lower switch voltage stress in open loop condition. Supporting this comparative performance with graphical comparison between voltage gain with duty ratio and switch voltage stress versus duty ratio for the proposed and other structures.

5.2 Future Work

The work done in this thesis can be further extended such that new improvements can be found. The feasible options are

- Modifying the converter structure by using other high gain techniques to improve the performance and to increase the voltage gain that make this converter suitable for several industrial applications.
- Studying the converter performance with maximum power point tracking for real implementation PV system.
- Using the proposed converter with grid connected PV system and study the performance of the system.

LIST OF PUBLICATIONS

[1] Arafa S. Mansour, Eman M. Sarhan, Awad E. El-Sabbe and Dina S. M. Osheba, "A Single Switch High Gain DC-DC Converter with Switched Inductor", IEEE 22nd International Middle East Power Systems Conference (MPCON), Assiut University, Egypt, pp.625-631, 14-16 December 2021**.**

[2] Arafa S. Mansour, Eman M. Sarhan, Awad E. El-Sabbe and Dina S. M. Osheba, "A Single-switch Non-isolated High Gain DC/DC Converter for PV Applications", Engineering Research Journal (ERJ), Menoufia University, Vol. 45, No. 3, pp. 261-271, July 2022.

REFERENCES

[1] N. Mohan, T. M. Undeland, and W. P. Robbins, Power Electronics: Converters, Applications and Design, second edition, New York. Wiley, 1995

[2] 1 R. W. Erickson and D. Maksimovic," Fundamentals of Power Electronics, Second Edition", New York: Kluwer Academic/Plenum Publishers, 2001.

[3] A. Tomaszuk, A. Krupa, "High efficiency high step-up DC/DC Converters – a review", Bulletin of the Polish Academy of Sciences Technical Sciences, Vol. 59, No. 4, pp. 475-483, Feb. 2011.

[4] A. Amir, A. Amir, H. S. Che, A. Elkhateb, N. Abd Rahim, "Comparative analysis of high voltage gain DC-DC converter topologies for photovoltaic systems", Renewable Energy, Vol. 136, No. 136, pp. 1147-1163, Jun. 2019.

[5] M. Das, V. Agarwal, "Design and Analysis of a High-Efficiency DC–DC Converter with Soft Switching Capability for Renewable Energy Applications Requiring High Voltage Gain", IEEE Transactions on Industrial Electronics, Vol. 63, No. 5, pp. 2936-2944, May 2016.

[6] B. P. R. Baddipadiga, V. A. K. Prabhala, M. Ferdowsi, "A Family of High-Voltage-Gain DC-DC Converters Based on a Generalized Structure", IEEE Transactions on Power Electronics, Vol. 33, No. 10, pp. 8399-8411, Oct. 2018.

[7] B. S. Revathi, M. Prabhakar, "Non isolated high gain DC-DC converter topologies for PV applications – A comprehensive review", Renewable and Sustainable Energy Reviews, Vol. 66, pp. 920-933, Dec. 2016.

[8] A. Kumar, P. Sensarma, "Ripple-Free Input Current High Voltage Gain DC–DC Converters with Coupled Inductors", IEEE Transactions on Power Electronics, Vol. 34, No. 4, pp. 3418-3428, Apr. 2019.

[9] V.A.K. Prabhala, V.S.P. Gouribhatla, M. SaT, P. Fajri, M. Ferdowsi, "A multiport DC-DC converter with high voltage gain," Telecommunications Energy Conference (INTELEC), 2014 IEEE 36th International, pp.1,8, Sept. 28 2014-Oct. 2 2014.

[10] M. Hoseinzadeh, R. Ebrahimi, H. M. Kojabadi, "A Cascade High Gain DC-DC Converter Employing Coupled Inductor and Diode Capacitor", 5th Conference on Knowledge Based Engineering and Innovation (KBEI), Tehran, Iran, pp. 205-209, 28 Feb.-1 March 2019.

[11] M. Amirbande, K. Yari, M. Forouzesh, A. Baghramian, "A Novel Single Switch High Gain DC-DC Converter Employing Coupled Inductor and Diode Capacitor", IEEE Power Electronics and Drive Systems Technologies Conference (PEDSTC), Tehran, Iran, pp. 1-6, 16-18 Feb. 2016.

[12] P. V. Suresh, A. Mittal, A. Ojha, "Review on High Gain DC/DC converters for Renewable Energy Applications and their comparison with proposed converter",

International Journal of Emerging Trends in Engineering Research (IJETER), Vol. 3, No. 6, pp. 471-476, Jun. 2015.

[13] D. Bao, A. Kumar, X. Pan, X. Xiong, A. R. Beig, S, K. Singh, "Switched Inductor Double Switch High Gain DC-DC Converter for Renewable Applications", IEEE Access, Vol. 9, pp. 14259-14270, Jan. 2021.

[14] K. R. Babu, M. R. Ramteke, H. M. Suryawanshi, K. R. Kothapalli, "A Novel High Gain Soft Switched Step-Up DC-DC Converter with Coupled Inductors", IEEE Texas Power and Energy Conference (TPEC), College Station, TX, USA, pp. 1-6, 6-7 Feb. 2020.

[15] X. Hu, C. Gong, "A High Voltage Gain DC–DC Converter Integrating Coupled-Inductor and Diode–Capacitor Techniques", IEEE Transactions on Power Electronics, Vol. 29, No. 2, pp. 789-800, Feb. 2014.

[16] R. Barzegarkhoo, P.Y. Siwakoti, N. Vosoughi, F. Blaabjerg, "Six-switch step-up common-grounded five-level inverter with switched-capacitor cell for transformerless grid-tied PV applications", IEEE Transactions on Industrial Electronics, Vol. 68, No. 2, pp. 1374–1387, Feb. 2021.

[17] H. Gholizadeh, S. Aboufazeli, Z. Rafiee, E. Afijei, M. Hamezeh, "A Non-Isolated High Gain DC-DC Converters with Positive Output Voltage and Reduced Current Stresses", IEEE 11th Power Electronics, Drive Systems, and Technologies Conference (PEDSTC), Tehran, Iran, pp. 4-6 Feb. 2020.

[18] H. E. Mohamed, A. A. Fardoum, "High Gian DC-DC Converter for PV Applications", IEEE 59th International Midwest Symposium on Circuits and Systems (MWSCAS), Abu Dhabi, United Arab Emirates, pp. 1-4, 6-19 Oct. 2016
.
[19] M. Forouzesh, Y. Shen, K. Yari, Y. P. Siwakoti, F. Blaabjerg, "High-Efficiency High Step-Up DC–DC Converter with Dual Coupled Inductors for Grid-Connected Photovoltaic Systems", IEEE Transactions on Power Electronics, Vol. 33, No. 7, pp. 5967-5982, Jul. 2018.

[20] H. J. Hoch, T. M. K. Faistel, M. M. da Silva, A. M. S. Andrade, M. L. da S. Martins, "High Voltage Gain DC-DC Converter based on a Simple Configuration of Switched Capacitor and Coupled Inductor", IEEE 15th Brazilian Power Electronics Conference and 5th IEEE Southern Power Electronics Conference (COBEP/SPEC), Santos, Brazil, pp. 1-6, 1-4 Dec. 2019.

[21] M. Fekri, N. Molavi, E. Adib, "High Voltage Gain Interleaved DC-DC Converter with Minimum Current Ripple", IET Power Electronics, Vol. 10, No. 14, pp. 1924-1931, Nov. 2017.

[22] G. Lin, Z. Zhang, " Low Input Ripple High Step-Up Extendable Hybrid DC-DC Converter", IEEE Access, Vol.7, pp. 158744-158752, Oct. 2019.

[23] M. D. Vecchia, G. V. den Broeck, S. Ravyts, J. Tant, J. Driesen, "A family of DC–DC converters with high step-down voltage capability based on the valley-fill switched capacitor principle", IEEE Transactions on Industrial Electronics, Vol. 68, No. 7, pp. 5810–5820, Jul. 2021.

[24] L. Wuhua and H. Xiangning, "An Interleaved Winding-Coupled Boost Converter With Passive Lossless Clamp Circuits," Power Electronics, IEEE Transactions on, vol. 22, pp. 1499-1507, 2007.

[25] S. Hasanpour, M. Forouzesh, Y. P. Siwakoti and F. Blaabjerg, "A Novel Full Soft-Switching High-Gain DC/DC Converter Based on Three-Winding Coupled-Inductor", IEEE Transactions on Power Electronics, Vol. 36, No.11, pp. 12656 – 12669, Nov. 2021.

[26] M. Rezaie, V. Abbasi, "Ultrahigh Step-Up DC–DC Converter Composed of Two Stages Boost Converter, Coupled Inductor, and Multiplier Cell" IEEE Transactions on Industrial Electronics", Vol.69, No. 6, pp. 5867 – 5878, June 2022.

[27] R. Rahimi, S. Habibi, P. Shamsi, M. Ferdowsi," A Dual-Switch Coupled Inductor-Based High Step- Up DC-DC Converter for Photovoltaic-Based Renewable Energy Applications" IEEE Texas Power and Energy Conference (TPEC), College Station, TX, USA, pp. , 2-5 Feb. 2021.

[28] T. Liang, P. Luo, K. Chen," A High Step-up DC-DC Converter with Three-winding Coupled Inductor for Sustainable Energy Systems" IEEE Transactions on Industrial Electronics (Early Access),pp. 1-1, Nov. 2021.

[29] P. Mohseni, S. Mohammadsalehian, Md. R. Islam, K. M. Muttaqi, D. Sutanto," Ultrahigh Voltage Gain DC–DC Boost Converter With ZVS Switching Realization and Coupled Inductor Extendable Voltage Multiplier Cell Techniques" IEEE Transactions on Industrial Electronics ,Vol. 69, No. 1, pp 323 – 335, Jan. 2022.

[30] R. Rahimi, S. Habibi, M. Ferdowsi, P. Shamsi," An Interleaved Quadratic High Step-Up DC-DC Converter with Coupled Inductor" IEEE Open Journal of Power Electronics, Vol.2, PP. 647 – 658, Dec.2021.

[31] B. Li, P. Wang, Z. Wang, X. Ma, H. Bi, "A New Coupled-Inductor-Based High-Gain Interleaved DC-DC Converter With Sustained Soft Switching" IEEE Transactions on Vehicular Technology, Vol. 70, No. 7, pp. 6527 – 6541, July 2021.

[32] A Mirzaei, M Rezvanyvardom, S Mekhilef," High step-up interleaved zero-voltage transition DC–DC converter with coupled inductors" IET Power Electronics, Vol. 13, No. 19, pp. 4518 – 4531,Dec.2021.

[33] B. Krishna, V. Karthikeyan," Active Switched-Inductor Network Step-Up DC–DC Converter With Wide Range of Voltage-Gain at the Lower Range of Duty Cycles" IEEE Journal of Emerging and Selected Topics in Industrial Electronics, Vol.2, No.4, pp. 431 – 441,Oct. 2021.

[34] S. Sadaf, M. S. Bhaskar, M. Meraj, A. Iqbal, N. Al-Emadi," A Novel Modified Switched Inductor Boost Converter With Reduced Switch Voltage Stress" IEEE Transactions on Industrial Electronics, Vol. 68, No.2, pp. 1275 – 1289, Feb. 2021.

APPENDIX (A)
MATLAB SIMULATION CIRCUITS

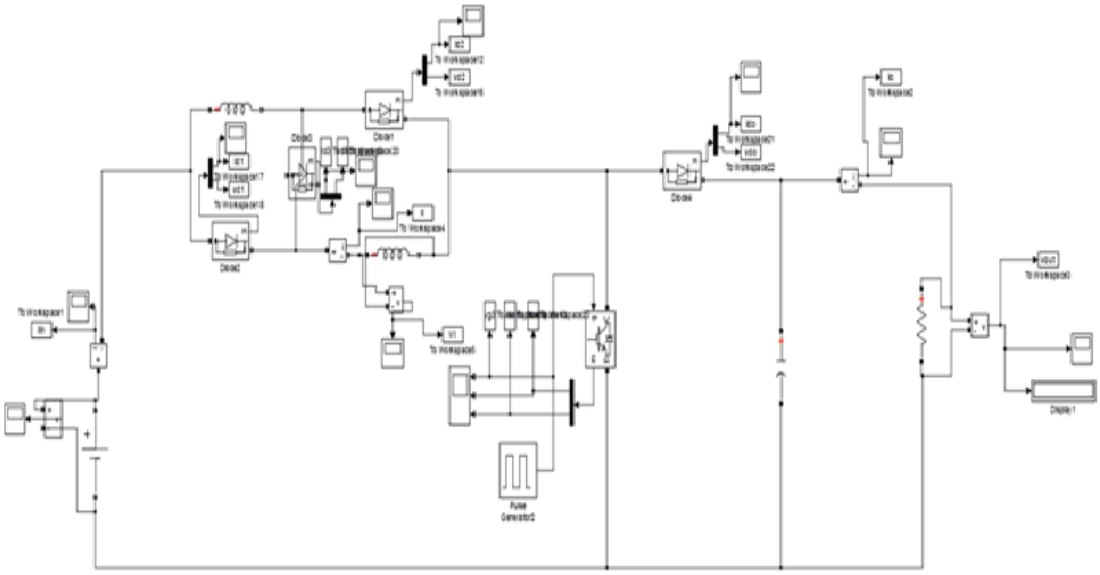

simulation circuit for the proposed converter

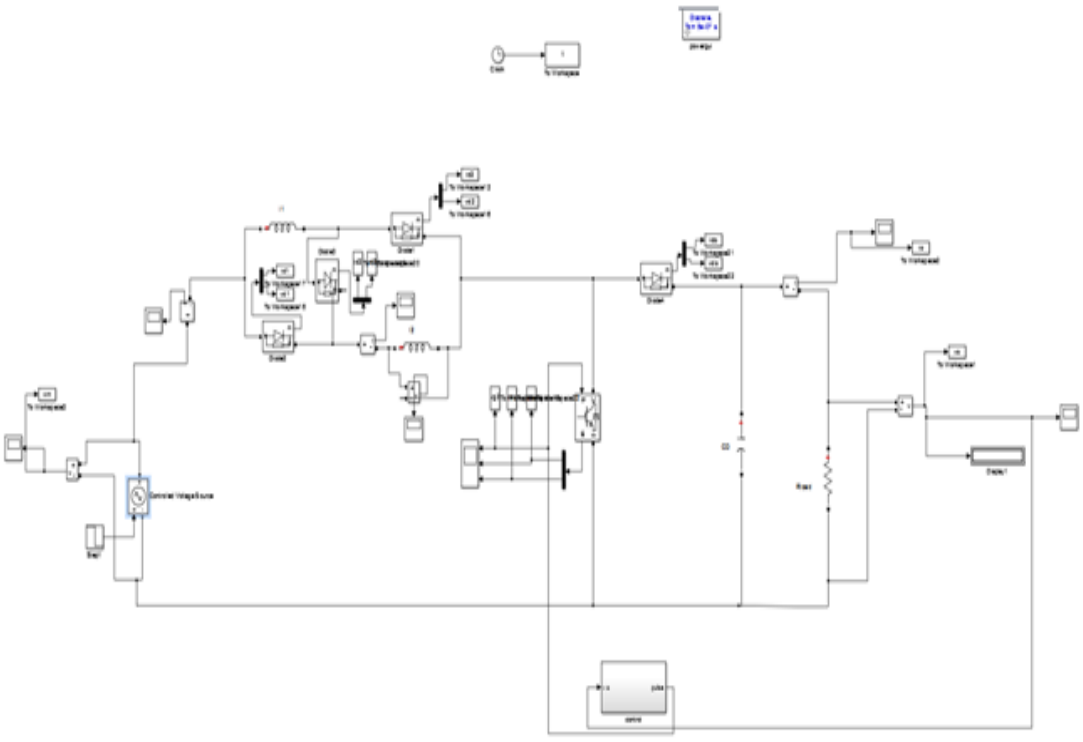

Simulation circuit for input change control

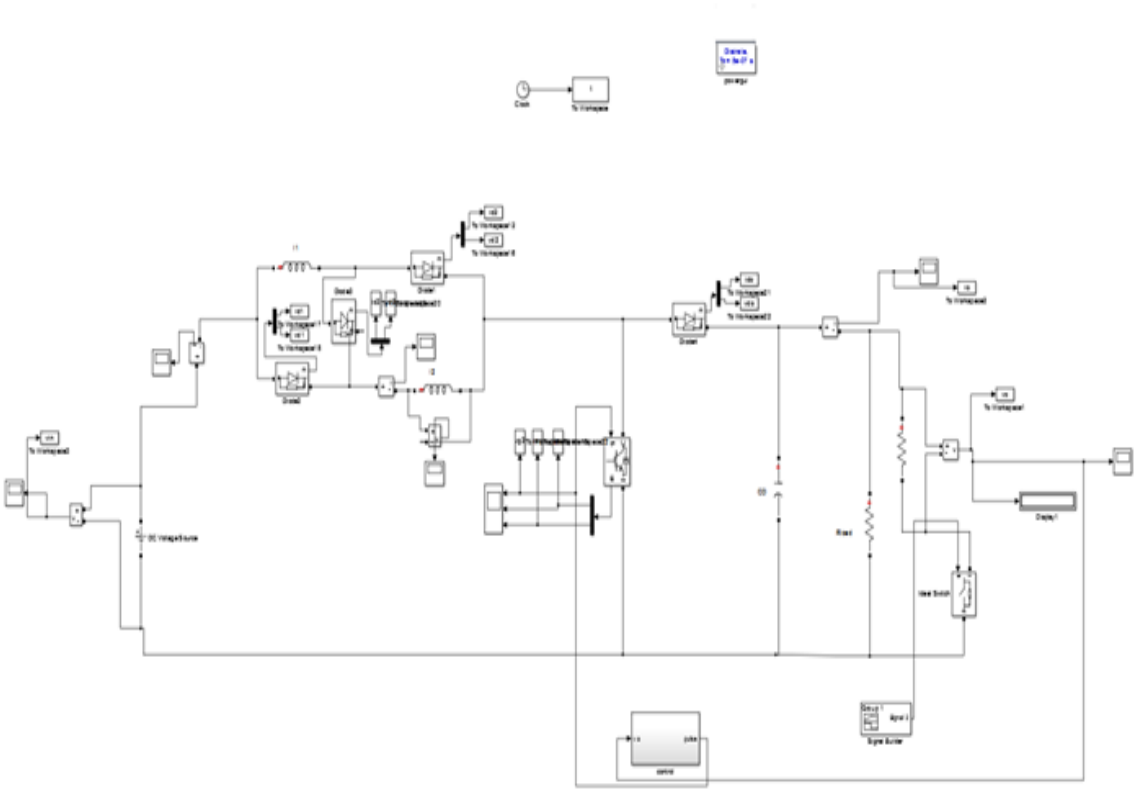

Simulation circuit for load change control

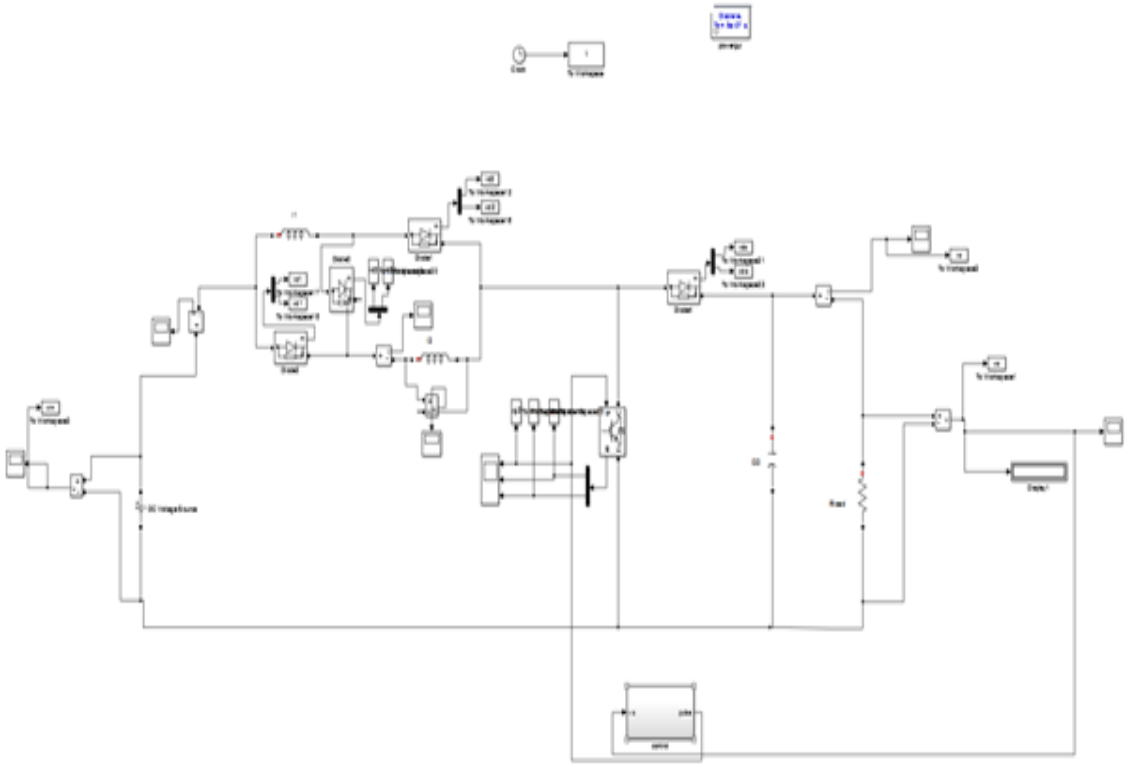

simulation circuit for reference voltage change

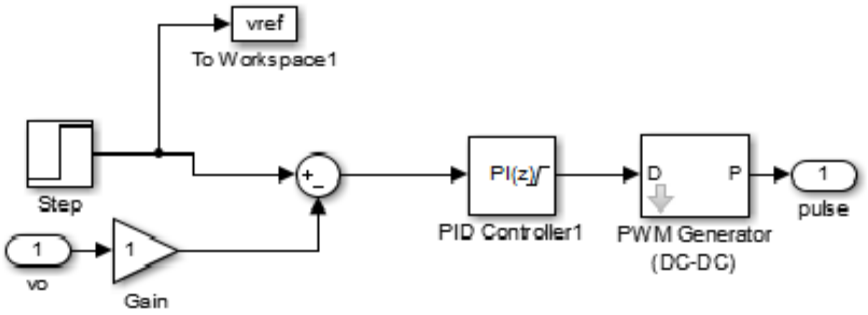

(a)

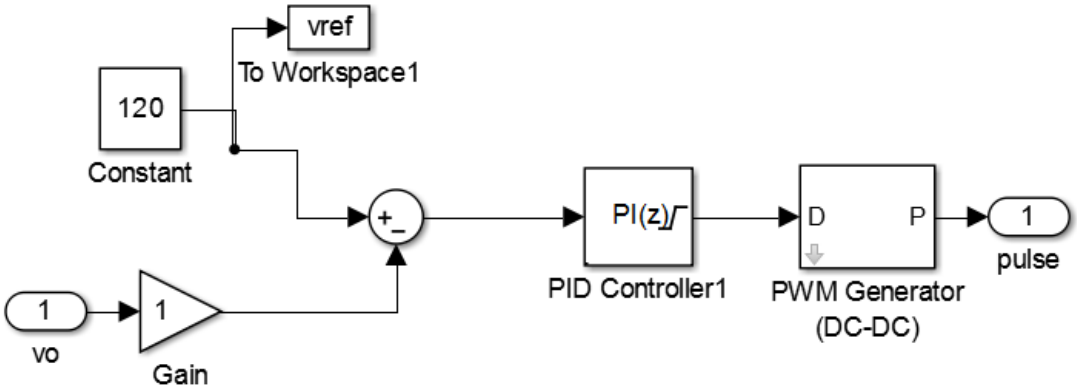

(b)

Block diagram for closed loop controller

Appendix (B)
IGBT DATA SHEET

MITSUBISHI IGBT MODULES

CM100DY-24H

HIGH POWER SWITCHING USE
INSULATED TYPE

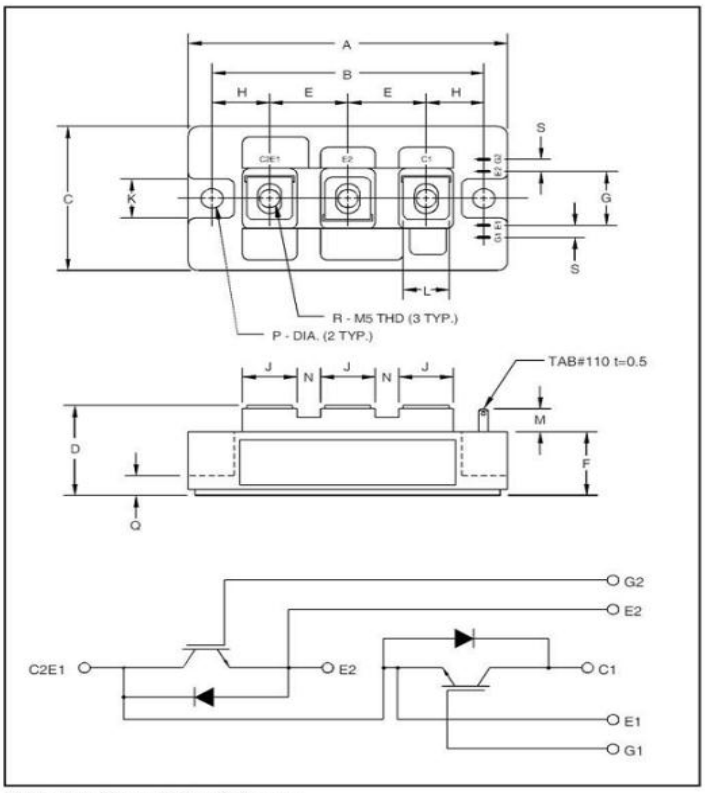

Outline Drawing and Circuit Diagram

Dimensions	Inches	Millimeters
A	3.70	94.0
B	3.150±0.01	80.0±0.25
C	1.89	48.0
D	1.18 Max.	30.0 Max.
E	0.90	23.0
F	0.83	21.2
G	0.71	18.0
H	0.67	17.0
J	0.62	16.0

Dimensions	Inches	Millimeters
K	0.51	13.0
L	0.47	12.0
M	0.30	7.5
N	0.28	7.0
P	0.256 Dia.	Dia. 6.5
Q	0.31	8.0
R	M5 Metric	M5
S	0.16	4.0

Description:
Mitsubishi IGBT Modules are designed for use in switching applications. Each module consists of two IGBTs in a half-bridge configuration with each transistor having a reverse-connected super-fast recovery free-wheel diode. All components and interconnects are isolated from the heat sinking baseplate, offering simplified system assembly and thermal management.

Features:
- ☐ Low Drive Power
- ☐ Low $V_{CE(sat)}$
- ☐ Discrete Super-Fast Recovery Free-Wheel Diode
- ☐ High Frequency Operation
- ☐ Isolated Baseplate for Easy Heat Sinking

Applications:
- ☐ AC Motor Control
- ☐ Motion/Servo Control
- ☐ UPS
- ☐ Welding Power Supplies

Ordering Information:
Example: Select the complete part module number you desire from the table below -i.e. CM100DY-24H is a 1200V (V_{CES}), 100 Ampere Dual IGBT Module.

Type	Current Rating Amperes	V_{CES} Volts (x 50)
CM	100	24

Sep.1998

MITSUBISHI ELECTRIC

MITSUBISHI IGBT MODULES

CM100DY-24H

HIGH POWER SWITCHING USE
INSULATED TYPE

Absolute Maximum Ratings, T_j = 25 °C unless otherwise specified

Ratings	Symbol	CM100DY-24H	Units
Junction Temperature	T_j	–40 to 150	°C
Storage Temperature	T_{stg}	–40 to 125	°C
Collector-Emitter Voltage (G-E SHORT)	V_{CES}	1200	Volts
Gate-Emitter Voltage (C-E SHORT)	V_{GES}	±20	Volts
Collector Current (T_C = 25°C)	I_C	100	Amperes
Peak Collector Current	I_{CM}	200*	Amperes
Emitter Current** (T_C = 25°C)	I_E	100	Amperes
Peak Emitter Current**	I_{EM}	200*	Amperes
Maximum Collector Dissipation (T_C = 25°C, $T_j \leq$ 150°C)	P_c	780	Watts
Mounting Torque, M5 Main Terminal	–	1.47 ~ 1.96	N · m
Mounting Torque, M6 Mounting	–	1.96 ~ 2.94	N · m
Weight	–	270	Grams
Isolation Voltage (Main Terminal to Baseplate, AC 1 min.)	V_{iso}	2500	Vrms

*Pulse width and repetition rate should be such that the device junction temperature (T_j) does not exceed $T_{j(max)}$ rating.
**Represents characteristics of the anti-parallel, emitter-to-collector free-wheel diode (FWDi).

Static Electrical Characteristics, T_j = 25 °C unless otherwise specified

Characteristics	Symbol	Test Conditions	Min.	Typ.	Max.	Units
Collector-Cutoff Current	I_{CES}	$V_{CE} = V_{CES}$, V_{GE} = 0V	–	–	1.0	mA
Gate Leakage Current	I_{GES}	$V_{GE} = V_{GES}$, V_{CE} = 0V	–	–	0.5	µA
Gate-Emitter Threshold Voltage	$V_{GE(th)}$	I_C = 10mA, V_{CE} = 10V	4.5	6.0	7.5	Volts
Collector-Emitter Saturation Voltage	$V_{CE(sat)}$	I_C = 100A, V_{GE} = 15V	–	2.5	3.4**	Volts
		I_C = 100A, V_{GE} = 15V, T_j = 150°C	–	2.25	–	Volts
Total Gate Charge	Q_G	V_{CC} = 600V, I_C = 100A, V_{GE} = 15V	–	500	–	nC
Emitter-Collector Voltage	V_{EC}	I_E = 100A, V_{GE} = 0V	–	–	3.5	Volts

** Pulse width and repetition rate should be such that device junction temperature rise is negligible.

Dynamic Electrical Characteristics, T_j = 25 °C unless otherwise specified

Characteristics		Symbol	Test Conditions	Min.	Typ.	Max.	Units
Input Capacitance		C_{ies}	V_{GE} = 0V, V_{CE} = 10V	–	–	20	nF
Output Capacitance		C_{oes}		–	–	7	nF
Reverse Transfer Capacitance		C_{res}		–	–	4	nF
Resistive	Turn-on Delay Time	$t_{d(on)}$	V_{CC} = 600V, I_C = 100A, $V_{GE1} = V_{GE2}$ = 15V, R_G = 3.1Ω	–	–	250	ns
Load	Rise Time	t_r		–	–	350	ns
Switching	Turn-off Delay Time	$t_{d(off)}$		–	–	300	ns
Time	Fall Time	t_f		–	–	350	ns
Diode Reverse Recovery Time		t_{rr}	I_E = 100A, di_E/dt = –200A/µs	–	–	250	ns
Diode Reverse Recovery Charge		Q_{rr}	I_E = 100A, di_E/dt = –200A/µs	–	0.74	–	µC

Thermal and Mechanical Characteristics, T_j = 25 °C unless otherwise specified

Characteristics	Symbol	Test Conditions	Min.	Typ.	Max.	Units
Thermal Resistance, Junction to Case	$R_{th(j-c)}$	Per IGBT	–	–	0.16	°C/W
Thermal Resistance, Junction to Case	$R_{th(j-c)}$	Per FWDi	–	–	0.35	°C/W
Contact Thermal Resistance	$R_{th(c-f)}$	Per Module, Thermal Grease Applied	–	–	0.065	°C/W

Sep.1998

MITSUBISHI ELECTRIC

MITSUBISHI IGBT MODULES

CM100DY-24H

HIGH POWER SWITCHING USE
INSULATED TYPE

OUTPUT CHARACTERISTICS (TYPICAL)

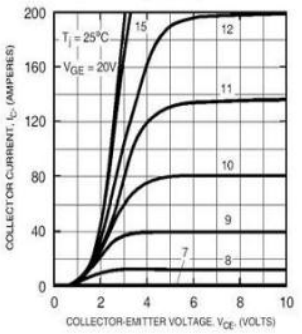

TRANSFER CHARACTERISTICS (TYPICAL)

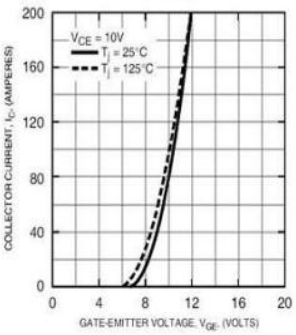

COLLECTOR-EMITTER SATURATION VOLTAGE CHARACTERISTICS (TYPICAL)

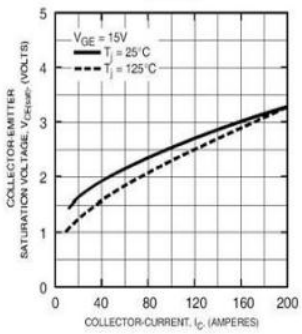

COLLECTOR-EMITTER SATURATION VOLTAGE CHARACTERISTICS (TYPICAL)

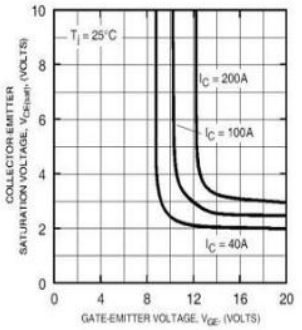

FREE-WHEEL DIODE FORWARD CHARACTERISTICS (TYPICAL)

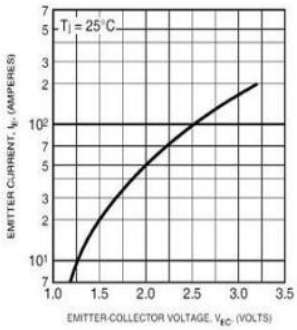

CAPACITANCE VS. V_{CE} (TYPICAL)

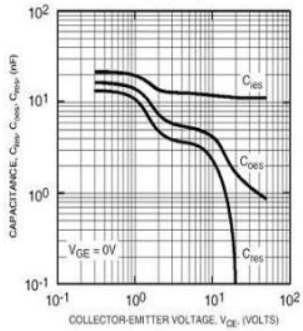

HALF-BRIDGE SWITCHING CHARACTERISTICS (TYPICAL)

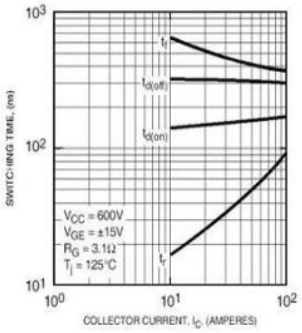

REVERSE RECOVERY CHARACTERISTICS (TYPICAL)

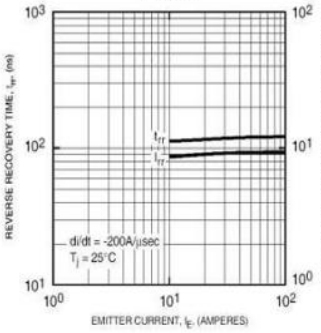

GATE CHARGE, V_{GE}

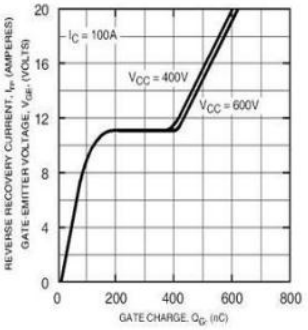

Sep.1998

MITSUBISHI ELECTRIC

حيث قله المكونات المستخدمه وزياده مستوى جهد الخرج وقله الاجهاد على المفتاح والصمامات الثنائيه وبالتالى تقل المفاقيد وتزيد الكفاءه للمحوال المستخدم.

تتكون هذه الرساله من خمسه فصول وفيما يلى عرض ملخص لما تحتويه فصول الرساله:

الفصل الاول:

يعرض الباحث مقدمه وعرضا لاهميه موضوع الرساله ودراسه للابحاث السابقه المتعلقه بموضوع الرساله واهداف الرساله واستعراض لبقيه ابواب الرساله.

الفصل الثانى:

يشرح هذا الفصل بالتفصيل تحليل المحوال المقترح في وضع التوصيل المستمر (CCM) ووضع التوصيل المتقطع (DCM) من حيث وصف المحوال ، وأوضاع التشغيل ، واشتقاق معادله تكبير الجهد ، ومنهجية التصميم.

الفصل الثالث:

يقدم هذا الفصل نتائج المحاكاة لكل من وضع التوصيل المستمر والمتقطع وكذلك نتائج المحاكاه فى التحكم في الحلقة المغلقة للمحوال المقترح عند الحمل الساكن. حيث تمت دراسة تغيير المدخلات وتغير الجهد المرجعي وتغيير الحمل في هذا الفصل للحمل الساكن .

الفصل الرابع:

يوضح هذا الفصل النتائج العمليه للمحوال المقترح لحاله التوصيل المستمر والمتقطع CCM و DCMوالمحوال ايضا تم اختباره فى حاله التحكم الحلقه المغلقه عند الحمل الساكن فى حاله تغيير دخل المحوال اوتغيير الحمل وكذالك تغيير الجهد المرجعى وايضا اختباره بالنسبه الى التحكم في السرعة والتحكم في الجهد في حالة الحمل الديناميكي.والتى تم تنفيذها معمليا على (DSP-1104)والحصول علي النتائج بواسطه جهاز الاوسليسكوب.

الفصل الخامس:

يقدم هذا الفصل مناقشه لما تم الحصول عليه فى الرساله من نتائج. وتم اقتراح نقاط بحثيه مستقبليه كامتداد لهذا البحث.

مقترح محوال الجهد المستمر عالى الكسب غير المعزول لتطبيقات الخلايا الفتوفولتيه

ملخص الرساله:

زياده الطلب على الطاقه الكهربيه نتيجه التقدم الصناعى وزياده الكثافه السكانيه ادى الى عدم كفايه مصادر الطاقه التقليديه. وحاليا تركز الاهتمام على النظم التى تعمل بمصادر الطاقه الجديده والمتجدده خاصه الطاقه الشمسيه كبديل للطاقه التقليديه حيث انها متوفره فى كل مكان فى مصر ولها مميزات عن الطاقه الغير متجدده مثل الاعتماديه والامان والاداء العالى وانخفاض تكلفه الصيانه وعدم وجود تكاليف استهلاك الوقود وايضا قله التلوث السمعى.

كل نظم الطاقه الشمسيه الموجوده فى السوق تعطى جهود منخفضه لكن متطلبات الحمل تحتاج لجهود اعلى لذلك يتم استخدام محوال التيار الستمر رافع للجهد. هذا المحوال يتم وضعه بين المصدر والحمل كوحده تحكم فى الجهد حيث انها تنظم وترفع جهد الخلايا الشمسيه الى الجهد المطلوب.

هناك العديد من التقنيات والاساليب المستخدمه لتطوير المحوالات عاليه الكسب لتعطى جهود عاليه مقارنه بالمحوالات التقليديه التى تعطى فقط جهد الخرج ضعف جهد الدخل وهذا الجهد قليل جدا لا يناسب تطبيقات الخلايا الفتوفولتيه بالاضافه الى الاجهاد العالى التى ينتج عن هذه المحوالات التقليديه وبالتالى زياده مفاقيد التوصيل ولذلك تم استخدام محوال الجهد المستمر عالى الكسب والتى تنقسم الى نوعين محوال معزول والاخر غير المعزول .

فى هذه الرساله تم استخدام نموذج مقترح لمحوال الجهد المستمر عالى الكسب من النوع الغير المعزول باستخدام تقنيه المحث المقطع التى يمكنها توفير جهد عالى عند الخرج مناسب لمستويات جهد الاستهلاك . وتمتاز هذه التقنيه عن غيرها باعطاء مستويات عاليه من الجهد عند الخرج بكفاءه عاليه ومفاقيد اقل للتغلب على عيوب المحوالات التقليديه.

فى هذه الرساله تم دراسه وتحليل كامل للمحوال المقترح من حيث اوضاع التشغيل والتحليل الرياضى لمعادلات الجهد والتيار واستنتاج معادله تكبير الجهد لكل من وضع التوصيل المستمر (CCM) وايضا وضع التوصيل المقطع (DCM) للتيار.

كما تم عرض نتائج المحاكاه للمقترح باستخدام برنامج الماتلاب والنتائج العمليه والتى تم فيها استخدام كلا من جهاز الاوسلسيكوب وجهاز معالج الاشارت التماثلى (DSP) وتم عمل مقارنه للمحوال المقترح مع غيره من المحوالات الاخرى والتى تؤكد مميزات المقترح عن غيره من

جامعة المنوفية
كلية الهندسة بشبين الكوم
قسم الهندسة الكهربية

مقترح محوال الجهد المستمر عالى الكسب غير المعزول لتطبيقات الخلايا الفتوفولتيه

رساله مقدمه من

المهندسه/ ايمان محمد عبدالغنى محمد سرحان

بكالوريوس الهندسه 2014/ جامعه الازهر

للحصول على درجه الماجستير
فى الهندسه الكهربيه

لجنه الحكم والمناقشه

ا0د / عزه محمد لاشين
استاذ الكترونيات القوى بقسم الهندسه الكهربيه
كليه الهندسه بشبين الكوم
جامعه المنوفيه
( )

ا.د/ عوض السيد السبع
استاذ الكترونيات القوى بقسم الهندسه الكهربيه
كليه الهندسه بشبين الكوم
جامعه المنوفيه
( )

ا.د / محمود محمد سالم
استاذ الكترونيات القوى
عميد كلية تكنولوجيا الصناعه والطاقه
جامعة الدلتا التكنولوجيه بقويسنا
( )

2022

جامعة المنوفية
كلية الهندسة بشبين الكوم
قسم الهندسة الكهربية

مقترح محوال الجهد المستمر عالى الكسب غير المعزول لتطبيقات الخلايا الفتوفولتيه

رساله مقدمه من

المهندسه/ ايمان محمد عبدالغنى محمد سرحان

بكالوريوس الهندسه 2014/ جامعه الازهر

للحصول على درجه الماجستير
فى الهندسه الكهربيه

تحت اشراف

ا.د/ عوض السيد السبع
استاذ الكترونيات القوى بقسم الهندسه الكهربيه
كليه الهندسه بشبين الكوم
جامعه المنوفيه
( )

د/ عرفه سيد منصور
استاذ مساعد بقسم الهندسه الكهربيه
كليه الهندسه بشبين الكوم
جامعه المنوفيه
( )

د/ دينا شعبان عشيبه
استاذ مساعد بقسم الهندسه الكهربيه
كليه الهندسه بشبين الكوم
جامعه المنوفيه
( )

2022